

**Exploring Hydrogen Bonding Interactions
in Multifunctional π Systems using
Matrix Isolation Infrared Spectroscopy and *Ab Initio* Computations**

**A thesis submitted in partial fulfillment of requirements
for the degree of Doctor of Philosophy**

By

Kanupriya Verma

PH12147

Research Advisor

Prof.K.S.Viswanathan



**Department of Chemical Sciences
Indian Institute of Science Education & Research Mohali
Sector-81, Knowledge City, S.A.S. Nagar Manauli PO, Mohali-140306
Punjab,India**

August 2017

Dedicated to...

My grandparents

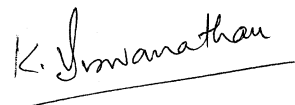
CERTIFICATE

I hereby certify that the thesis titled “ Exploring Hydrogen Bonding Interactions in Multifunctional π systems using Matrix Isolation Infrared Spectroscopy and *Ab Initio* Computations” submitted for the degree of Doctor of Philosophy by Ms. Kanupriya Verma is the record of research work carried out by her during the period May 2013 to August 2017 under my guidance and supervision and further state that this work has not formed the basis for the award of any degree, diploma or a fellowship to any other University or Institute. I further state that this work in this thesis was carried out independently by Ms. Kanupriya Verma.

In my capacity as the supervisor of the candidate's PhD thesis work, I certify that the above statements are true to the best of my knowledge.

Place: Mohali

Date: 23rd January, 2018



Prof. K.S Viswanathan

(Research Supervisor)

DECLARATION

The work presented in this thesis has been carried out by me under the guidance of Prof. K.S.Viswanathan at the Indian Institute of Science Education and Research Mohali. This work has not been submitted in part or in full for a degree, diploma or a fellowship to any other University or Institute. Whenever contributions of others are involved, every effort has been made to indicate this clearly, with due acknowledgement of collaborative research and discussions. This thesis is a bonafide record of original work done by me and all sources listed within have been detailed in the bibliography.

Place: Mohali

Date: 23rd January, 2018



Kanupriya Verma

Acknowledgements

I would like to express my deep sense of gratitude and indebtedness to my supervisor Prof.K.S.Viswanathan for giving me an opportunity to work under his guidance. His excellent supervision, skilled guidance, unfailing support and constant encouragement have been invaluable to me. His humility and patience are unparalleled. I thoroughly enjoyed the freedom that was given to me during the course of this research work that allowed me to explore and learn more than I otherwise might have. I feel extremely fortunate to have a supervisor who cared so much about my work and was always available for scientific discussions, questions and queries. He has made this journey a wonderful and memorable experience for me.

My sincere thanks to my doctoral committee members Dr. Sugumar Venkataramani and Dr. P. Balanarayan for their constant assessment of my thesis work and giving me productive ideas and suggestions to improve my work.

My humble thanks to the former director of IISER Mohali, Prof. N. Sathyamurthy for providing me with all the experimental and computational facilities. I would also like to thank Prof. Debi Prasad Sarkar, Director of IISER Mohali. I am thankful to Dr. S. Arulananda Babu, Head, Department of Chemistry, IISER Mohali. I want to thank MHRD for the funding and infrastructure. I am thankful to the administrative staff, stores, library, hostel, housekeeping, maintenance and the security staff of IISER Mohali.

I would like to thank my colleagues Dr. Anamika, Jyoti, Ginny and Pankaj, for creating a healthy and positive atmosphere in the lab. I would like to thank Dr. Bishnu Prasad Kar for all his help and encouragement. I am thankful to Dr. Sanjay Singh and his colleague Mr. Deependra Bawari for their help in the synthesis of borazine.

This thesis could not be completed without the support of my best friend, Piyush Mishra. I thank him for his constant inspiration, patience and support. He was always there to help me throughout my thesis work. He made my stay in IISER a memorable one. I am glad and very fortunate that I would also be sharing my life with him. My friends, Monika, Jyoti, Srijit, Mariyam, Shruti, Satyam, Aniket, Parth, Shivangi, Anandi, Banpreet and Bhavna for their support.

I am very grateful to Mrs. Chitra Viswanathan and Dr. Deepika Janakiraman for their constant encouragement and help. I would like to express my deep and sincere gratitude to Mrs. Sunita Mishra and Prof. A.K.Mishra for their support and encouragement.

I would like to thank Mr. Biswajit Ghosh, Mr. Saavan and Mr. Rohit in my hostel canteen who always provided me with good food.

I am very thankful to my grandparents, Late Smt. Sanyoglata Abrol and Late Shri. Baldev Raj Abrol for their unconditional love and affection. They will always be missed. They always believed in my abilities and their blessings constantly motivate me in whatever I do.

I would like to extend a heartfelt thanks to my mother, Mrs. Sunita Verma for being very patient with me and giving me her support throughout my doctoral work. She has always been by my side during difficult times and helped me to recover from my fears and disappointments. Her love and affection were the main driving force which led this thesis to a successful completion. I am also very grateful to my father, Mr. Yogesh Verma and my brother Karan Verma for their unconditional love and support.

Finally and most importantly, I would like to thank the Almighty for always blessing me and being by my side throughout this journey.

Kanupriya Verma

CONTENTS

	Page Number
List of Figures	i
List of Tables	iv
List of Abbreviations	vii
Synopsis	viii
CHAPTER 1 INTRODUCTION	1
1.1 Scope of present work	9
References	10
CHAPTER 2 EXPERIMENTAL AND COMPUTATIONAL DETAILS	16
2.1 Matrix Isolation Infrared Spectroscopy	16
2.2 Matrix Isolation Setup	22
2.3 Experimental Procedure	23
2.4 Computations	28
2.4.1 Geometry optimization and frequency calculation	28
2.4.2 Interaction energy calculation of complexes	30
2.4.3 Atoms in Molecules Analysis	31
2.4.4 Energy Decomposition Analysis	32
2.4.5 Natural Bond Orbital Analysis	33
References	37
CHAPTER 3 PHENYLACETYLENE-ACETYLENE COMPLEXES	
3.1 Introduction	41
3.2 Experimental Details	42
3.3 Computations	43
3.4 Results and Discussion	45
3.4.1 Computational	45
3.4.2 Experimental	46
3.5 Vibrational Assignments	49

3.5.1	\equiv C-H asym.stretch in C_2H_2 submolecule	49
3.5.2	\equiv C-H stretch in PhAc submolecule	52
3.5.3	\equiv C-H bend in C_2H_2 submolecule	52
3.5.4	\equiv C-H bend in PhAc submolecule	52
3.5.5	\equiv C-D stretch in PhAc _D	52
3.6	AIM Analysis	53
3.7	EDA Analysis	57
3.8	NBO analysis	57
3.9	Conclusions	60
	References	63
CHAPTER 4	STUDY OF HYDROGEN BONDED INTERACTIONS IN BORAZINE-ACETYLENE	
4.1	Introduction	67
4.2	Experimental Details	68
4.2.1	Synthesis of $B_3N_3H_6$	68
4.2.2	Matrix Isolation IR Experiments	69
4.3	Computations	70
4.4	Results and Discussions	74
4.4.1	Computational	74
4.4.2	Experimental	74
4.5	Vibrational Assignments	75
4.5.1	N-H stretch in $B_3N_3H_6$	75
4.5.2	C-H asymmetric stretch in C_2H_2	77
4.5.3	C-H bend in C_2H_2	77
4.6	Atoms-in-Molecules analysis	78
4.7	Energy Decomposition Analysis	78
4.8	Natural Bond Orbital (NBO) Analysis	83
4.9	Comparison Between $C_6H_6-C_2H_2$ and $B_3N_3H_6-C_2H_2$ Dimers	83
4.10	Conclusions	85
	References	86

CHAPTER 5	BORAZINE DIMER	
5.1	Introduction	88
5.2	Experimental Details	89
5.2.1	Synthesis	89
5.2.2	Matrix Isolation IR Experiments	89
5.3	Computational Details	89
5.4	Results and Discussion	90
5.4.1	Computational	90
5.4.2	Experimental	94
5.5	Vibrational Assignments	94
5.5.1	N-H stretch in $B_3N_3H_6$	94
5.5.2	Ring bending mode in $B_3N_3H_6$	97
5.6	AIM Analysis	97
5.7	EDA Analysis	99
5.8	NBO Analysis	99
5.9	Conclusions	103
	References	104
CHAPTER 6	BORAZINE-BENZENE AND BORAZINE-PHENYLACETYLENE COMPLEXES	
6.1	Introduction	107
6.2	Experimental details	107
6.2.1	Synthesis	108
6.2.2	Matrix Isolation IR Experiments	108
	Section I: $B_3N_3H_6-C_6H_6$ Complexes	
6.3	Computational Details	108
6.4	Results and Discussion	111
6.4.1	Computational	111
6.4.2	Experimental	111
6.5	Vibrational Assignments	113

6.5.1	N-H stretch in $B_3N_3H_6$	113
6.5.2	Ring bending mode in $B_3N_3H_6$	113
	Section II: $B_3N_3H_6$-PhAc Complexes	
6.6	Computational Details	113
6.7	Results and Discussion	116
6.7.1	Computational	116
6.7.2	Experimental	116
6.8	Vibrational Assignments	119
6.8.1	N-H stretch in $B_3N_3H_6$	119
6.8.2	C-H symmetric stretch in PhAc	119
6.8.3	C-D stretch in PhAc _D	120
6.9	AIM Analysis	120
6.10	Energy Decomposition Analysis	124
6.11	Natural Bond Orbital Analysis	124
6.12	Phenylacetylene-Benzene Complexes	124
6.13	Conclusions	125
	References	132
CHAPTER 7	SUMMARY AND CONCLUSIONS	133
7.1	Scope for Future Work	137
	LIST OF PUBLICATIONS	138

LIST OF FIGURES

Fig.No.	Figure Caption	Page No.
2.1	Cage effects and frequency shifts for the sample molecule	19
2.2	Radiation shield of the cryostat	24
2.3	Cryostat, Compressor and the temperature controller	25
2.4	Diffusion pump, Pirani Gauge and Penning Gauge readouts	26
2.5	a) The mixing chamber; b) The fine flow needle valve; c) The double jet setup mounted on the cryostat	26
2.6	The MI-FTIR setup at IISER Mohali	27
2.7	Schematic NBO perturbation diagram for '2-e stabilizing' delocalization interaction.	36
3.1	PhAc and C ₂ H ₂ structures with multifunctional sites	44
3.2	Optimized structures of PhAc-C ₂ H ₂ complexes at M06-2X/aug-cc-pVDZ	47
3.3	Panel A (a) C ₂ H ₂ :N ₂ annealed (1:1000) (b) PhAc: N ₂ annealed (1:1000) (c) C ₂ H ₂ : PhAc: N ₂ (1:1:1000) at 12K (d) annealed spectrum of (c). Panel B (a) C ₂ H ₂ annealed (1:1000) (b) PhAc annealed (1:1000) (c) C ₂ H ₂ : PhAc: N ₂ (1:1:1000) at 12K (d) annealed spectrum of (c). Panel C (a) C ₂ H ₂ annealed (1:1000) (b) PhAc annealed (1:1000) (c) C ₂ H ₂ : PhAc: N ₂ (1:1:1000) at 12K (d) annealed spectrum of (c). Matrix isolation infrared spectra showing the concentration dependence over the spectral region 3300-3200 cm ⁻¹ in N ₂ matrix Panel A of a) PhAc:C ₂ H ₂ :N ₂ (0.25:0.1:1000), b) PhAc:C ₂ H ₂ :N ₂ (0.5:0.1:1000) c) PhAc: C ₂ H ₂ :N ₂ (1:0.2:1000). Panel B shows the spectral region 3330-3300 cm ⁻¹	50
3.4	a) PhAc:C ₂ H ₂ : N ₂ (1:0.25:1000), b) PhAc:C ₂ H ₂ : N ₂ (3:0.25:1000) and c) PhAc:C ₂ H ₂ :N ₂ (6:0.5:1000). Panel C shows the spectral region 770-730 cm ⁻¹ of (a) PhAc:C ₂ H ₂ :N ₂ (1:0.25:1000), b) PhAc:C ₂ H ₂ : N ₂ (3:0.25:1000) and c) PhAc:C ₂ H ₂ : N ₂ (6:0.5:1000).	51

3.5	Matrix isolation infrared annealed spectra of PhAc-C ₂ H ₂ in a N ₂ matrix over the region 3350-3200 cm ⁻¹ (Panel A), 3335-3285 cm ⁻¹ (Panel B) and 770-740 cm ⁻¹ (Panel C). Spectra shown in (a) is experimental spectra recorded after annealing the matrix; (b), (c) and (d) show the computed spectra of complexes 3, 2 and 1 respectively.	55
3.6	Matrix isolation infrared spectra showing the concentration dependence over the spectral region 2620-2580 cm ⁻¹ (Panel A) of a) PhAcD:C ₂ H ₂ (0.25:0.1:1000), b) PhAcD:C ₂ H ₂ (0.5:0.1:1000) and c) PhAcD:C ₂ H ₂ (1:0.2:1000). Panels A and B show the N ₂ and Ar spectra respectively.	56
3.7	AIM analysis of the complexes at M06-2X/aug-cc-pVDZ.	59
4.1	Possible geometries of the B ₃ N ₃ H ₆ -C ₂ H ₂ complexes at the MP2/aug-cc-pVDZ.	72
4.2	Infrared spectrum of (a) B ₃ N ₃ H ₆ (x:1000) (b) C ₂ H ₂ :N ₂ (1:1000) (c) B ₃ N ₃ H ₆ : C ₂ H ₂ :N ₂ (x:1:1000) at 12K (d) spectrum of (c) annealed at 27K, (e) B ₃ N ₃ H ₆ : C ₂ H ₂ :N ₂ (x:2:1000) annealed at 27 K. Panels A, B and C show the regions 3500-3400, 3300-3200 and 760-730 cm ⁻¹ respectively.	76
4.3	Comparison of experimental and computed spectra of the various B ₃ N ₃ H ₆ -C ₂ H ₂ complexes.	80
4.4	AIM analysis for the stable B ₃ N ₃ H ₆ -C ₂ H ₂ complexes at MP2/aug-cc-pVDZ level of theory.	82
5.1	Optimised geometries of the B ₃ N ₃ H ₆ dimers at MP2/aug-cc- pVDZ	91
5.2	Matrix isolation IR spectra of (a) B ₃ N ₃ H ₆ :N ₂ (0.5x:1000) annealed at 27 K (b) B ₃ N ₃ H ₆ :N ₂ (x:1000) deposited at 12 K. (c) Spectrum of sample in 'b' annealed at 27K, (d) Spectrum 'b' subtracted from 'c'. Negative going peaks are product peaks formed during annealing. Panels A and B show features in the N-H stretch region and bending region, respectively.	95
5.3	(a) Experimental spectrum of the B ₃ N ₃ H ₆ :N ₂ (x:1000) (b) Subtracted spectrum; computed spectrum for the (c) H··H complex (d) T _N complex (e) PD complex, (f) AS complex. Panels A and B show features in the N-H stretching and bending region, respectively.	98
5.4	AIM analysis for the B ₃ N ₃ H ₆ dimers at MP2/aug-cc-pVDZ. The atom labels in this figure are those shown in Fig. 5.1.	101
6.1	Optimised structures of B ₃ N ₃ H ₆ -C ₆ H ₆ complexes at MP2/aug-cc-pVDZ level of theory.	109

6.2	Panel A shows matrix isolation infrared spectra from 3500-3425 cm^{-1} (a) $\text{C}_6\text{H}_6:\text{N}_2$ (3:1000) (b) $\text{B}_3\text{N}_3\text{H}_6:\text{N}_2$ (x:1000) (c) $\text{B}_3\text{N}_3\text{H}_6:\text{C}_6\text{H}_6:\text{N}_2$ (x:3:1000) at 12K (d) $\text{B}_3\text{N}_3\text{H}_6:\text{C}_6\text{H}_6:\text{N}_2$ (x:3:1000) annealed at 27K (e) $\text{B}_3\text{N}_3\text{H}_6:\text{C}_6\text{H}_6:\text{N}_2$ (x:6:1000) annealed at 27K. Panel B shows the bending region of $\text{B}_3\text{N}_3\text{H}_6$ from 925-910 cm^{-1} . (a) $\text{C}_6\text{H}_6:\text{N}_2$ (3:1000) (b) $\text{B}_3\text{N}_3\text{H}_6:\text{N}_2$ (x:1000) (c) $\text{B}_3\text{N}_3\text{H}_6:\text{C}_6\text{H}_6:\text{N}_2$ (x:3:1000) at 12K (d) $\text{B}_3\text{N}_3\text{H}_6:\text{C}_6\text{H}_6:\text{N}_2$ (x:3:1000) annealed at 27K (e) $\text{B}_3\text{N}_3\text{H}_6:\text{C}_6\text{H}_6:\text{N}_2$ (x:6:1000) annealed at 27K.	112
6.3	Panel A showing (a) experimental spectrum of $\text{B}_3\text{N}_3\text{H}_6:\text{PhAc}:\text{N}_2$ (x:6:1000) (b) Computed spectrum of NH-C complex; (c) Computed spectrum of T-NH complex; (d) Computed spectrum of PD complex.	115
6.4	Optimised structures of $\text{B}_3\text{N}_3\text{H}_6$ -PhAc complexes at MP2/aug-cc-pVDZ level of theory.	117
6.5	Infrared spectrum of (a) $\text{PhAc}:\text{N}_2$ (1:1000) (b) $\text{B}_3\text{N}_3\text{H}_6:\text{N}_2$ (x:1000) (c) $\text{B}_3\text{N}_3\text{H}_6:\text{PhAc}:\text{N}_2$ (x:1:1000) at 12 K (d) spectrum of (c) annealed at 27K. (a) $\text{PhAc}_D:\text{N}_2$ (1:1000) (b) $\text{B}_3\text{N}_3\text{H}_6:\text{PhAc}_D:\text{N}_2$ (x:1:1000) at 12 K (c) $\text{B}_3\text{N}_3\text{H}_6:\text{PhAc}_D:\text{N}_2$ (x:1:1000) annealed at 27 K. Panels A, B and C show the regions 3550-3400, 3340-3300 and 2610-2590 cm^{-1} respectively.	121
6.6	Panel A showing the (a) Experimental spectrum of $\text{B}_3\text{N}_3\text{H}_6:\text{PhAc}:\text{N}_2$ (x:1:1000) annealed at 27K (b) Computed spectrum of Bent NH-C complex (c) T-NH complex (d) Stacked complex.	122
6.7	AIM analysis of $\text{B}_3\text{N}_3\text{H}_6$ - C_6H_6 complexes at MP2/aug-cc-pVDZ.	126
6.8	AIM analysis of $\text{B}_3\text{N}_3\text{H}_6$ -PhAc complexes at MP2/aug-cc-pVDZ	127
6.9	Optimized geometries of PhAc- C_6H_6 complexes at MP2/aug-cc-pVDZ	131
7.1	The various multifunctional π systems explored in this thesis.	133

LIST OF TABLES

Table No.	Table Caption	Page No.
3.1	Raw uncorrected/ZPE/BSSE interaction energies in kcal/mol for the various PhAc-C ₂ H ₂ complexes at the M06-2X and MP2 levels using 6-311++G** and aug-cc-pVDZ basis sets.	44
3.2	Selected geometrical parameters for the PhAc-C ₂ H ₂ complexes at the M06-2X/aug-cc-pVDZ level of theory	47
3.3	Experimental, computed scaled vibrational frequencies and mode assignments for the C ₂ H ₂ -PhAc complexes in N ₂ matrix at the M06-2X/aug-cc-pVDZ level of theory.	53
3.4	AIM calculations showing the electron densities $\rho(r)$ and $\nabla^2\rho(r)$ at the bond critical point for PhAc-C ₂ H ₂ complexes at M06-2X/aug-cc-pVDZ.	57
3.5	Energy Decomposition analysis of PhAc-C ₂ H ₂ complexes at MP2/aug-cc-pVDZ.	61
3.6	NBO analysis for the PhAc-C ₂ H ₂ heterodimers, performed at M06-2X/aug-cc-pVDZ level of theory. The atom numbering indicated in the table is as shown in Fig. 2. E is the second order perturbation energy, E(j)-E(i) is the donor-acceptor energy difference and F(i,j) is the overlap between the donor and acceptor orbitals.	61
4.1	Interaction energy values (ΔE in kcal/mol) obtained using the M06-2X, MP2 and CCSD(T) methods for different isomers of B ₃ N ₃ H ₆ -C ₂ H ₂ .	69
4.2	Selected structural parameters for the B ₃ N ₃ H ₆ -C ₂ H ₂ complexes at the MP2/aug-cc-pVDZ level of theory. The distances are given in angstroms (Å) and the angles are given in degrees (°) The atom numbering is as given in figure 4.1.	73
4.3	Experimental (N ₂ matrix) and scaled computed vibrational wavenumbers (in cm ⁻¹) and mode assignments for the B ₃ N ₃ H ₆ -C ₂ H ₂ complex. Computations were performed at the MP2/aug-cc-pVDZ level of theory.	79
4.4	AIM calculations showing the values of the electron density $\rho(r_c)$ and its Laplacian $\nabla^2\rho(r_c)$, λ_1/λ_3 at the bond critical point, local kinetic energy density $G(r_{CP})$, local electronic potential energy density $V(r_{CP})$ and the interaction energy ΔE , for the B ₃ N ₃ H ₆ -C ₂ H ₂ complex, computed at MP2/aug-cc-pVDZ level of theory. The values of $\rho(r_c)$, $\nabla^2\rho(r_c)$, $G(r_{CP})$ and $V(r_{CP})$ are in atomic units and ΔE in kcal/mol.	81
4.5	Energy decomposition analysis of the B ₃ N ₃ H ₆ -C ₂ H ₂ complexes at the MP2/aug-cc-pVDZ level of theory.	81
4.6	NBO analysis for the B ₃ N ₃ H ₆ -C ₂ H ₂ dimers, performed at MP2/aug-cc-pVDZ level of theory. The atom numbering indicated in the table is as shown in Fig. 1. E is the second order perturbation energy, E(j)-E(i) is the donor-acceptor energy difference and F(i,j) is the overlap between the donor and acceptor orbitals.	84
5.1	Interaction energies of the various complexes of B ₃ N ₃ H ₆ dimer given as uncorrected/ZPE corrected/BSSE corrected energies (kcal/mol) using the MP2 and M06-2X methods and 6-311++G(d,p) and aug-cc-pVDZ basis sets.	92

5.2	Selected structural parameters for the $B_3N_3H_6$ dimers at the MP2/aug-cc-pVDZ level of theory. The distances are given in angstroms (Å) and the angles are given in degrees (°). The atom numbering is as shown in figure 5.1.	93
5.3	Experimental wavenumbers (cm^{-1}) in N_2 matrix and scaled computed wavenumbers for the $B_3N_3H_6$ dimer, together with mode assignments. Computations were performed at the MP2/aug-cc-pVDZ level.	96
5.4	AIM calculations showing the electron densities $\rho(r)$ and Laplacian of electron densities at the MP2/aug-cc-pVDZ level of theory.	100
5.5	Energy decomposition analysis (LMO-EDA) for the various $B_3N_3H_6$ dimers computed at the MP2/aug-cc-pVDZ level. All energies are in kcal/mol.	100
5.6	NBO analysis for the $B_3N_3H_6$ dimers, performed at MP2/aug-cc-pVDZ level of theory. The atom numbering indicated in the table is as shown in Fig. 1. E is the second order perturbation energy, $E(j)-E(i)$ is the donor-acceptor energy difference and $F(i,j)$ is the overlap between the donor and acceptor orbitals.	102
6.1	Interaction energies, in $kcal\ mol^{-1}$, of the various complexes of $B_3N_3H_6-C_6H_6$ heterodimers given as Uncorrected/ZPE corrected/BSSE corrected energies ($kcal\ mol^{-1}$) at MP2 and M06-2X levels of theory using the 6-311++G** and aug-cc-pVDZ basis sets.	105
6.2	Selected structural parameters for the $B_3N_3H_6-C_6H_6$ at the MP2/aug-cc-pVDZ level of theory. The distances are given in angstroms (Å) and the angles are given in degrees (°)	110
6.3	Experimental (N_2 matrix), scaled computed vibrational wavenumbers (in cm^{-1}) and mode assignments for $B_3N_3H_6-C_6H_6$ complexes. Computations were performed at MP2/aug-cc-pVDZ level.	114
6.4	Interaction energies, in $kcal\ mol^{-1}$, of the various complexes of $B_3N_3H_6-PhAc$, given as uncorrected/ZPE corrected/BSSE corrected energies ($kcal\ mol^{-1}$) at M06-2X and MP2 levels of theory using 6-311++G(d,p) and aug-cc-pVDZ basis sets.	117
6.5	Selected structural parameters for the various $B_3N_3H_6-PhAc$ complexes at the MP2/aug-cc-pVDZ level of theory.	118
6.6	Experimental (N_2 matrix), scaled computed vibrational wavenumbers (in cm^{-1}) and mode assignments for $B_3N_3H_6-PhAc$ and $B_3N_3H_6-PhAc_D$ complexes at MP2/aug-cc-pVDZ level.	123
6.7	AIM calculations showing the values of the electron density $\rho(r_c)$ and its Laplacian $\nabla^2\rho(r_c)$, λ_1/λ_3 at the bond critical point for the $B_3N_3H_6-C_6H_6$ complexes computed at MP2/aug-cc-pVDZ level of theory. The values of $\rho(r)$, $\nabla^2\rho(r)$ are in atomic units.	128
6.8	AIM calculations showing the values of the electron density $\rho(r_c)$ and its Laplacian $\nabla^2\rho(r_c)$, λ_1/λ_3 at the bond critical point for the $B_3N_3H_6-PhAc$ complexes computed at MP2/aug-cc-pVDZ level of theory.	128
6.9	Values of the interaction energy (ΔE) and its different components (in kcal/mol units), for the various $B_3N_3H_6-C_6H_6$ complexes using LMO-EDA at MP2/aug-cc-pVDZ level of theory.	129
6.10	Values of the interaction energy (ΔE) and its different components (in kcal/mol units), for the various $B_3N_3H_6-PhAc$ complexes using LMO-EDA at MP2/aug-cc-pVDZ level of theory.	129

- 6.11 NBO analysis for the $B_3N_3H_6-C_6H_6$ dimers, performed at MP2/aug-cc-pVDZ level of theory. The atom numbering indicated in the table is as shown in Fig. 6.1. E is the second order perturbation energy, $E(j)-E(i)$ is the donor-acceptor energy difference and $F(i,j)$ is the overlap between the donor and acceptor orbitals. 130
- 6.12 NBO analysis for the $B_3N_3H_6-PhAc$ dimers, performed at MP2/aug-cc-pVDZ level of theory. The atom numbering indicated in the table is as shown in Fig. 6.4. E is the second order perturbation energy, $E(j)-E(i)$ is the donor-acceptor energy difference and $F(i,j)$ is the overlap between the donor and acceptor orbitals. 131

LIST OF ABBREVIATIONS

AIM	Atoms in molecules
BCP	Bond Critical Point
BSSE	Basis Set Superposition Error
CBS	Complete Basis Set
CCSD(T)	Coupled Cluster Singles and Doubles
CP	Critical Point
HSAB	Hard Soft Acid Base
LMO-EDA	Localized Molecular Orbital-Energy Decomposition Analysis
MP2	Moller Plesset Perturbation
M06	Minnesota Functional
NBO	Natural Bond Orbital
PhAc	Phenylacetylene
SAPT	Symmetry Adapted Perturbation Theory
ZPE	Zero Point Energy

SYNOPSIS

The study of hydrogen bonding interactions, both experimental and computational, has elicited enormous interest, as it plays a crucial role in many chemical and biological processes, crystal engineering and supramolecular chemistry¹⁻⁴. Hydrogen bonds involving π systems as proton acceptors are a special class of interactions involving O-H $\cdots\pi$, N-H $\cdots\pi$, C-H $\cdots\pi$ and S-H $\cdots\pi$ contacts. All these contacts manifest interaction energies ranging from 1 to 10 kcal/mol. Electronic structure calculations have been extensively used to study these interactions, and advances in computational methodologies have resulted in a more accurate description of these weak interactions. Together with the computations, experiments using a number of different methods, have further improved our understanding of these weak but important interactions. The synergism offered by computations and experiments in the understanding of these interactions cannot be overemphasized.

A brief description of the chapters has been given below.

Chapter 1: Introduction

Non-covalent interactions involving π -systems is a topic that has been and is being extensively studied, as these interactions are responsible for the assembly of a vast array of supramolecular architectures². C-H $\cdots\pi$ interactions have been reported to be present in more than 35% of the organic crystals⁵. The interaction energy of the complexes having π - π and C-H $\cdots\pi$ contacts can vary over the range 1-5 kcal/mol, depending on the nature of the aromatic ring/substituent(s) and the acidity of the C-H bond⁶⁻⁸. Using the Pearson's HSAB concept, these were classified as soft acid-soft base interactions and were shown to have contributions from both electrostatic and dispersion interactions, as opposed to hydrogen bonded interactions involving hard acid-hard base, hard acid-soft base or soft acid-hard base precursors, which were essentially dominated by electrostatic interactions. This chapter gives an overview of the weak hydrogen bonding systems based on prevailing literature and puts the present work in perspective.

In this work, we have explored a number of multifunctional π systems which have competitive binding sites and addressed the question as to which amongst the various isomers of the hydrogen bonded complexes would be the global minimum. The molecules considered in this

study are phenylacetylene, acetylene, borazine and benzene, which are π systems with competitive binding sites. All of these molecules have the potential to serve as proton donors and acceptors and thus, it was interesting to study the competition between the different isomeric forms of the complexes. Towards this end, we have used matrix isolation infrared spectroscopy together with *ab initio* computations. In addition to providing infrared spectral features with small line widths, so essential in studying weak non-covalent interactions, matrix isolation spectroscopy, also offers the possibility of trapping both global and local minima, thus providing a better panorama of the hydrogen bonding landscape.

One of the first systems we studied, was the phenylacetylene-acetylene heterodimer. Both precursors could potentially serve as proton acceptors or donors and our experiments unambiguously pointed to the complex where acetylene was the proton donor to be the global minimum. Other systems we chose, were the complexes of borazine with a number of π systems. Borazine, also known as inorganic benzene is the isoelectronic analogue of benzene. It is highly moisture sensitive and decomposes rapidly in the presence of water, which makes it a challenge to study this system. The main motivation behind studying the borazine systems was to compare it with the much studied benzene systems. While many studies in the literature are known on the benzene systems, very little work has been done on borazine. One of the first studies on borazine done in the group was the borazine-water system. Borazine-water showed the N-H group of borazine acting as the proton donor to the O atom of water as the global minimum, which was very different from the benzene water system which displays an $\text{H}\cdots\pi$ interaction⁹. This N-H \cdots O contact in the borazine-water complex structure was observed experimentally and corroborated by computations. Thus, it was concluded in our work that the borazine water system had a different landscape compared with the benzene water system, which led us to further explore the nature of interaction of borazine with π systems. Hence the study of borazine was considered interesting as it was expected to show similarities and fascinating differences from its organic counterpart, benzene. The results on borazine-acetylene, borazine dimer, borazine-benzene and borazine-phenylacetylene will be discussed.

Chapter 2: Experimental and Computational Details

Details of the experimental technique employed and the computational procedures used to corroborate the experimental results are given in this chapter.

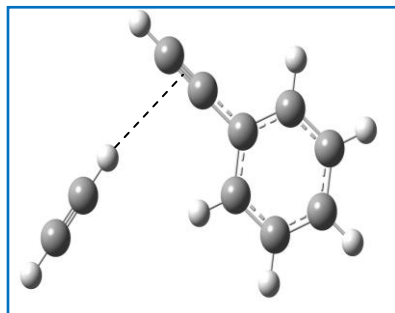
Single jet and double jet effusive sources were used to deposit the analyte molecules and the matrix gases (Ar/N₂) on a cold KBr substrate, maintained at 12 K. After deposition, a matrix isolated spectrum was taken using an IR spectrometer operated at a resolution of 0.5 cm⁻¹. The matrix was then annealed at an elevated temperature, typically 27 K for N₂ and 32 K for Ar for about an hour and the annealed spectrum was taken. Annealing was performed to encourage diffusion to enable complex formation.

Ab initio computations were performed using the GAUSSIAN 09 suite of programs, at the M06-2X and MP2 levels with 6-311++G (d, p) and aug-cc-pVDZ basis sets. Single point calculations were also done using the CCSD(T)/aug-cc-pVDZ level for the complexes. Vibrational frequency calculations were done using analytical gradients to ensure that these frequencies did correspond to minima on the potential energy surface and to assign the observed features in the matrix isolation experiments. AIM, NBO and LMO-EDA calculations were also done for all the systems to further explore the nature of interactions involved in such complexes.

Chapter 3: Phenylacetylene-Acetylene

The role of competitive complexation has been explained in this chapter by describing the study of phenylacetylene-acetylene complexes through matrix isolation IR and *ab initio* quantum chemical studies. Since phenylacetylene and acetylene have multifunctional binding sites, it was interesting to see which of these molecules would serve as the proton donor and which would serve as the proton acceptor. At the M06-2X/aug-cc-pVDZ level of theory, it was found that two complexes, one where the ≡C-H of acetylene interacted with the π cloud of phenyl ring in phenylacetylene and the other where, the ≡C-H group of acetylene interacted with the π cloud of acetylene in phenylacetylene were almost isoenergetic. However, we were able to discern only the latter complex in our matrix isolation experiments. The experimental frequency shift of this complex, in the C-H stretch region of acetylene was found to be 30 cm⁻¹ which corroborated excellently with a theoretical shift of 29.9 cm⁻¹ at the M06-2X/aug-cc-pVDZ level of theory. We could also find evidences of adduct features in the C-H stretching region of phenylacetylene and in the bending region of acetylene. The stacked structure was not observed as it did not present discernible shifts in the vibrational wavenumbers. Experiments were also performed using phenylacetylene deuterated at the acetylenic hydrogen to study the isotopic effects on the vibrational spectra of complexes. The isotopic studies further confirmed the structure of the

complex trapped in the matrix, thereby presenting unambiguous evidence that acetylene served as the proton donor. AIM, NBO and LMO-EDA analysis were also performed to further understand the nature of interactions in this system.



C₂H₂: proton donor

Fig.1. Experimentally observed structure for the phenylacetylene-acetylene complex: acetylene serving as the proton donor to the π cloud of acetylene in phenylacetylene.

Chapter 4: Borazine-acetylene and comparison with benzene-acetylene

The interaction of borazine with acetylene has been studied in this chapter, using both matrix isolation IR and *ab initio* calculations. This system was compared with the well studied benzene-acetylene system^{7,10}. It was found that the structure where the N-H group of borazine interacted with one of the carbon atoms of acetylene was the global minimum. This structure was referred to as the bent NH \cdots C structure. The BSSE corrected interaction energy of this complex was found to be 2.03 kcal/mol at the MP2/aug-cc-pVDZ level of theory. This complex was identified in our matrix isolation experiments through the perturbations in the N-H stretching modes of borazine and C-H stretching mode of acetylene. In addition to this complex, we were also able to observe, through shifts in the C-H stretching modes of acetylene, the bent CH \cdots N complex where the C-H of acetylene served as the proton donor to the N atom of borazine. This system was compared with the acetylene-benzene system where the C-H of acetylene was found to be the proton donor to the π cloud in benzene, thus indicating that the borazine interactions were markedly different from those of benzene.

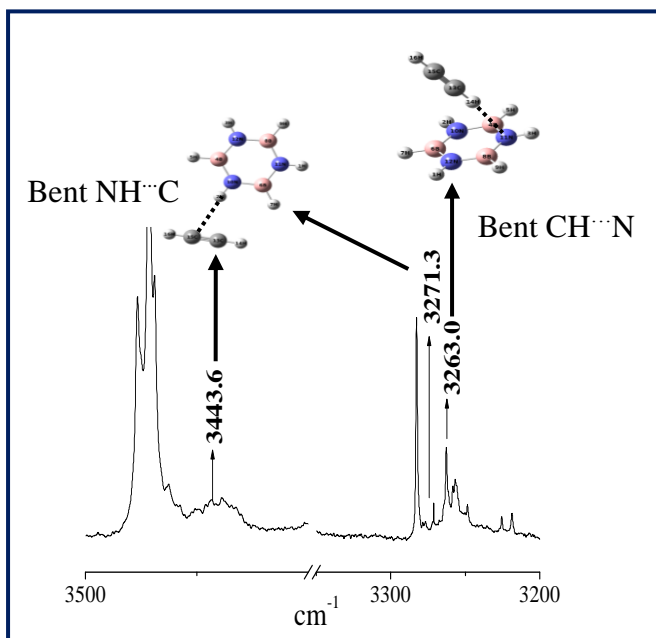


Fig.2. Experimentally observed structures: Bent $\text{NH}\cdots\text{C}$ and Bent $\text{CH}\cdots\text{N}$ for the borazine-acetylene complex, in the N-H stretching region of borazine ($3500\text{-}3400\text{ cm}^{-1}$) and the C-H stretching region of acetylene ($3300\text{-}3200\text{ cm}^{-1}$).

Chapter 5: Borazine dimer

The homodimers of borazine were studied using matrix isolation IR spectroscopy and *ab initio* calculations. The aligned stacked structure and the parallel displaced structure were found to be the global minima at the MP2/aug-cc-pVDZ level of theory. These structures were however not seen in our matrix isolation experiments because of insignificant shifts in the vibrational wavenumbers of the borazine monomer. We observed a T_N isomer in the matrix, where the N-H of one borazine interacted with the N atom of another borazine. Interestingly, we also located both experimentally and computationally, a dihydrogen bonded complex, in which the hydrogen attached to the nitrogen of borazine (of an N-H group) interacted with the hydrogen attached to the boron atom (of a B-H group) of another borazine. This is probably the first experimental observation of such a bond in a system other than that involving a metal hydride. In this structure, *two* dihydrogen bonds were in operation, probably cooperatively, which therefore placed it in terms of stability, behind the classical hydrogen bonded T_N dimer, by just about 0.5 kcal/mol. The borazine dimer was, thus, found to be a different and richer landscape than the benzene dimer system, already studied in literature.

Chapter 6: Borazine-benzene and borazine-phenylacetylene complexes

The hydrogen bonded complexes of borazine-benzene and borazine-phenylacetylene were explored in this chapter. It was found that in both the systems, the experimentally observed structure was the one where the N-H group of borazine interacted with the carbon atom of benzene and the acetylenic carbon in phenylacetylene. In case of the borazine-benzene system, we were also able to observe the T-NH complex in the matrix, which corresponded to the interaction between N-H group of borazine and the π cloud in benzene. The BSSE corrected interaction energy for the NH \cdots C complex and the T-NH complex were found to be almost same at the MP2/aug-cc-pVDZ level of theory, thus making them isoenergetic.

Chapter 7: Conclusions

This chapter discusses the significant conclusions drawn from the study of the various multifunctional π systems described in this thesis and gives an insight into the nature of weak hydrogen bonding interactions operating in such systems. The molecules chosen for the study have a potential to serve both as proton donors and acceptors. While the CH \cdots π interactions are explored in detail using the phenylacetylene-acetylene system, the borazine systems throw light on the interactions of an N-H system with π systems, such as acetylene, benzene and phenylacetylene. The study of borazine was also undertaken to compare it with its organic analogue, benzene. In the phenylacetylene-acetylene system, the acetylene was found to be the proton donor to the π cloud of acetylene in phenylacetylene. In the borazine-acetylene system, it was found that the N-H of borazine was found to be the proton donor to one of the carbon atoms in acetylene. This work was compared with the well studied benzene-acetylene system already studied in literature, where the C-H of acetylene was found to be the proton donor to the π cloud in benzene. In our work on the borazine dimer, a dihydrogen bonded complex was found, both experimentally and computationally and was one of the rare examples of a dihydrogen bonded 1:1 complex, not involving a metal hydride. In case of the borazine-benzene and borazine-phenylacetylene systems, complex where the N-H of borazine interacted with one of the carbon atoms of benzene and acetylene in phenylacetylene respectively, was observed in our experiments. Thus, it was concluded in this thesis that the borazine systems presented a different and richer landscape than the benzene systems studied in literature.

REFERENCES

- (1) Kim, K.S.; Tarakeshwar, P; Lee, J.Y. *Chem. Rev.* **2000**, *100*, 4145-4186.
- (2) Nishio, M; Hirota, M; Umezawa, Y. The CH/ π Interaction, Evidence, Nature and Consequences. Wiley–VCH, New York. **1998**, *6*, 178-181.
- (3) Nishio, M. CH/ π hydrogen bonds in crystals. *Cryst. Eng. Commun.* **2004**, *6*, 130-158.
- (4) Matsuura, H; Yoshida, H; Hieda, M; Yamanaka, S; Harada, T; Shin-ya, K; Ohno, K. Experimental Evidence for Intramolecular Blue-Shifting CH \cdots O Hydrogen Bonding by Matrix Isolation Infrared Spectroscopy. *J. Am. Chem. Soc.* **2003**, *125*, 13910-13911.
- (5) Umezawa, Y.; Tsuboyama, S.; Honda, K.; Uzawa, J.; Nishio, M. CH/ π Interaction in the Crystal Structure of Organic Compounds: A database study. *Bull. Chem. Soc. Jpn.* **1998**, *71*, 1207-1213.
- (6) Sankaran, K.; Viswanathan, K. S.; Kulkarni, A. D.; Gadre, S. R. H \cdots π complexes of Acetylene-Ethylene: A Matrix Isolation and Computational Study. *J. Phys. Chem. A.* **2002**, *106*, 1504-1510.
- (7) Sundararajan, K.; Viswanathan, K. S.; Kulkarni, A. D.; Gadre, S. R. H- π Complexes of Acetylene–Benzene: A Matrix-Isolation and Computational Study. *J. Mol. Struct.* **2002**, *613*, 209-222.
- (8) Sundararajan, K.; Sankaran, K; Viswanathan, K.S. A Matrix Isolation and *ab initio* study of the Hydrogen Bonded Complexes of Acetylene with Pyridine. *J. Mol. Struct.* **2005**, *733*, 187-192.
- (9) Engdahl, A.; Nelander, B. A matrix isolation study of the benzene-water interaction. *J. Phys. Chem.* **1985**, *89*, 2860-2864.
- (10) Majumder, M., Mishra, B.K.; Sathyamurthy, N. CH \cdots π and $\pi\cdots\pi$ interactions in benzene-acetylene clusters. *Chem. Phys. Lett.* **2013**, *557*, 59-65.

CHAPTER 1: INTRODUCTION

The importance of studying hydrogen-bonding interactions, both experimental and theoretical, stems from the fact that these are responsible for a large number of important chemical and biological processes.¹⁻⁶ The classical definition of a hydrogen bond is a bond where the hydrogen is attached to an electronegative atom, such as oxygen or nitrogen and forms a bond with another electronegative atom. While this definition of the hydrogen bond was first proposed by Latimer and Rodebush⁷ in 1920, a number of examples of the hydrogen bond observed in recent times have warranted a redefinition of this bond. One of the first examples which did not conform to the above definition was recognized when June Sutor proposed that the hydrogen attached to carbon could be involved in a hydrogen bond. While her proposal was initially met with stiff opposition, it later came to be recognized as a very important class of a hydrogen bond. Later, electron donors other than electronegative atoms, such as π systems, were shown to be good proton acceptors in a hydrogen bond. Clearly, the definition of Latimer and Rodebush had to be revisited. The definition of hydrogen bond had to be constantly modified and in the year 2011, IUPAC formed a committee which came up with the following definition for the hydrogen bond:

*“The hydrogen bond is an attractive interaction between a hydrogen atom from a molecule or a molecular fragment X–H in which X is more electronegative than H, and an atom or a group of atoms in the same or a different molecule, in which there is evidence of bond formation.”*⁸

The IUPAC recommendation also points out that directionality is a defining characteristic of a hydrogen bond and that *evidence* of bond formation was a requirement in classifying the hydrogen bond.

Hydrogen bonding is an important component of the three major macromolecules in biochemistry; proteins, nucleic acids, and carbohydrates. Hydrogen bonds provide most of the directional interactions that underpin protein folding, protein structure and molecular recognition.⁹ It is also responsible for holding the complementary strands of DNA together. Nucleotides pair precisely based on the position of possible hydrogen bond donors and acceptors.

The three-dimensional shape of antibodies is also aided by hydrogen bonding, due to which it is able to shape itself like a key in a lock, to bind to its specific antigen.¹⁰

Hydrogen bonds involving π systems as proton acceptors have also been reported, such as the O-H $\cdots\pi$, N-H $\cdots\pi$, and C-H $\cdots\pi$ systems. All these interactions manifest interaction energies ranging from a few kJ/mol to many tens of kJ/mol. Electronic structure calculations have been extensively used to study these interactions, and advances in computational methodologies have led to increasing use of methods, to accurately describe these weak interactions. Computations together with experiments, has remarkably improved our understanding of these weak but important interactions.

Nishio and Hirota¹¹ classified the hydrogen bonding interactions into four categories, based on the HSAB (Hard and Soft Acids and Bases) principle. They are; (1) conventional hydrogen bond, (2) XH/ π hydrogen bonds, where X is an electronegative atom, such as O, N or S (3) CH/ n hydrogen bonds, where 'n' is an electron lone pair and (4) CH/ π hydrogen bonds, where the carbon is usually in an 'sp' or 'sp²' hybridization. Contribution from the electrostatic forces was found to be dominant in the first three interactions, while dispersion was considered to be significant in the CH/ π contact.

C-H $\cdots\pi$ interactions constitute one of the important factors in controlling the crystal packing of molecules. In recent years, the study of hydrogen bonds involving C-H $\cdots\pi$ interactions has generated enormous interest, as these interactions appear to be the driving force in the packing of a number of organic crystals and proteins.¹²⁻¹³ From a study of crystal structure databases, Umezawa *et al.* observed that C-H $\cdots\pi$ interactions are present in more than 35% of the organic crystals.¹⁴ It has been suggested that the C-H $\cdots\pi$ interaction plays important roles in determining the conformation¹⁵⁻¹⁶ and chiroptical property¹⁷ of organic compounds, in stereoselective reactions¹⁸ and chiral recognitions.¹⁹ This type of interaction also plays a role in the solid structure of supramolecules such as clathrates (lattice-inclusion²⁰ or cavity-inclusion type²¹) and mesogenic compounds.²² The hybridization of the carbon atom to which the hydrogen is attached, plays a critical role in these interactions, as it determines the acidity of the hydrogens attached to it and therefore its ability to form hydrogen bonds. The interaction energy of complexes having π - π and C-H $\cdots\pi$ contacts can vary over the range of 1-5 kcal/mol depending

on the nature of the aromatic ring/substituent(s) and the acidity of the C-H bond.²³⁻²⁵ Hirota determined the energy of C-H $\cdots\pi$ hydrogen bond involving CHCl₃ and aromatic hydrocarbons to be 1.5-3 kcal mol⁻¹ depending on the interaction system.²⁶ The C-H $\cdots\pi$ hydrogen bond plays its role in polar protic media such as water, and therefore in the physiological environment. This is because the energy of this bond comes mostly from the dispersion force. This is of supreme importance when considering the effect of non polar or weak hydrogen bonds in the biochemical process. The Coulomb force and the ordinary hydrogen bond, on the contrary, are not very effective in polar solvents. Steiner and Koellner²⁷ described hydrogen bonded proteins involving aromatic acceptors, and Brandl *et al.*²⁸ exhaustively surveyed the occurrence of interactions involving all possible C-H groups (C_{aliphatic}-H and C_{aromatic}-H) as donors and all possible side chain π systems as acceptors. The cases in which C-H $\cdots\pi$ interactions have been described in proteins include the formation of complexes of proteins with ligands or cofactors such as the heme group (Nishio *et al.*) and design of serine proteases inhibitors (Shimohigashi *et al.*)²⁹ Previous studies by Brandl *et al* have also revealed that C-H $\cdots\pi$ interactions are responsible for the stabilization of structural elements such as alpha helices or non-proline cis peptide bonds.²⁸ C-H $\cdots\pi$ interactions involving aromatic groups either as donor or as acceptor are found mostly in the interior of the protein. The more hydrophilic the participating groups are, the closer to the surface are the interactions located. An excellent article on the C-H $\cdots\pi$ interaction by Nishio has discussed the unique features of this interaction in the context of molecular conformations and supramolecular assemblies.^{2,30} These interactions were shown to have contributions from both electrostatic and dispersion interactions, as opposed to hydrogen bonded interactions involving hard acid-hard base, hard acid-soft base or soft acid-hard base precursors, which were essentially dominated by electrostatic interactions.

Investigation of such weak interactions is challenging both experimentally and theoretically.³¹ Many experimental techniques, such as X-ray, NMR, calorimetry and optical spectroscopy have been employed for studies on hydrogen bonding interactions. Of the optical spectroscopic techniques, infrared spectroscopy has been a popular method, employed for the study of such weak hydrogen bonds. Shifts in the vibrational frequencies of donor and acceptor groups in hydrogen bonded complexes, indicate the presence, nature and strength of hydrogen

bonds. Study of weak interactions by matrix isolation infrared spectroscopy has been a subject of interest for many years. In particular, matrix isolation and supersonic jet expansion³²⁻³³ methods have become the techniques of choice, because of the highly resolved spectra that they offer, which consequently makes it possible to make unambiguous assignments of hydrogen bonded structures.³⁴⁻³⁵ In addition, the two techniques very often prove to be complementary; while the supersonic jet technique traps species in their lowest energy structure, the global minimum, matrix isolation spectroscopy can often trap both global and local minima.³⁶ The two studies therefore allow for a better understanding of the potential energy surface of the weak complexes.

Where the interactions are weak, the perturbations are small, but the small linewidths in matrix isolation spectroscopy allows for the identifications of small perturbations in infrared features. One of the earliest matrix isolation studies was done in 1950 where the hydrogen bonding of water was studied by Pimentel *et al.*³⁷ The H₂O dimers were reported by Ayers and Pullin³⁸, followed by the work of Bentwood *et al.*³⁹, who through a careful study of the concentration dependence identified the dimer and higher oligomers of water. They also reported that the dimer and trimer of water exhibit an open chain structure, whereas the tetramer and higher polymers display a cyclic structure. Over the years, work on weak hydrogen bonded interaction using matrix isolation spectroscopy has been a popular area of research.

While molecules containing π systems present the possibility of acting as proton acceptors to form H $\cdots\pi$ contacts, it is possible that the same molecule may also have a potential proton donor site. Molecules with such multifunctional sites provide an interesting scenario, as to whether it would serve as a proton donor or a proton acceptor. An example of such a molecule is acetylene, C₂H₂. It can act as a proton donor, using the hydrogen attached to the sp carbon. Alternatively, C₂H₂ can also play the role of a proton acceptor, through its π -cloud. Studies on the hydrogen bonded complexes of C₂H₂-MeOH, C₂H₂-CHCl₃, C₂H₂-C₂H₄ and C₂H₂-C₆H₆ have been reported, where the dual behavior of C₂H₂ has been documented.^{23,24,40,41} While in the C₂H₂-CHCl₃ complexes, C₂H₂ played the role of a proton acceptor,⁴¹ in the complexes of C₂H₂-C₂H₄, both types of complexes were found experimentally and computationally; one where C₂H₂ was the proton donor and another where it served as a proton acceptor, with C₂H₄ serving as the proton donor.²³ In the C₂H₂-C₆H₆ complex, only the complex where C₂H₂ was the proton donor was found experimentally.²⁴

Another molecule that has the potential to show such dual behavior is phenylacetylene (PhAc), an alkyne hydrocarbon. It has four hydrogen bonding sites; benzene ring and the acetylenic triple bond, both of which can act as proton acceptor sites and an acetylenic C-H or the phenyl C-H group, which can act as proton donors. In this study, we addressed the question as to what the nature of interaction would be, if two π systems, both capable of dual behavior, were allowed to interact with each other, such as PhAc and C_2H_2 . It was interesting to see which of the two molecules would serve as the proton acceptor/donor and what the nature of the interactions would be. We therefore studied the PhAc- C_2H_2 system both experimentally, using matrix isolation infrared spectroscopy and computationally, using *ab initio* quantum chemical studies.

We followed it up with our work on the complexes of borazine ($B_3N_3H_6$) with π systems, such as C_2H_2 , C_6H_6 and PhAc. $B_3N_3H_6$, popularly known as inorganic benzene, is the isoelectronic analog of C_6H_6 and has many similar physical and chemical properties to C_6H_6 . It has many industrial applications in ceramics industries and is also used as a precursor to boron nitride. $B_3N_3H_6$ precursors for Si-B-C-N ceramics have been used several times. Silylsubstituted vinylborazines⁴²⁻⁴³, silylmethylborazines⁴⁴ and other derivatives⁴⁵ have been used as molecular precursors. $B_3N_3H_6$ materials have also been demonstrated to be a new class of multifunctional and thermally stable materials with high electron and moderate hole mobilities for many applications in electroluminescent devices.⁴⁶

$B_3N_3H_6$ is an inorganic compound which has three alternate N-H and B-H units. In $B_3N_3H_6$, the difference in electronegativities of boron (2.0) and nitrogen (3.0) leads to a charge distribution which makes it susceptible to both nucleophilic and electrophilic attack, respectively. Due to this difference in electronegativity between the N and B atoms, the B-N bond is polar which makes $B_3N_3H_6$ more reactive towards polar reagents, as compared with C_6H_6 . Fornarini *et al* conducted some *ab initio* calculations and revealed that the most basic sites in $B_3N_3H_6$ are the nitrogen atoms and its conjugate acid, $H_3B_3N_3H_4^+$, is similar in structure to the benzenium ion.⁴⁷ Kiran *et al.* computed the protonation and methylation energies of benzene, cyclobutadiene, and borazine.⁴⁸ Since C_6H_6 shows an ability to undergo substitution reactions readily than addition, the energetics of these reactions could be an indicator of aromaticity. On this basis they concluded that $B_3N_3H_6$ should be considered as an aromatic

molecule, though its aromaticity is about half of that in C_6H_6 . Understandably, the chemistry of $B_3N_3H_6$ is dominated by addition reactions. However, recent experiments of Chiavarino *et al.* demonstrate that $B_3N_3H_6$ undergoes electrophilic aromatic substitution in the gas phase much like its organic counterpart.⁴⁷ Kartha *et al* studied the infrared spectra of $B_3N_3H_6$ and its isotopic species.⁴⁹ Niedenzu *et al* reported an extensive gas phase infrared and liquid Raman spectroscopic studies of various isotopically labelled forms of $B_3N_3H_6$.⁵⁰ They confirmed the findings of Kartha *et al* and assigned all the active fundamentals. Perhaps the first matrix isolation study on $B_3N_3H_6$ was done by Kaldor and Porter when they recorded the infrared spectra of $B_3N_3H_6$ in an Ar matrix.⁵¹ The $B_3N_3H_6$ dimer has been studied by Kawahara *et al.* who showed, using the second order Møller–Plesset perturbation theory (MP2) and 6-311G(d,p) basis set, that the gauche parallel sandwich structure with the boron atoms of one $B_3N_3H_6$ stacking on top of the nitrogen atoms of the other $B_3N_3H_6$ to be the most stable geometry.⁵² Unlike the C_6H_6 dimer, for which both the parallel displaced and T-shaped dimers are nearly isoenergetic, the T-shaped $B_3N_3H_6$ dimer was found to be less stable by 0.4 kcal/mol than the gauche structure, at the MP2/aug(d)-6-311G* level of theory. In all the geometries considered, the contribution from electrostatic interaction was found to be very small.⁵² Bettinger *et al* studied the $B_3N_3H_6$ homodimers and the $B_3N_3H_6$ - C_6H_6 heterodimers at the coupled cluster singles, doubles and perturbative triples [CCSD(T)] level of theory and described how the intermolecular interactions get modified when a C-C bond gets replaced by a B-N bond.⁵³ In the case of the $B_3N_3H_6$ - C_6H_6 heterodimers, the authors reported the T shaped geometry (T-NH-1) in which the N-H of the $B_3N_3H_6$ molecule served as the proton donor to the π cloud of C_6H_6 through $NH\cdots\pi$ interaction as the lowest energy minimum among the geometries they considered.

While numerous theoretical studies are present in the literature on $B_3N_3H_6$, very few experimental reports can be found. $B_3N_3H_6$ is highly moisture sensitive and decomposes rapidly in the presence of water. It has a very high vapor pressure at room temperature which thus makes it a challenge to experimentally study this system. We have in this work, performed a number of experimental studies on the $B_3N_3H_6$ complexes. The main purpose of carrying out this work was to compare the hydrogen bonding interactions in the much studied C_6H_6 systems with the $B_3N_3H_6$ systems.

The first experimental study on $B_3N_3H_6$ carried out by our group was on the $B_3N_3H_6-H_2O$ system. The motivation was to compare it with the well studied $C_6H_6-H_2O$ system. Theoretical studies on the $C_6H_6-H_2O$ system have already been carried out by many groups and it was shown to have an H- π interaction.⁵⁴⁻⁶³ It has been reported that this complex is extremely floppy, where the H_2O can freely rotate across the C_6H_6 ring. This process has been described by Zwier *et al* as “hydrogen bond swapping”.⁵⁸ This internal rotation of H_2O has also been described in the matrix isolation studies done on the $C_6H_6-H_2O$ system by Engdahl and Nelander.⁵⁹ The global minimum in case of $C_6H_6-H_2O$ was found to be the complex where the H atom of water interacted with the π electron cloud of the C_6H_6 ring. Our studies on $B_3N_3H_6-H_2O$ confirmed the presence of an $NH\cdots O$ interaction as the global minimum, thus making it clearly different from the $C_6H_6-H_2O$ system. Thus, the N-H of $B_3N_3H_6$ was found to be the proton donor to the O atom of H_2O , a result very different from that observed for the $C_6H_6-H_2O$ complex.⁶⁴

Matrix isolation infrared and *ab initio* studies on the complexes of $B_3N_3H_6$ with π systems such as C_2H_2 , C_6H_6 and PhAc have been carried out in this work. Such studies on the $C_6H_6-C_2H_2$ system, done by Sundararajan *et al*, showed the presence of a structure where the C-H of acetylene served as the proton donor to the π cloud of C_6H_6 as the global minimum.²⁴ This study motivated us to further explore the interaction of $B_3N_3H_6$ with multifunctional π systems such as C_2H_2 , C_6H_6 and PhAc in the matrix. We also investigated the $B_3N_3H_6$ dimer complexes and compared it with the C_6H_6 dimer complexes. *Ab initio* computations were used to corroborate our experimental results. AIM and NBO analysis helped us to predict the nature of interactions in the various complexes. LMO-EDA analysis was employed to partition the total energy of the complexes into various fractions such as electrostatic, dispersion, repulsion and polarization. Details of the computations and experimental procedure adopted are presented in chapter 2.

Chapter 3 describes the complexes of PhAc and C_2H_2 . This work helped us to understand the role of proton donor/acceptor in multifunctional molecules. This study also aids in explaining the role of competitive complexation in the matrix for molecules having both proton acceptor and donor sites.

Chapter 4 describes the $B_3N_3H_6-C_2H_2$ system and a comparison of this work has been done with the $C_6H_6-C_2H_2$ system studied in the literature. In the experiments on the $C_6H_6-C_2H_2$ system, a T-shaped $H\cdots\pi$ complex was observed in the matrix.²⁴ In the $B_3N_3H_6-C_2H_2$ system too, a similar complex was located as one of the local minima in the computations. The nature of the interaction has been studied in detail.

The $B_3N_3H_6$ dimer system has been discussed in Chapter 5. This work highlights the comparison of the $B_3N_3H_6$ dimer with the C_6H_6 dimer. The C_6H_6 homodimer also was shown computationally and experimentally to have a T-shaped geometry, with one C_6H_6 serving as a proton donor to the π -system of the second C_6H_6 unit.⁶⁵⁻⁶⁷ A parallel displaced π -stacked structure was also indicated by computations, though it has never been observed in any experiment.⁶⁷ While the *ab initio* studies on the $B_3N_3H_6$ dimer by Bettinger *et al*⁵³ confirmed the presence of a sandwich structure and the T_N structure, in our computations at the M06-2X and MP2 level of theory in conjunction with 6-311++G(d,p) and aug-cc-pVDZ basis sets and in the matrix isolation experiments, a third structure, which was the dihydrogen bonded structure was also observed. In this structure, both the N-H and B-H groups were involved in proton donation. This is the first experimental observation of a dihydrogen bond in a system other than in a metal hydride.

Chapter 6 describes the hydrogen bonded complexes of $B_3N_3H_6$ with C_6H_6 . Our computations and experiments reveal the $NH\cdots C$ complex, where the N-H of $B_3N_3H_6$ interacting with one of the carbon atoms in C_6H_6 as the global minimum structure. Bettinger *et al* failed to locate this structure in their work on the $B_3N_3H_6-C_6H_6$ system at the MP2/aug-cc-pVQZ level of theory. We also observed the T-NH structure, where the N-H of $B_3N_3H_6$ interacted with the π cloud in C_6H_6 . The heterodimer studied in this work seemed to be similar to the C_6H_6 homodimer. In both cases, it was the local minimum, a T-shaped dimer, that has been experimentally observed. The nature of interactions were further studied using AIM, NBO and LMO-EDA analysis.

This chapter also describes the study of hydrogen bonded complexes of $B_3N_3H_6$ with PhAc. $B_3N_3H_6$ and PhAc both being multifunctional molecules, it was again interesting to study the hydrogen bonded landscape in these systems.

Summary and conclusions derived from these studies are discussed in Chapter 7.

1.1 Scope of Present Work

The aim of this thesis is to explore the hydrogen bonding interactions in multifunctional π systems both experimentally, using matrix isolation infrared spectroscopy and computationally, using *ab initio* quantum chemical studies. The computational studies were employed to corroborate the experimental results. Various π systems such as PhAc, C₂H₂, C₆H₆ and B₃N₃H₆ were used for this study. AIM, NBO and LMO-EDA analysis were carried out in order to explore the nature of interactions involved. This work also demonstrates an interplay between the C-H $\cdots\pi$ systems and the N-H $\cdots\pi$ systems. While the PhAc-C₂H₂ system gave us an insight into the C-H $\cdots\pi$ interactions, the B₃N₃H₆ systems described the significance of studying the N-H systems in the matrix and a comparison of hydrogen bonding in these systems with the well studied C₆H₆ systems has been discussed. These studies also provided an insight into competitive binding sites operative in multifunctional molecules. As a result of these studies, we were also able to identify the dihydrogen bonding interactions not reported earlier, except in systems involving the metal hydrides.

REFERENCES

- (1) Kim, K.S.; Tarakeshwar, P; Lee, J.Y. Molecular Clusters of π systems: Theoretical studies of structures, spectra and origin of interaction energies. *Chem. Rev.* **2000**, *100*, 4145-4186.
- (2) Nishio, M; Hirota, M; Umezawa, Y. The CH/ π Interaction, Evidence, Nature and Consequences. Wiley-VCH, New York. **1998**, *6*, 178-181.
- (3) Nishio, M. CH/ π Hydrogen Bonds in Crystals. *Cryst. Eng. Commun.* **2004**, *6*, 130-158.
- (4) Matsuura, H; Yoshida, H; Hieda, M; Yamanaka, S; Harada, T; Shin-ya, K; Ohno, K. Experimental evidence for Intramolecular Blue Shifting C-H--O Hydrogen Bonding by Matrix Isolation Infrared Spectroscopy. *J. Am. Chem. Soc.* **2003**, *125*, 13910-13911.
- (5) Steiner, T. The Hydrogen Bond in the Solid State. *Angew. Chem. Int. Ed.* **2002**, *41*, 48-76.
- (6) Espinoza, C.; Szczepanski, J.; Vala, M.; Polfer, C. N. Glycine and its Hydrated Complexes: A matrix isolation infrared study. *J. Phys. Chem. A.* **2010**, *114*, 5919-5927.
- (7) Latimer, W.M.; Rodebush, W. H. Polarity and ionization from the standpoint of the Lewis theory of valence. *J. Am. Chem. Soc.* **1920**, *42*, 1419-1433.
- (8) Arunan, E.; Desiraju, G.R.; Klein, R.A.; Sadlej, J.; Scheiner, S.; Alkorta, I.; Clary, D. C.; Crabtree, R.H.; Dannenberg, J.J.; Hobza, P.; Kjaergaard, H.G.; Legon, A.C.; Mennucci, B.; Nesbitt, D.J. Definition of the Hydrogen Bond. *Pure Appl. Chem.*, **2011**, *83*, 1637-1641.
- (9) Hubbard, E.R; Kamran, M. John Wiley & Sons, 2010.
- (10) Sherriff, S.; Silverton, E.W.; Padlan, E.A.; Cohen, G.H.; Smith-Gill, S.J.; Finzel, B.C.; Davies, D.R. Three-dimensional structure of an antibody-antigen complex. *Proc. Nat. Acad. Sci.* **1987**, *84*, 8075-8079.
- (11) Nishio, M. and Hirota, M. CH/ π interaction: implications in organic chemistry. *Tetrahedron* **1989**, *45*, 7201-7245.
- (12) Tsuzuki, S.; Honda, K.; Uchimara, T.; Mikami, M; Tanabe, K. The Magnitude of CH/ π Interactions between Benzene and some Model Hydrocarbons. *J. Am. Chem. Soc.* **2000**, *122*, 3746-3753.
- (13) Samanta, U.; Chakrabarti, P.; Chandrashekhar, J. Ab Initio Study of Energetics of X-H \cdots π Interactions involving a Heteroaromatic Ring. *J. Phys. Chem.* **1998**, *102*, 8964-8969.
- (14) Umezawa, Y.; Tsuboyama, S.; Honda, K.; Uzawa, J.; Nishio, M. The Importance of π

Interactions in Crystal Engineering. *Bull. Chem. Soc. Jpn.* **1998**, *71*, 1207-1213.

(15)Umezawa, Y.; Tsuboyama, S.; Takahashi, H.; Uzawa, J.; Nishio, M. CH/ π interaction in the conformation of organic compounds. A database study. *Tetrahedron* **1999**, *55*, 10047–10056.

(16)Umezawa, Y.; Tsuboyama, S.; Takahashi, H.; Uzawa, J.; Nishio, M. CH/ π interaction in the conformation of peptides. A database study. *Bioorg. Med. Chem.* **1999**, *7*, 2021-2026.

(17)Araki, S.; Sakakibara, K.; Hirota, M.; Nishio, M. Tsuzuki, S.; Tanabe, K. Theoretical study of CH- π interaction. Significant enhancement of CD spectra due to the participation of CH- π interaction. *Tetrahedron Lett.* **1991**, *32*, 6587-6590.

(18)Yoshimura, T.; Tsukurimichi, E.; Iizuka, Y.; Mizuno, H.; Isaji, H. Shimasaki, C. The Ei reaction of substituted threo- and erythro-1-Phenylethyl Phenyl Sulfoxides. *Bull. Chem. Soc. Jpn* **1989**, *62*, 1891–1899.

(19)Tomori, H.; Yoshihara, H.; Ogura, K. Facile Optical Resolution of a Dibenzopyrazinoazepine Derivative and the Nature of Molecular Recognition of Amines by Chiral 2,3-Di-O-(arylcabonyl) tartaric acids. *Bull. Chem. Soc. Jpn* **1996**, *69*, 3581–3590.

(20)Moody, G. J.; Owusu, R. K.; Slawin, A. M. Z.; Spencer, N.; Stoddart, J. F.; Thomas, J. D. R.; Williams, D.J. Noncovalent Bonding Interactions between Tetraphenylborate Anions and Paraquat and Diquat Dications. *Angew. Chem., Int. Ed. Engl.* **1987**, *26*, 890–892.

(21)Ashton, P. R.; Philp, D.; Spencer, N.; Stoddart, J. F.; Williams, D. J. *J. Chem. Soc., Chem. Commun.* **1994**, 181–184.

(22)Miyamura, K.; Mihara, A.; Fujii, T.; Gohshi, Y.; Ishii, Y. Unusually strong interactions mediated by both π - π stacking and CH \cdots π interactions present in the dimer of nickel (II) complex coordinated with n-butyl substituted Salen. *J. Am. Chem. Soc.* **1995**, *117*, 2377-2378.

(23)Sankaran, K.; Viswanathan, K. S.; Kulkarni, A. D.; Gadre, S. R. H- π Complexes of Acetylene-Ethylene: A Matrix Isolation and Computational Study. *J. Phys. Chem. A.* **2002**, *106*, 1504-1510.

(24)Sundararajan, K.; Viswanathan, K. S.; Kulkarni, A. D.; Gadre, S. R. H- π Complexes of Acetylene–Benzene: A Matrix-Isolation and Computational Study. *J. Mol. Struct.* **2002**, *613*, 209-222.

-
- (25) Sundararajan, K.; Sankaran, K.; Viswanathan, K.S. A Matrix Isolation and *ab initio* study of the Hydrogen Bonded Complexes of Acetylene with Pyridine. *J. Mol. Struct.* **2005**, *733*, 187-192.
- (26) Ehama, R.; Yokoo, A.; Tsushima, M.; Yuzuri, T.; Suezawa, H and Hirota, M. Substituent effect on the enthalpies of formation of CH- π complexes of aromatic π -bases. *Bull. Chem. Soc. Jpn.*, **1993**, *66*, 814-818.
- (27) Steiner, T.; Koellner, G. Hydrogen bonds with π -acceptors in proteins: frequencies and role in stabilizing local 3D structures. *J. Mol. Biol.* **2001**, *305*, 535-557.
- (28) Brandl, M., Weiss, M. S., Jabs, A., Sühnel, J. & Hilgenfeld, R. C-H $\cdots\pi$ interactions in proteins. *J. Mol. Biol.* **2001**, *307*, 357-377.
- (29) Shimohigashi, Y.; Maeda, I.; Nose, T.; Ikesue, K.; Sakamoto, H.; Ogawa, T.; Ide, Y.; Kawahara, M. Chymotrypsin inhibitory conformation induced by amino acid side-chain side-chain intramolecular CH/ π interaction. *J. Chem. Soc., Perkin Trans.* **1996**, *1*, 2479-2485.
- (30) Nishio, M. The CH/ π hydrogen bond in chemistry. Conformation, supramolecules, optical resolution and interactions involving carbohydrates. *Phys. Chem. Chem. Phys.* **2011**, *13*, 13873-13900.
- (31) Dethlefs, M.; Hobza, P. Non covalent interactions: A Challenge for experiment and theory. *Chem. Rev.* **2000**, *100*, 143-167.
- (32) Futami, Y.; Kudoh, S.; Ito, F.; Nakanaga, T.; Nakata, M Structures of methyl halide dimers in supersonic jets by matrix isolation infrared spectroscopy and quantum chemical, calculations. *J. Mol. Str.* **2004**, *690*, 9-16.
- (33) Ito, F.; Nakanaga, T.; Futami, Y.; Kudoh, S.; Takayanagi, M.; Nakata, M. Isomeric Structures of CH₃I dimers in a supersonic jet studied by matrix isolation infrared spectroscopy and ab initio calculation. *Chem. Phys. Lett.* **2001**, *343*, 185-191.
- (34) Viswanathan, K.S.; Sankaran, K. and Sundararajan, K. *Encyclopedia of Analytical Chemistry*, edited by J. B. Myers **2000**, Wiley, New York.
- (35) Whittle, E.; Dows, D.A.; Pimentel, G.C. Infrared and Raman Matrix Isolation Spectroscopy. *J. Chem. Phys.* **1954**, *22*, 1943-1944.

-
- (36) Verma, K.; Viswanathan, K.S.; Sathyamurthy, N.; Majumder, M. How different is the Borazine–Acetylene Dimer from the Benzene–Acetylene Dimer? A Matrix Isolation Infrared and *Ab Initio* Quantum Chemical Study *Mol. Phys.* **2017**, DOI: 10.1080/00268976.2017.1284357.
- (37) Thiel, M.V.; Becker, E.D.; Pimentel, G.C. Infrared studies of Hydrogen bonding of water by the Matrix Isolation Technique. *J. Chem. Phys.* **1957**, *27*, 486-490.
- (38) Ayers, G. P. and Pullin, A. D. E. IR Spectra of Matrix-Isolated Water Species. Assignment of Bands to (H₂O)₂, (D₂O)₂ and HDO Dimer Species in Argon Matrices. *Spectrochim. Acta* **1976**, *32*, 1629-1639.
- (39) Bentwood, R.M.; Barnes, A.J.; Thomas, W.J.O. Studies of intermolecular interactions by matrix isolation vibrational spectroscopy Self association of water. *J. Mol. Spectrosc.* **1980**, *84*, 391-404.
- (40) Jovan Jose, K.V.; Gadre, S.R.; Sundararajan, K. and Viswanathan, K.S. Effect of matrix on IR frequencies of acetylene and acetylene-methanol complex: Infrared matrix isolation and *ab initio* study. *J. Chem. Phys.* **2007**, *127*, 104501-104505.
- (41) Jemmis, E.D.; Giju, K.T.; Sundararajan, K.; Sankaran, K.; Vidya, V.; Viswanathan, K.S.; Leszczynski, J. An *ab initio* and matrix isolation study of the 1:1 C₂H₂-CHCl₃ adduct. *J. Mol. Str.* **1999**, *510*, 59-68.
- (42) Haberecht, J.; Krumeich, F.; Grutzmacher, H.; Nesper, R. High yield molecular borazine precursors for Si-B-N-C ceramics. *Chem. Mater.* **2004**, *16*, 418-423.
- (43) Krummland, A.; Nesper, R.; Grutzmacher, H. 2nd International Conference on Inorganic Materials, Santa Barbara, 2000.
- (44) Jaeschke, T.; Jansen, M. J. Synthesis, Crystal Structure and Spectroscopic Characterisation of the Borazine Derivatives [B{CH₂(SiCl₃)}NH]₃ and [B{CH₂(SiCl₂CH₃)}NH]₃ *Inorg. and Gen. Chem.* **2004**, *630*, 239-243.
- (45) Jaschke, B.; Klingebiel, U.; Riedel, R.; Doslik, N.; Gadow, R. Cyclosilazanes and borazines: polymer precursors to silicon- and boron-containing ceramics. *Appl. Organomet. Chem.* **2000**, *14*, 671-685.
- (46) Sham, I. H. T.; Kwok, C-C.; Che, C-M; Zhu, N. Borazine materials for organic optoelectronic applications. *Chem. Comm.* **2005**, 3547- 3549.

-
- (47) Chiavarino, B.; Crestoni, M. E.; Fornarini, S. Electrophilic substitution of gaseous borazine. *J. Am. Chem. Soc.* **1999**, *121*, 2619-2620.
- (48) Kiran, B.; Phukan, A.K.; Jemmis, E.D. Is borazine aromatic? Unusual parallel behavior between hydrocarbons and corresponding B-N analogues. *Inorg. Chem.* **2001**, *40*, 3615-3618.
- (49) Kartha, V.B.; Krishnamachari, S.L.N.G.; Subramaniam, C.R. The infrared spectra of borazine and its isotopic species. Assignment of the “a₂” fundamental modes. *J. Mol. Spec.* **1967**, *23*, 149-157.
- (50) Niedenzu, K.; Sawodny, W.; Watanabe, H.; Dawson, J.W.; Totani, T.; Weber, W. The vibrational spectrum of borazine. *Inorg. Chem.* **1967**, *6*, 1453-1461.
- (51) Kaldor, A.; Porter, R.F. Matrix Isolation study of borazine and boroxine. Vibrational Analysis. *Inorg. Chem.* **1971**, *10*, 775-785.
- (52) Kawahara, S.-I.; Tsuzuki, S.; Uchamaru, T. *Ab initio* calculation of interaction nature of borazine (B₃N₃H₆) dimer. *J. Chem. Phys.* **2003**, *119*, 10081-10087.
- (53) Bettinger, H.F.; Kar, T.; Sanchez-Garcia, E. Borazine and benzene homo- and heterodimers. *J. Phys. Chem. A.* **2009**, *113*, 3353-3359.
- (54) Suzuki, S.; Green, P.G.; Bumgarner, R.E.; Dasgupta, S.; Goddard, W.A.; Blake, G.A. Benzene forms hydrogen bonds with water. *Science* **1992**, *257*, 942-945.
- (55) Feller, D. Strength of the benzene-water hydrogen bond. *J. Phys. Chem. A.* **1999**, *103*, 7558-7561.
- (56) Li, S.; Cooper, V.R.; Thonhauser, T.; Puzder, A.; Langreth, D.C. A density functional theory study of the benzene-water complex. *J. Phys. Chem. A.* **2008**, *112*, 9031-9036.
- (57) Ma, J.; Alfe, D.; Michaelides, A.; Wang, E. The water-benzene interaction: Insight from electronic structure theories. *J. Chem. Phys.* **2009**, *130*, 154303-6.
- (58) Gotch, A.J.; Zwier, T.S. Multiphoton ionization studies of clusters of immiscible liquids. I. C₆H₆-(H₂O)_n, n=1,2. *J. Chem. Phys.* **1992**, *96*, 3388-3401.
- (59) Engdahl, A.; Nelander, B. A matrix isolation study of the benzene-water interaction. *J. Phys. Chem.* **1985**, *89*, 2860-2864.
- (60) Augspurger, J.D.; Dykstra, C.E.; Zwier, T.S. Hydrogen bonding swapping in the benzene-water complex: A Model Study of the Interaction Potential. *J. Phys. Chem.* **1992**, *96*, 7252-7257.

-
- (61) Cheng, B.M.; Grover, J.R.; Walters, E.A. Dissociation energy of the benzene-water van der Waals complex. *Chem. Phys. Lett.* **1995**, *232*, 364-369.
- (62) Alberti, M.; Lago, N.F.; Pirani, F. Benzene water interaction: From gaseous dimers to solvated aggregates. *Chem. Phys.* **2012**, *399*, 232-239.
- (63) Gutowsky, H.S.; Emilsson, T.; Arunan, E. Low J-Rotation Spectra, internal rotation, and structures of several benzene-water dimers. *J. Chem. Phys.* **1993**, *99*, 4883-4893.
- (64) Mishra, P.; Verma, K.; Bawari, D.; Viswanathan, K.S. Does borazine-water behave like benzene-water? A matrix isolation infrared and *ab initio* study. *J. Chem. Phys.* **2016**, *144*, 234307-16.
- (65) Arunan, E.; Gutowsky, H. The rotational spectrum, structure and dynamics of a benzene dimer. *J. Chem. Phys.* **1993**, *98*, 4294-4296.
- (66) Sinnokrot, M.O.; Valeev, E.F.; Sherrill, C.D. Estimates of the *ab initio* limit for π - π interactions : The benzene dimer. *J. Am. Chem. Soc.* **2002**, *124*, 10887-10893.
- (67) Hobza, P.; Selzle, H.L.; Schlag, E.W. Potential Energy Surface for the benzene dimer. Results of the *ab initio* CCSD(T) Calculations Show two nearly isoenergetic structures: T-shaped and Parallel displaced. *J. Phys. Chem* **1996**, *100*, 18790-18794.

CHAPTER 2: EXPERIMENTAL AND COMPUTATIONAL PROCEDURES

This section describes the experimental procedures employed in this work and the computational methods adopted to corroborate the experimental results.

2.1. Matrix Isolation Infrared Spectroscopy

Matrix isolation is a technique where the molecules under study are trapped in solid inert gas matrices at high dilution. In a typical matrix isolation experiment, the molecules of interest are mixed with a rare gas, such as Ar or N₂, at sample to matrix ratios of approximately 1:1000. This gas mixture is then effused through a nozzle and is allowed to deposit on a KBr substrate maintained at a low temperature of ~12 K. At the analyte/matrix ratios employed, there is a large probability that the analyte molecules are isolated in the inert gas matrices. The use of inert gas matrices for the study of reactive species was originally proposed independently by Porter and Pimentel¹ and the technique of matrix isolation itself was initially developed by Pimentel, in the mid 1950s, for the study of free radicals.²⁻⁶

Reactive species isolated in such inert gas matrices have long lifetimes for want of reaction partners and can be studied leisurely by spectroscopic techniques such as infrared, UV-visible, microwave, electron spin resonance etc. This technique also offers other advantages such as small line widths for the spectral features of the trapped species, which has been exploited in the study of weakly bound complexes, such as hydrogen bonded and van der Waals complexes.⁷⁻⁹

Of the various spectroscopic methods, infrared spectroscopy is the most commonly used technique for the study of matrix isolated species. In a matrix isolation experiment, as the molecules are immobilized in an inert matrix at extremely low temperatures, broadening due to collision and Doppler effects are absent. The low temperature in the matrix also ensures that only the lowest rovibrational and electronic levels are populated, resulting in a significant reduction of spectral congestion.

The choice of the matrix material is crucial in the success of any matrix isolation experiment. The matrix material should be chemically inert to avoid reactions or strong interactions with the analyte. In addition to chemical inertness, a good matrix material must also be free from impurity, rigid at low temperature and transparent in the spectral region of interest. Also, the substance should have enough vapor pressure at room temperature, to enable it to be

deposited onto the cold substrate. Inert gases and nitrogen meet the above criteria to be used as matrix gases. In many cases, gases like methane are also used for this purpose.¹⁰ Solid para hydrogen has also been used as a matrix. Many excellent studies on the use of para hydrogen as a matrix have been carried out by Anderson and co workers.¹¹⁻¹³ In one of their recent work, they have studied the matrix isolation spectroscopy and spin conversion of NH₃ and ND₃ using solid para-hydrogen as a matrix.¹¹ In our experiments, Ar and N₂ were used as matrix gases and these are also transparent in mid IR region. However, a number of effects that can cause the spectrum of matrix isolated species to be complicated, do operate and these are briefly discussed in the following section.

A proper interpretation of infrared spectra of matrix isolated species demands a better understanding of the various effects that the matrix can have on the vibrational features of the analyte. The most important among the matrix effects is the perturbation of the vibrational features of analyte. The guest molecules are subjected to analyte-matrix interactions, albeit weak due to the inertness of the matrix material. These weak interactions can result either in a shift in the frequency relative to isolated gas molecules, or splitting of the vibrational bands, due to the analyte molecules residing in sites of differing symmetry. The frequency shift, $\Delta\nu$, in a matrix with respect to the gas phase value arises from electrostatic ($\Delta\nu_{elec}$), inductive ($\Delta\nu_{ind}$), dispersive ($\Delta\nu_{dis}$) and repulsive interactions ($\Delta\nu_{rep}$) and is given by the expression,

$$\Delta\nu = (\nu_{matrix} - \nu_{gas}) = \Delta\nu_{elec} + \Delta\nu_{ind} + \Delta\nu_{dis} + \Delta\nu_{rep} \dots \dots \dots (2.1)$$

where, ν_{matrix} and ν_{gas} are the frequencies of the vibrational mode in the matrix and gas phase respectively.⁸ Thus, matrix shift provides information regarding the interaction between the analyte and the matrix. In inert gas matrices, the long-range London dispersion forces and short range repulsive forces are the two dominant interactions. A theoretical treatment of a matrix induced frequency shift was given by Pimentel and Charles.¹⁴

The Buckingham expression which calculates the frequency shift, $\Delta\nu$, in solutions arising from the perturbation due to solvent interactions is given by

$$\Delta\nu = (\nu_{solvent} - \nu_{gas}) = [B_e/hc\omega_e][U'' - (3aU'/\omega_e) \dots \dots \dots (2.2)$$

where $B_e = h/(8\pi^2\mu r_e^2)$, is the rotational constant,

a = Anharmonicity constant,

U = Energy due to solute-solvent interaction¹⁵,

ω_e = Harmonic oscillator frequency for the normal vibration.

This expression can be used to explain the frequency shift occurring in the matrix. Fig. 2.1 shows the interaction potential curves between the trapped molecule and matrix atoms when trapped in a matrix cage. When R_{CM} is greater than R_1 (Fig. 2.1), i.e. when one of the atoms, C, of the trapped molecule is more distant from the matrix atom, M than R_e , U' and U'' are negative and since 'a', the anharmonicity constant, is also negative, the term Δv is negative (Eq. 2.2). Here the molecule experiences a loose cage effect resulting in a red shift. When R_{CM} is less than R_e , U' and U'' are positive and hence Δv is positive, which is a blue shift. The molecule experiences, in this case, a tight cage effect. It was reported that when polyatomic molecules are trapped in matrices, the high frequency stretching vibrations display red shifts as in a loose cage and the low frequency stretching, bending or rocking vibrations, manifest blue shifts as in a tight cage.¹⁵

Since nitrogen and noble gases, which are the popularly used matrices, are not reactive, the shifts in the vibrational frequencies are usually small. In more reactive matrix materials, such as carbon monoxide, carbon dioxide, sulfur hexafluoride and hydrocarbons, the shifts will be larger.

In addition to the shift in the vibrational features discussed above, there are many other factors operating in the matrix, which can lead to multiple band structures for a vibrational feature in the matrix. These are:

- 1) Rotation or libration of the solute molecules in its trapping site
- 2) Multiple trapping site effects
- 3) Aggregation of the solute
- 4) Lifting of degeneracy of the vibrational levels
- 5) Inactive modes may also be rendered active due to interactions with the matrix.¹⁶⁻¹⁷

Rotation of analyte in matrix cage

Analyte species trapped in inert matrix cages at low temperatures are generally rotationally cold. Furthermore, the matrix cage also prevents rotational motion, particularly for large molecules. However, a number of small molecules, such as HX (X=F, Cl), H₂O, NH₃ and OH have been shown to rotate in noble gas matrices. In general, rotation seems not to occur in matrices with unsymmetrical matrix sites, although there are exceptions (e.g. H₂ in N₂ matrix).

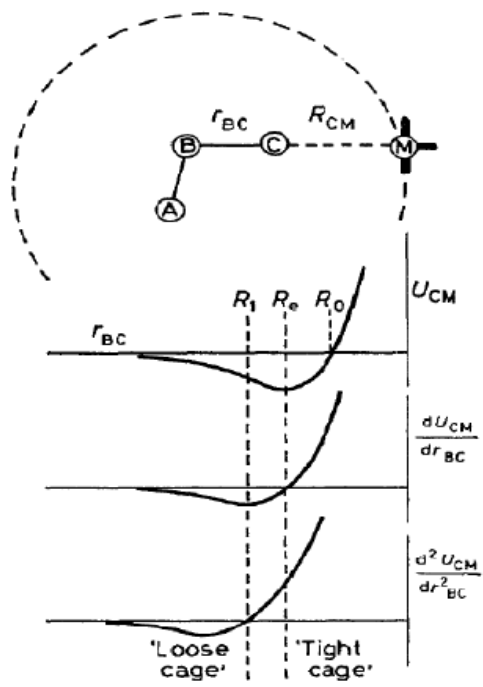


Fig. 2.1 Cage effects and frequency shifts for the sample molecule
(Reference 14)

Confirmation that these small molecules rotate in noble gas matrices has been provided by observation of the pure rotational transitions in the far infrared or Raman spectrum.¹⁸⁻²¹ The features due to rotations also show a temperature cycling effect, i.e. these bands can increase or decrease in intensity with changes in temperature, which is also used to confirm that these features are due to rotations.

Multiple trapping site effects

It may also happen that the analytes may be trapped in sites in the matrix of differing symmetry. The different matrix sites perturb the vibrational potential differently leading to a splitting in vibrational features. The common matrix materials, the noble gases, generally crystallize in cubic closed packed (face centre cubic f.c.c.) structure. A small amount of nitrogen or oxygen in solid argon can render hexagonal close packed (h.c.p.) structure to be more stable. In f.c.c. structure, each atom is surrounded by 12 equidistant nearest neighbors and its symmetry is found to be an octahedron, O_h . The h.c.p. structure is less stable compared to f.c.c. and it has also 12 equidistant nearest neighbor of symmetry D_{3h} . The inert gases crystallize in f.c.c. structure at cryogenic temperatures when no impurity is present. The closed packed lattices can have three possible guest sites; substitutional, in which the guest molecule replaces one or more host species and two types of interstitial sites viz. tetrahedral and octahedral. A tetrahedral hole is in itself not tetrahedral in shape but is so named because a small guest atom trapped in such a hole would have four neighboring matrix spheres arranged at the corners of tetrahedron. Additionally, there are tetrahedral holes from three spheres of top layer and one from the bottom; thus there is also one tetrahedral hole above each sphere of the bottom layer. In the crystal as a whole, there is one tetrahedral hole above and one below every close-packed sphere. Similarly an octahedral site is surrounded by six close-packed spheres situated on the corners of an octahedron. By simple geometry, it can be shown that the radius of an octahedral site is $0.414r$. In a column of spheres, octahedral sites and spheres alternate, for f.c.c. lattices. Thus there is one octahedral site for every sphere in lattice, i.e. there are half as many octahedral sites in a closest-packed lattice as there are tetrahedral sites.

Vacancies in the crystal lattice may alter the existing site symmetry and crystal imperfections may provide further sites viz. dislocation sites. Generally solids grown by rapid condensation from vapor are unlikely to form perfect crystal as the possibility of formation of

grain boundaries and dislocation sites are quite high. The most likely site is the substitutional site since it alone is large enough to accommodate a normal size diatomic guest. The octahedral interstitial sites are much smaller than the substitutional sites but can possibly accommodate smaller diatomic molecules whereas tetrahedral interstitial sites must be too small to be seriously considered. Small molecules like H₂, HCl, can occupy interstitial sites, which have a diameter less than 2 Å in argon or nitrogen matrix. Larger guest molecules must occupy sites formed by removing two or more lattice molecules.

For solute molecules trapped in different sites, for example, in a substitutional site formed by removal of n or n+1 matrix atoms, each vibrational mode will exhibit more than one band since the interaction of the solute with the matrix environment will be different for different trapping sites. The relative intensity of multiplets due to different trapping sites is usually not dependent on the solute concentration but can change on annealing at higher temperatures or by altering the rate of deposition.²²⁻²⁵

Multiple bands can, however arise from other causes; concentration and annealing studies are necessary to identify the effects due to multiple trapping sites. In addition, in a matrix, coupling may occur between certain internal vibrational modes of a molecule with low energy lattice vibrations of the matrix leading to splitting and broadening of spectral features.

Aggregation

True isolation is achieved only at matrix/analyte (M/A) ratios, of about 1000:1; at M/A ratios where the analyte concentration is higher, molecular aggregates may be formed and trapped in addition to monomers. A sample to matrix ratio of 1:1000 gives about 98.8% isolation of a small molecule undergoing weak interactions. A larger trapped species has a larger cage and hence a larger probability of interaction. This probability has been found to be 99.9% when the sample to matrix ratio is 1:10000 for a weak interaction.²⁶ Multiple features due to self-association can be readily identified from their concentration dependence and from warm-up experiments in which monomers diffuse to form dimer and higher multimers.

In the above discussion, the effect of diffusion during and after deposition are ignored. It is found experimentally, for example, that carbon monoxide forms dimers or higher aggregates to the extent of several percent at a matrix ratio of 1:1000 in argon, rather than the 1% expected on the basis of our analysis. Lithium atoms, on the other hand, will dimerise completely even with matrix ratios of 1:10000, unless matrices that rigidify at a very fast rate are used.²⁷⁻²⁸

It is also important that the matrix gas used must be free from impurities, even if these impurities do not interfere. The presence of, for instance, 1% of nitrogen in argon would result in some 12% of all sites having a cage containing at least one nitrogen molecule even if only single substitutional sites are considered.

Lifting of degeneracy of vibrational levels

The symmetry of the site occupied by the molecule may also contribute to matrix effects. The perturbation of the molecule trapped in a particular site will be different for different vibrations and hence will have different frequency shifts. In case of degenerate vibrational modes, asymmetric sites can lead to a lifting of the degeneracy, resulting in the splitting of the vibrational features, such as that occurs in CO_2 ²⁹⁻³¹ and C_2H_2 ^{32,33}.

2.2. Matrix Isolation Setup

Main component of this set up involves: (a) Cryostat; (b) Vacuum system; (c) Sample introduction system and (d) Fourier transform infrared spectrometer.

Cryostat

Fig. 2.2 shows the radiation shield of the cryostat. Experiments were performed using closed cycle Helium compressor. The cryostat used is a Sumitomo closed cycle Helium compressor (HC-4E1) (Fig. 2.3) that uses continuous expansion-compression cycle of He for cooling.

The region of the cryostat tip is maintained at high vacuum conditions and at a temperature of 12K while recording the spectra. During annealing, the temperature is increased to 27K in the case of N_2 and to 32K in the case of Ar, and maintained at this temperature for a period of 30-60 minutes. The temperature is controlled using a temperature controller unit (Lakeshore Instruments). The compressor is cooled by 3kW water chiller system (Werner Finley) that provides flowing water at an approximate temperature of 15°C.

Vacuum Systems

An efficient pumping system is very crucial for any matrix isolation experiment, not only to minimise the heat load on the cryostat, but also to ensure a clean environment around the cryotip during deposition. The vacuum is obtained in this setup in two steps. First, a mechanical rotary pump (Hind Hivac; ED6) operating at a pumping speed of 200 L/min is used to rough the system to a pressure of $\sim 10^{-2}$ mbar. This is followed by pump-down using a vapor diffusion

pump (Edwards, Diffstack MK2 series 100/300) operating at a pumping speed of 300L/sec, which produces a vacuum to about 10^{-6} mbar. The walls of the diffusion pump are cooled by water from a chiller (Werner-Finley). The vacuum is measured using a digital Penning gauge (Hind Hivac) and a Pirani Gauge 26 (Edwards APG 100 Active Pirani Gauge). Figure 2.4 shows the diffusion pump, the Pirani and Penning gauge readouts.

Sample introduction system

The analyte/matrix gas mixture was prepared in a stainless steel mixing chamber of 1 L capacity, using manometric procedures. (Figure 2.5(a)) The gas mixture was then introduced into the vacuum system using a single jet effusive nozzle. In some experiments, such as when studying $B_3N_3H_6$ complexes, deposition was carried out using a double jet nozzle system. In these experiments, the matrix gas was allowed to effuse out through one nozzle, while $B_3N_3H_6$ was introduced through the second nozzle. .

The rate of deposition was controlled by using a fine flow needle valve (Model: EVN 116, Pfeiffer vacuum) at typical deposition rates of ~ 3 mmol/hr.

2.3. Experimental procedure

C_2H_2 (Sigma Gases, 99.9%), PhAc (Sigma Aldrich, 98%) and C_6H_6 (Sigma Aldrich, anhydrous, $\geq 99\%$) were used without further purification. However, the liquid samples were subjected to several freeze-pump-thaw cycles before use.

$B_3N_3H_6$ was prepared in our lab and the method of preparation will be discussed in Chapter 4. $B_3N_3H_6$, being highly moisture sensitive, was handled with great care during the experiments. It was loaded in the sample bottle in an argon atmosphere in a glove box to minimize its contact with moisture. These liquid samples were equilibrated at the required temperature, to obtain the desired vapor pressure to prepare the analyte/matrix gas mixture of the required ratio. The temperature of the sample was maintained using an ethanol-liquid nitrogen slush bath, and equilibrated for an hour to ensure that the desired vapor pressure over the sample was obtained. The temperature of the slush bath was measured using a platinum resistance thermometer. Vapor pressure data, where available was used to determine the temperature at which the desired vapor pressure could be obtained, by using the Clausius-Clapeyron equation.



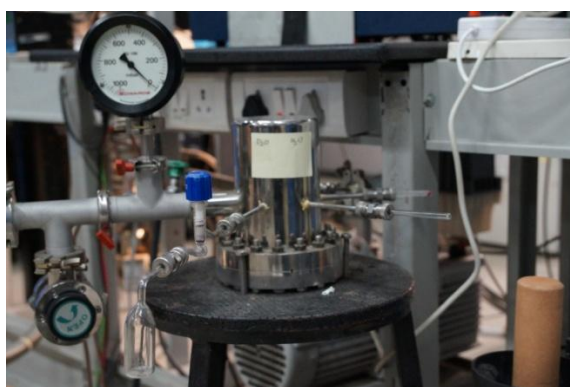
Fig. 2.2: Radiation shield of the cryostat



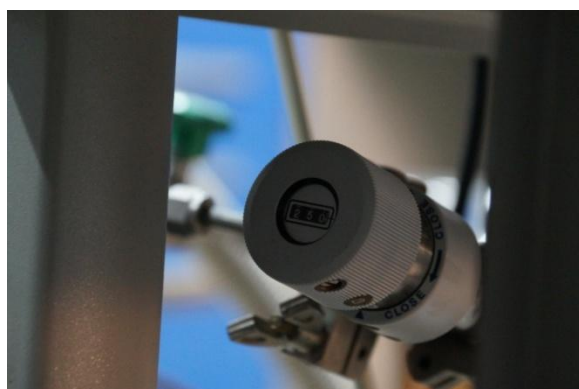
Fig 2.3. Cryostat, Compressor and the temperature controller



Fig. 2.4. (L-R) Diffusion pump, Pirani Gauge and Penning Gauge readouts



(a)



(b)



(c)

Fig. 2.5: a) The mixing chamber; b) The fine flow needle valve (Model: EVN 360); c) The double jet setup mounted on the cryostat



Fig. 2.6: The MI-FTIR setup at IISER Mohali

Spectra of matrix isolated molecules were recorded using a Bruker-Tensor 27 FTIR spectrophotometer with KBr optics. The instrument was operated at a resolution fixed at 0.50 cm^{-1} . In all the experiments, 8 scans were recorded which yielded spectra with a good signal to noise ratio. Spectra were also recorded after annealing the matrix at an elevated temperature such as 27K for N_2 and 32K for Ar to promote diffusion of the species and to aid in complex formation.

2.4. Computations

Ab initio computations were carried out using the Gaussian 09W package³⁴ on a Fujitsu workstation. Molecular properties such as structures, energies and frequencies were computed which were then used to corroborate the experimental results. AIM2000 package was used to examine the nature of the interactions between the precursors of the complexes³⁵⁻³⁷, by studying the electron density topology. (3,-1) bond critical points were located and electron densities (ρ) and Laplacian ($\nabla^2\rho$) at these critical points were obtained for an understanding of the nature of the bonding. NBO (3.1 version) implemented using Gaussian 09 was used to understand the delocalization interactions present in molecules under study.³⁸ These calculations provide an insight into the nature of the orbital interactions, thereby presenting a clear picture of the bonding characteristics of the non-covalent interactions. Energy Decomposition Analysis (EDA) was also done using the LMO-EDA method implemented through GAMESS, in order to partition the total energy of the complexes into various components, such as electrostatic, dispersion, exchange-repulsion and polarization.³⁹⁻⁴⁰ A brief discussion regarding the computational methods employed is given in the following sections.

2.4.1 Geometry optimization and frequency calculation

Geometry Optimization was done to arrive at the structures corresponding to minimum on the potential energy surface. This process of optimization begins with a guess molecular structure specified as input. The energy and gradient are first computed at this point on the potential surface, corresponding to the initial geometry. This information is used to determine how far and in which direction the next step is taken to improve the geometry. At the minimum (or more generally a stationary point), forces will be zero. In the case of Gaussian program, the optimization was achieved when the forces, the root mean square of forces, the calculated displacement and the root mean square of the displacement for the subsequent steps are below preset threshold values.

Optimization calculations were performed at various levels of theories using M06-2X, Moller-Plesset second order perturbation (MP2) using 6-311++G(d,p) and augmented basis sets. Vibrational frequency calculations were performed at the same level of theory used for geometry optimization. The frequency computations were done, first, to ensure that the computed structures did correspond to minima on the potential surface and also to assign the vibrational features observed in the experiments. The computed vibrational frequencies were scaled to bring them in agreement with experimental results. To arrive at the scaling factor, the experimentally observed strongest feature was correlated with the strongest computed feature. The scaling factor that would bring the computed frequency in good agreement with that of experiment was used to scale all other vibrational frequencies. The method of determining the scaling factors is discussed in detail in Chapter 3.

The computed scaled frequencies were used to simulate vibrational spectra by the help of the SYNSPEC program.⁴¹ The simulated spectra were generated assuming a Lorentzian line profile with full width at half maximum (FWHM) of 1 cm^{-1} . Zero point vibrational energies (ZPE) were also obtained from frequency calculations which were used to calculate ZPE corrected energies.

M06 and related methods

The M06 set of functionals were developed by Truhlar et. al.⁴² The M06 functionals are set of four meta-hybrid GGA functionals (generalised gradient approximation- it depends on the up and down spin densities and their reduced gradient). Recently, a new functional, called as the M06-L functional has been introduced to this family of Minnesota functionals for main-group and transition element thermochemistry, thermochemical kinetics, and noncovalent interactions.⁴³ M06-L is very fast for large systems, and is an excellent choice for transition metals and for calculating geometries for any system. M06-HF is recommended for problems that are extremely sensitive to self-interaction, such as long-range charge transfer excitations. All four functionals have good performance for van der Waals interactions, but M06-2X is the best for such interactions, especially for the very difficult case of π - π stacking. The 2X is referred to the percentage of HF exchange which roughly amounts to 54% in this case. The M06 functionals are thus best suited to model dispersion interactions.⁴⁴ All the M06-2X calculations were performed using OPT=TIGHT and INT=ULTRAFINE option.

Møller Plesset Perturbation Theory

The methods employing Møller Plesset Perturbation Theory are non DFT methods and work by brute force solutions of quantum mechanical wavefunctions. The main problem with the Hartree-Fock approach is that it does not account for electron correlation in molecular and atomic systems. However, there exist several methods for treating the electron correlation problem starting from a Hartree-Fock (HF) single determinantal wave function. Configuration interaction (CI), Møller Plesset (MP) (or many-body) perturbation and the coupled cluster (CC) are some of the widely used formalisms to calculate the electron correlation energy. The MP Perturbation Theory was developed in the year 1934 by Christian Møller and Milton S. Plesset.⁴⁵ Since then, this theory has widely developed over the years. This method essentially treats the electron correlation using the Rayleigh-Schrodinger perturbation theory to second (MP2), third (MP3) and fourth (MP4) order. The accuracy of MP2, in particular, has been systematically improved by introducing spin scaling, dispersion corrections, orbital optimization, or explicit correlation.

2.4.2 Interaction energy calculation of complexes

The interaction energy (ΔE) of a complex is given by:

$$\Delta E = E_{AB} - (E_A + E_B) \dots \dots \dots (2.3)$$

where, E_A , E_B and E_{AB} represent the energies for the monomers A, B and complex AB respectively. If the value of ΔE is negative, the complex is more stable relative to the precursors. The interaction energy of the complex was also computed by separately correcting for zero point energy (ZPE) and Basis Set Superposition Error (BSSE).

The BSSE arises for the following reason. When the energy of complex (E_{AB}) is computed, the basis functions used are those of both the monomer subunits. When computing the energy of the individual precursors (i.e. E_A and E_B), the basis functions pertaining to only the corresponding precursor are used. As the number of basis functions used is larger in the computation of the complex, the energy obtained will be lower, as basically each monomer can use the basis functions of other. Interaction energies thus derived from the calculated energies E_A , E_B and E_{AB} will be overestimated and the error is referred to as the basis set superposition error (BSSE).⁴⁶⁻⁵⁰ The best way to eliminate the BSSE is to increase the basis set until the interaction energy is stable to the desired accuracy, which of course implies large computation times for even small systems. The commonly used method to correct for BSSE is by

counterpoise correction proposed by Boys and Bernardi.⁴⁶ In this scheme, one calculates all quantities (energies of monomer E_A , E_B and the complex E_{AB}) in the same basis set spanned by the functions of the complex AB and the difference in energies is obtained as follows:

$$\Delta E = E_{AB}(AB) - \{E_A(AB) + E_B(AB)\} \dots \dots \dots (2.4)$$

where, $E_A(AB)$ = Energy of the monomer A using the basis set AB

$E_B(AB)$ = Energy of the monomer B using the basis set AB

$E_{AB}(AB)$ = Energy of the complex AB using the basis set AB

It is to be noted that the energy corrections for ZPE and BSSE simultaneously were not included as these values are known to overcorrect the stabilization values.⁵¹⁻⁵²

To address the problem of BSSE arising from the limited size of the basis sets, the energy values were also computed at the complete basis set (CBS) limit, obtained using the two-point extrapolation scheme proposed by Helgaker *et al*⁵³, which relies on the fact that correlation energy is proportional to X^3 for aug-cc-pVXZ basis sets. For example, the extrapolation of $\Delta E_{MP2/aug-cc-pVQZ}$ and $\Delta E_{MP2/aug-cc-pVTZ}$ energy values leads to the simple formula:

$$\Delta E_{MP2/CBS} = (4^3 \times \Delta E_{MP2/aug-cc-pVQZ} - 3^3 \times \Delta E_{MP2/aug-cc-pVTZ}) / (4^3 - 3^3) \dots \dots \dots (2.5)$$

We have used the $\Delta E_{MP2/aug-cc-pVQZ}$ and $\Delta E_{MP2/aug-cc-pVTZ}$ values for the extrapolation purpose for most of the geometries. For a few geometries, energy values did not converge at the MP2/aug-cc-pVQZ level of theory. In that case, $\Delta E_{MP2/aug-cc-pVDZ}$ and $\Delta E_{MP2/aug-cc-pVTZ}$ values were used for extrapolation. Finally the estimated CCSD(T)/CBS energy was obtained using the following formula:

$$\Delta E_{CCSD(T)/CBS} = \Delta E_{MP2/CBS} + (\Delta E_{CCSD(T)/aug-cc-pVDZ} - \Delta E_{MP2/aug-cc-pVDZ}) \dots \dots \dots (2.6)$$

2.4.3 Atoms-in-Molecules analysis

Bader first proposed the “atoms in molecules” theory, which uses an analysis of the electron density topology³⁵. The wavefunction corresponding to the optimized geometry of a molecule or complex are generated using the Gaussian 09 package. From the electron density plots, bond critical points, charge density ρ , Laplacian of charge density $\nabla^2\rho$, can be obtained through AIM2000 package. The charge density, $\rho(r)$, is a physical quantity which has a definite value at each point in space. It is a scalar field defined over three dimensional space. Each topological feature of $\rho(r)$, whether it is a maximum, a minimum, or a saddle point, has associated with it in a space called a critical point. At this point, the first derivative of $\rho(r)$ vanish. The sign of its second derivative or curvature at this point determines whether a function

is maximum or minimum. The rank of critical point, denoted by ω , is equal to the number of non-zero eigenvalues or non-zero curvature of ρ at the critical point. The signature denoted by σ , is the algebraic sum of the signs of the eigenvalues. The critical point (CP) is labeled by giving the duo values (ω, σ).

For example, (3, -1) critical point means, three non-zero curvatures and one positive and two negative eigenvalues. A (3, -1) CP corresponds to a bond between two atoms, a (3, +1) CP to a ring, a (3, +3) CP to a cage and a (3, -3) CP corresponds to a maximum. The numbers of critical points of all types, which can coexist in a system with a finite number of nuclei, are governed by the Poincare-Hopf relationship.

$$n - b + r - c = 1 \dots\dots (2.7)$$

where, n is the number of nuclei, b is the number of bond critical points, r is the number of ring critical points and c is the number of cage critical points.

The sum of three Hessians ($\lambda_1, \lambda_2, \lambda_3$) at a bond critical point, gives the value of $\nabla^2\rho$, which provides the electronic charge density distribution in the inter nuclear region. If the value of charge density ρ ($<10^{-1}$ a.u) and the curvature of charge density are large, Laplacian of charge density may be positive or negative usually of the same order of magnitude as ρ then the interaction is of shared type, typical of covalent interaction. For the closed shell interactions, such as hydrogen bond complexes, van der Waals complexes and ionic systems, the charge density ρ ($\sim 10^{-2}$ to 10^{-3} a.u) at the bond critical point is quite small and the Laplacian of the charge density is positive. Koch and Popelier have proposed values of ρ and $\nabla^2\rho$ to characterize the hydrogen bonds, which we have used in this work.⁵⁴

2.4.4. Energy Decomposition Analysis

Energy decomposition analysis (EDA) is a powerful method for a quantitative interpretation of chemical bonds and is used to partition the total energy of the complexes into various fractions like electrostatic, polarization, dispersion and exchange-repulsion. One of the earlier approaches to this analysis was proposed by Morokuma⁵⁵ and further extended by Kitaura and Morokuma.⁵⁶⁻⁵⁷ Their energy decomposition approach (EDA, also called sometimes the KM analysis) has become standard and has been widely used for over 30 years now. The original method was applied to the analysis of binding between two units (e.g., molecules), and it was extended into a general case of an arbitrary number of units by Chen and Gordon.⁵⁸ An energy decomposition analysis method is implemented for the analysis of both

covalent bonds and intermolecular interactions on the basis of single-determinant Hartree–Fock (HF) (restricted closed shell HF, restricted open shell HF, and unrestricted open shell HF) wavefunctions and their density functional theory analogs. For HF methods, the total interaction energy from a supermolecule calculation is decomposed into electrostatic, exchange, repulsion, and polarization terms. Dispersion energy is obtained from second-order Møller–Plesset perturbation theory and coupled-cluster methods such as CCSD and CCSD(T). Tests on various systems show that this algorithm is simple and robust. The symmetry-adapted perturbation theory (SAPT)⁵⁹ is another method for calculating the intermolecular interaction. It is a well established method of calculating the interaction energy of non-covalent complexes. The SAPT method provides detailed information on the intermolecular interaction, as this method directly calculates the magnitude of each energy term (electrostatic, dispersion, *etc.*) of the intermolecular interaction. DFT-SAPT calculation provides very accurate interaction energy, if a reasonably large basis set is used. Another method used to carry out the energy decomposition is the Localized Molecular Orbital-EDA method (LMO-EDA), developed by Su and Li.³⁹ The LMO-EDA scheme was employed in our work, using GAMESS⁴⁰, for the various complexes to decompose the total interaction energies of the complexes. This method can be successfully applied to both closed-shell and open shell systems and is insensitive to the quality of basis set employed. An added advantage of this method is its applicability to high-level quantum chemical methods, such as MP2, CCSD and CCSD(T), thus making it a robust model. Inclusion of such methods enhances the EDA to the wide range of intermolecular interactions.⁶⁰ As stated before, this method can be applied to open systems as well, hence making it useful for covalent bond analysis.

2.4.5. Natural Bond Orbital Analysis

Natural Bond Orbital (NBO) analysis is based on a method for optimally transforming a given wave function into localized form, corresponding to the one-center ("lone pairs") and two-center ("bonds") elements of the Lewis structure picture. In NBO analysis, the input atomic orbital basis set is transformed via natural atomic orbitals (NAOs) and natural hybrid orbitals (NHOs) into natural bond orbitals (NBOs). The NBOs obtained this way correspond to the widely used Lewis picture, in which two-center bonds and lone pairs are localized. Natural (localized) orbitals are used in computational chemistry to calculate the distribution of electron density in atoms and in bonds between atoms. They have the "maximum-occupancy character" in localized 1-center and 2-center regions of the molecule. Natural bond orbitals (NBOs) include

the highest possible percentage of the electron density, ideally close to 2.000, providing the most accurate possible “natural Lewis structure” of ψ . The concept of *natural orbitals* was first introduced by Per-Olov Löwdin in 1955, to describe the unique set of orthonormal 1-electron functions that are intrinsic to the N -electron wavefunction. The NBOs are localized few-centered orbitals that describe the Lewis-like molecular bonding pattern of electron in optimally compact form. More precisely, NBOs are an orthonormal set of localized maximum occupancy orbitals whose leading $N/2$ members give the most accurate possible Lewis-like description of the total N -electron density. The NBOs are obtained as local block eigenfunctions of the one-electron density matrix, and are hence natural in the sense of Löwdin, having optimal convergence properties for describing the electron density. Delocalization effects appear as weak departures from this idealized localized picture.

The estimates of energy effects are based on second-order perturbation theory, or on the effect of deleting certain orbitals or matrix elements and recalculating the total energy to determine the associated vibrational energy lowering. This analysis is performed by

- 1) Deleting specified elements or block of elements from the NBO Fock matrix,
- 2) Diagonalizing this new Fock matrix to obtain a new density matrix, and
- 3) Passing this density matrix to the SCF routines for a single pass through the SCF energy evaluator.

The difference between this deletion energy and the original SCF energy provides useful measure of the energy contribution of the deleted terms. This way one can decompose the total energy into components associated with covalent and non-covalent contributions

$$E = E_{\sigma} - E_{\sigma^*} \dots \dots \dots (2.8)$$

where, σ and σ^* are referred to filled and unfilled orbitals respectively. The filled orbital can be core orbital, lone pair, σ or π bond and the unfilled orbital can be σ or π antibond, Rydberg orbital etc. Schematic NBO perturbation diagram for 2-e stabilizing interaction (hyperconjugative interactions) is shown in Fig. 2.7. This figure depicts the interaction of a filled orbital σ of the formal Lewis structure with one of the unfilled antibonding orbitals σ^* to give the second order energy lowering, $\Delta E_{\sigma \rightarrow \sigma^*}^{(2)}$. In SCF–MO theory this lowering in energy is given by the formula,

$$\Delta E_{\sigma \rightarrow \sigma^*}^{(2)} = q \langle \sigma | F | \sigma^* \rangle^2 / [\epsilon_{\sigma^*} - \epsilon_{\sigma}] \dots \dots \dots (2.9)$$

Where, q is the donor orbital occupancy, F is the Fock operator and ϵ_{σ} , ϵ_{σ^*} are NBO orbital energies. The NBO perturbative framework permits one to apply qualitative concepts of valence theory to describe the non-covalent energy lowering. Since the non-covalent delocalization effects are associated with $\sigma \rightarrow \sigma^*$ interactions between filled (donor) and unfilled (acceptor) orbitals, it is natural to describe them as being of “donor-acceptor”, “charge transfer”, or generalized “Lewis base-Lewis acid” type.

In our work, NBO analysis (Version 3.1)³⁸ was performed at MP2/aug-cc-pVDZ using GAUSSIAN 09 to explore the nature of delocalization interactions in the various π systems studied.

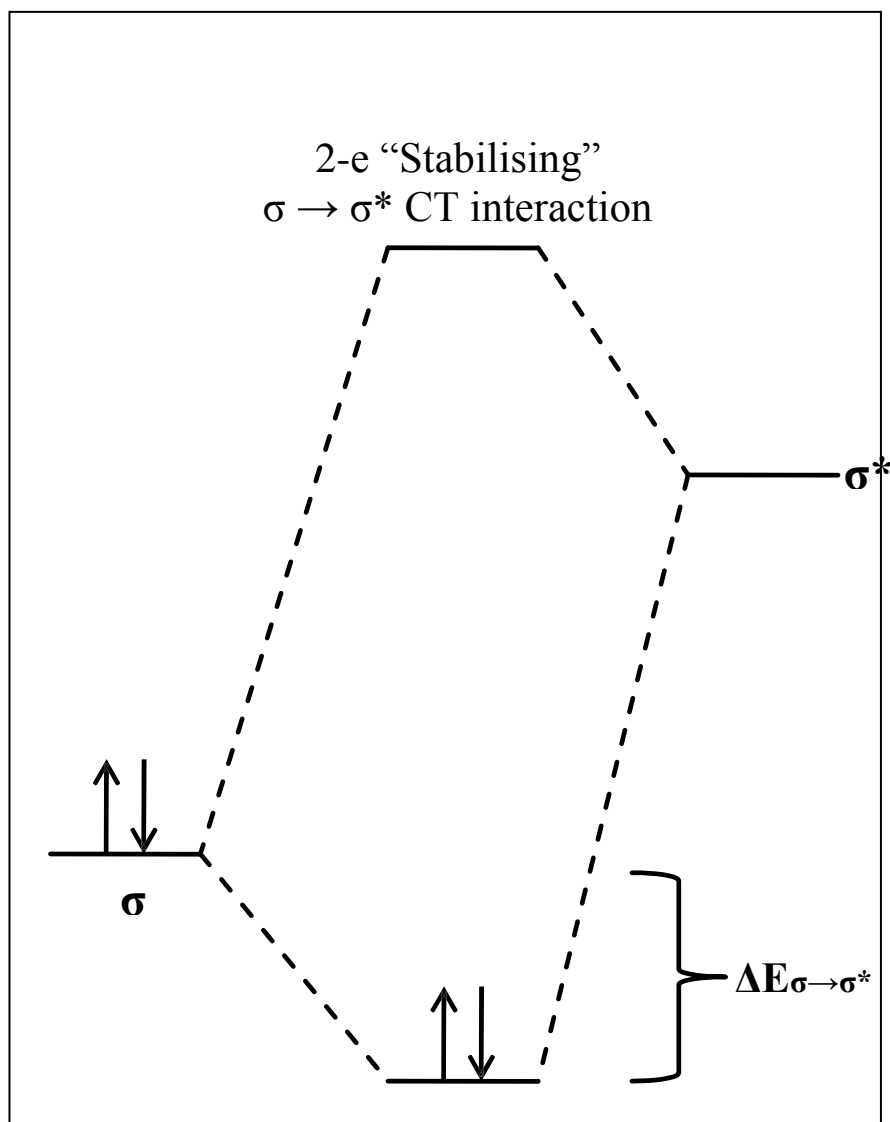


Fig. 2.7. Schematic NBO perturbation diagram for ‘2-e stabilizing’ delocalization interaction.

REFERENCES

- (1) Norman, I.; Porter, G. *Nature*, **1954**, *174*,508; Whittle, E.; Dows, D.A.; Pimentel, G.C. *J. Chem. Phys.* **1954**, *22*, 1943.
- (2) Thiel, M.V.; Becker, E.D.; Pimentel, G.C. Infrared studies of Hydrogen Bonding of Water by the Matrix Isolation Technique. *J. Chem. Phys.* **1957**, *27*,486-490.
- (3) Becker, E.D.; Pimentel, G.C. Spectroscopic Studies of Reactive Molecules by the Matrix Isolation Method. *J. Chem. Phys.* **1956**, *25*,224-228.
- (4) Thiel, M.V.; Becker, E.D.; Pimentel, G.C. Infrared studies of Hydrogen Bonding of Methanol by the Matrix Isolation Technique. *J. Chem. Phys.* **1957**, *27*, 95-99.
- (5) Becker, E.D.; Pimentel, G.C.; Thiel, M.V. Matrix Isolation Studies: Infrared Spectra of Intermediate Species in the Photolysis of Hydrazoic Acid. *J. Chem. Phys.* **1957**, *26*,145-150.
- (6) Milligen, D.E.; Pimentel, G.C. Matrix isolation studies: Possible infrared spectra of Isomeric Forms of Diazomethane and of Methylene, CH₂. *J. Chem. Phys.* **1958**, *29*,1405-1412.
- (7) Meyer, M. *Low Temperature Spectroscopy* Elsevier Publishing Company New York,1971.
- (8) Hallam, H.E. *Vibrational Spectroscopy of Trapped Species*. J.Wiley, London,1973.
- (9) Moskovits, M.; Ozin, G.A. *Cryochemistry*. J.Wiley, London,1973.
- (10) Poliakoff, M.; Turner, J.J. *J.Chem.Soc* 2276 **1974**.
- (11) Ruzi, M.; Anderson, D.T. Matrix Isolation spectroscopy and Nuclear Spin Conversion of NH₃ and ND₃ in Solid Parahydrogen. *J.Phys.Chem.A* **2013**,*117*,9712-9724.
- (12) Yoshioka, K.; Anderson, D.T. Infrared Spectra of CH₃F (ortho-H₂)_n clusters in solid parahydrogen. *J. Chem. Phys.* **2003**,*119*,4731-4742.
- (13) Paulson, L.O.; Anderson, D.T. High resolution vibrational spectroscopy of trans-formic acid in solid parahydrogen. *J.Phys. Chem. A* **2009**,*113*,1770-1778.
- (14) Pimentel, G. C.; Charles, S. W. Infrared spectral perturbations in matrix isolation experiments. *Pure and Appl. Chem.*, **1963**, *7*, 111-123.
- (15) Buckingham, A. D. *Proc. Roy.Soc. (London)* **1958**,248,169.
- (16) Warren, J. A.; Smith, G. R.; Guillory, W. A. The infrared spectrum of matrix isolated hydrogen and deuterium. *J. Chem. Phys.*, **1980**, *72*, 4901-4908.
- (17) Carr, B. R.; Chadwick, B. M.; Edwards, C. S.; Long, D. A.; Wharton, G. C. The infrared activation of the NN stretching vibration in nitrogen matrices. *J. Mol. Struct.* **1980**, *62*, 291-295.

-
- (18) Bowers, M. T.; Kerley, G. I.; Flygare, W. H. Vibrational Spectra of Monomeric HF in the Rare-Gas Lattices. *J. Chem. Phys.*, **1966**, *45*, 3399-3414.
- (19) Robinson, D. W. *J. Chem. Phys.*, 1963, *39*, 3430.
- (20) Bowers, M. T.; Flygare, W. H. Vibration-Rotation Spectra of monomeric HCl, DCl, HBr, DBr and HI in the rare gas lattices and N₂ doping experiments in the rare gas lattices. *J. Chem. Phys.*, **1966**, *44*, 1389-1404.
- (21) Prochaska, F. T.; Andrews, L. Vibration-Rotational and pure rotational laser-Raman spectra of H₂, D₂ and HD in matrices at 12K. *J. Chem. Phys.*, **1977**, *67*, 1139-1143.
- (22) Mile, B. Free radical studies at low temperatures. *Angew. Chem. Int. Ed.*, **1968**, *7*, 507-519.
- (23) Pollack, G. L. The solid state of rare gases. *Rev. Mod. Phys.*, **1964**, *36*, 748.
- (24) Purnell, C. J.; Barnes, A. J.; Suzuki, S.; Ball, D. F.; Orville-Thomas, W. J. Infrared and Raman matrix isolation studies of methylamine. *Chem. Phys.*, **1976**, *12*, 77-87.
- (25) Swanson, B. I.; Jones, L. H. *J. Chem. Phys.*, **1980**, *73*, 986.
- (26) Cradock, S.; Hinchcliffe, A. J. Matrix Isolation: A technique for the study of reactive inorganic species. Cambridge Univ. Press, London.
- (27) Andrews, L.; Pimentel, G. C. Visible Spectra of Lithium in Inert-Gas Matrices. *J. Chem. Phys.*, **1967**, *47*, 2905.
- (28) Welker, T.; Martin, T. P. Optical absorption of matrix isolated Li, Na and Ag clusters and microcrystals. *J. Chem. Phys.*, **1979**, *70*, 5683.
- (29) Jones, L. H.; Swanson, B. I. High resolution infrared studies of dynamics in low temperature matrices: Vibrational dephasing for SeF₆ in noble gas solids. *J. Chem. Phys.*, **1981**, *74*, 3216-3224.
- (30) Dubs, M.; Gunthard, H. H. IR hole burning and line shape of matrix isolated 1,2-difluoroethane with tunable diode lasers. *Chem. Phys. Lett.*, **1979**, *64*, 105-107.
- (31) Poliakov, M.; Turner, J. J. Infrared laser photochemistry in matrixes in chemical and biological application of lasers, Ed. C. B. Moore, Academic Press, New York, 1980.
- (32) Sundararajan, K.; Viswanathan, K. S. A matrix isolation and *ab initio* study of the C₂H₂-MeOH complex. *J. Mol. Struct.*, **2006**, *798*, 109-116.

-
- (33) Jose, K. V. J.; Gadre, S. R.; Sundararajan, K.; Viswanathan, K. S. Effect of matrix on IR frequencies of acetylene and acetylene-methanol complex: Infrared matrix isolation and ab initio study. *J. Chem. Phys.*, **2007**, *127*, 104501-104505.
- (34) Frisch, M.J.; Trucks, G.W.; Schlegel, H.B.; Scuseria, G.E. ; Robb, M.A.; Cheeseman, J.R.; Scalmani, G.; Barone, V.; Mennucci, B.; Petersson et. al, Gaussian, Inc., Wallingford CT, 2010.
- (35) Bader, R.F.W. Atoms in Molecules. A Quantum Theory (Clarendon Press, Oxford, 1994).
- (36) Bone, R.G.A.; Bader, R.F.W. Identifying and analyzing intermolecular bonding interactions in van der Waals molecules. *J. Phys. Chem.* **1996**, *100*, 10892-10911.
- (37) Bieger-König, F.; Bayles, D.; Schönbohn, J. AIM2000 (Version 1.0); Chemical Adviser: R. F. W. Bader.
- (38) Glendening, E.D.; Reed, A. E.; Carpenter, J.E.; Weinhold, F. NBO Version 3.1.
- (39) Su, P. F.; Li, H.; Energy Decomposition Analysis of Covalent Bonds and Intermolecular Interactions. *J. Chem. Phys.* **2009**, *131*, 014102-014115.
- (40) Schmidt, M.W. ; Baldridge, K.K; Boatz, J.A.; Elbert, S.T.; Gordon, M.S.; Jensen, J.H.; Koseki, S; Matsunaga, N. Nguyen, K.A.; Su, S. *et. al.* General Atomic and Molecular Electronic Structure System. *J. Comp. Chem.* **1993**, *14*, 1347-1363.
- (41) The spectra were simulated using SYNSPEC made available by K. Irikura, National Institute of Standards and Technology, Gaithersburg, MD 20899, USA, **1995**.
- (42) Zhao, Y.; Truhlar, D. G. A new local density functional for main-group thermochemistry, transition metal bonding, thermochemical kinetics and non-covalent interactions. *J. Chem. Phys.* **2006**, *125*, 194101-18
- (43) Zhao, Y.; Truhlar, D. G. Applications and validations of the Minnesota Density Functionals. *Chem. Phys. Lett.* **2011**, *502*, 1-13.
- (44) Raju, R. K.; Ramraj, A.; Hillier, I. H.; Vincent, M. A.; Burton, N.A. Carbohydrate-aromatic π interactions: a test of density functionals and the DFT-D method. *Phys. Chem. Chem. Phys.* **2009**, *11*, 3411-3416.
- (45) Moller, C.; Plesset, M.S. Note on an approximate treatment for many-electron systems. *Phys. Rev.* **1934**, *46*, 618-622.
- (46) Boys, S.F.; Bernardi, F. The calculation of small molecular interactions by the differences of separate total energies. Some procedures with reduced errors. *Mol. Phys.*, **1970**, *19*, 553-566.

-
- (47) Jensen, F. The magnitude of intramolecular basis set superposition error. *Chem. Phys. Lett.*, **1996**, *261*, 633-636.
- (48) Mayer, I.; Surjan, P. R. Monomer geometry relaxation and the basis set superposition error *Chem. Phys. Lett.*, **1992**, *191*, 497-499.
- (49) Schwenke, D. W.; Truhlar, D. G. Systematic study of basis set superposition errors in the calculated interaction energies of two HF molecules *J. Chem. Phys.*, **1985**, *82*, 2418-2426.
- (50) Turi, L.; Dannenberg, J.J. Correcting for basis set superposition error in aggregates containing more than two molecules: ambiguities in the calculation of the counterpoise correction. *J. Phys. Chem.* **1993**, *97*, 2488-2490.
- (51) Turi, L.; Dannenberg, J.J. Molecular Orbital Studies of the Nitromethane-Ammonia complex. An unusually strong CH \cdots N hydrogen bond. *J. Phys. Chem.* **1995**, *99*, 639-641.
- (52) Wong, N.B.; Cheung, Y.S; Wu, D. Y.; Ren, Y.; Wang, X.; Tian, A. M.; Li, W.K. A theoretical study of the C-H \cdots N hydrogen bond in the methane-ammonia complex. *J. Mol. Struct.* **2000**, *507*, 153-156.
- (53) Helgaker, T.; Klopper, W.; Koch, H.; Noga, Basis set convergence of correlated calculations on water. *J. Chem. Phys.* **1997**, *106*, 9639-9646.
- (54) Koch, U.; Popelier, P.L.A. Characterization of CH \cdots O hydrogen bonds on the basis of charge density *J. Phys. Chem.* **1995**, *99*, 9747-9754.
- (55) Morokuma, K. Molecular Orbital Studies of Hydrogen Bonds. C \equiv O \cdots H-O hydrogen bond in H₂CO-H₂O and H₂CO-2H₂O. *J. Chem. Phys.* **1971**, *55*, 1236.
- (56) Kitaura, K.; Morokuma, K. A new energy decomposition scheme for molecular interactions within the Hartree-Fock approximation. *Intl. J. Quant. Chem.* **1976**, *10*, 325-340.
- (57) Kitaura, K.; Morokuma, K. In *Molecular Interactions*, Vol. **1**; Ratajczak, H.; Orville-Thomas, W. J., Eds.; Wiley: Chichester, England, 1980; p. 21.
- (58) Gordon, M. S.; Jensen, J. H. In *Encyclopedia of Computational Chemistry*, Vol. **5**; Schleyer, P. V. R., Ed.; Wiley: Chichester, England, **1998**; p. 3198.
- (59) Jeziorski, B.; Moszynski, R.; Szalewicz, K. Perturbation theory approach to intermolecular potential energy surfaces of van der Waals complexes. *Chem. Rev.* **1994**, *94*, 1887-1930.
- (60) Romero, J.; Reyes, A.; David, J.; Restrepo, A. Understanding microsolvation of Li⁺: structural and energetical analyses. *Phys. Chem. Chem. Phys.* **2011**, *13*, 15264-15271.

CHAPTER 3: HYDROGEN BONDED COMPLEXES OF PHENYLACETYLENE- ACETYLENE

3.1. Introduction

PhAc is an interesting multifunctional molecule which presents competitive hydrogen bonding sites. There have been many theoretical and experimental studies in the literature in order to understand the hydrogen bonding interactions in PhAc. Patwari and co-workers have studied hydrogen bonded complexes of PhAc with various molecules such as water, methanol, ammonia and methylamine experimentally using IR-UV Double Resonance Spectroscopy and theoretically using high level *ab initio* calculations.¹⁻¹⁰ Goswami and Arunan have also studied the complexes of PhAc using gas phase microwave spectroscopy.¹¹⁻¹² As can be expected, PhAc forms a variety of intermolecular structures which results from a fine balance of intermolecular forces. For example, the phenylacetylene-methanol complex has an O-H $\cdots\pi$ hydrogen bond, where the O-H group of methanol interacts with the π cloud of the benzene ring.¹ Likewise, the phenylacetylene-methylamine complex is characterized by the presence of an N-H $\cdots\pi$ hydrogen bond, with the N-H group of methylamine interacting with the π electron density of the C₆H₆ ring.¹ On the other hand, PhAc forms a linear C-H \cdots N, σ hydrogen-bonded complex with ammonia, which is very similar to acetylene-ammonia complex, whereas in addition, it forms a quasiplanar cyclic complex with water, involving both O-H $\cdots\pi$ and C-H \cdots O hydrogen bonds. Interestingly, in this complex the O-H group of a water molecule interacts with the π electron density of the C-C triple bond, while the C-H group of the C₆H₆ ring in the ortho position is hydrogen-bonded to the oxygen atom of the water molecule. Even though PhAc has features of both C₆H₆ and C₂H₂, the structure of the PhAc-H₂O complex is different from both the C₆H₆-H₂O and C₂H₂-H₂O complexes.¹³⁻¹⁴ These results indicate that while studying interactions with multifunctional molecules, even small changes in the interacting partner can result in a remarkable change in the intermolecular structure.

In order to understand weak non-covalent interactions, specially π -hydrogen bonded systems and π - π interactions, we have chosen to study PhAc and C₂H₂ heterodimer in this work. The prime motivation behind choosing this system is that PhAc is a molecule with multifunctional sites for hydrogen bonding (Fig.3.1). It has two hydrogen bonding acceptor sites

in the benzene ring and the acetylenic C-C triple bond, and proton donor sites as the acetylenic and the phenyl C-H group. Similarly, C_2H_2 has a C-C triple bond, which can act as proton acceptor, and an acetylenic C-H group, which can act as a proton donor (Fig.3.1).

Studies on the hydrogen bonded complexes of C_2H_2 -MeOH, C_2H_2 -CHCl₃, C_2H_2 -C₂H₄ and C_2H_2 -C₆H₆ have been reported, where the dual behavior of C_2H_2 has been well documented.¹⁵⁻¹⁹ While in the C_2H_2 -CHCl₃ complex, C_2H_2 played the role of a proton acceptor, in the complexes of C_2H_2 -C₂H₄ and C_2H_2 -C₆H₆, it played the role of a proton donor.

It is thus interesting to study this system, to understand the nature of the PhAc- C_2H_2 heterodimer. Since this system is expected to present a number of minima on the potential surface, the problem turns out to be even more interesting. While in gas phase experiments, the lowest energy complex is usually observed, the matrix isolation experimental technique that we have employed is known to trap local minima. It was therefore worthwhile to see how many of these minima can be discerned in the experiments.

Experiments were also performed using PhAc deuterated at the acetylenic hydrogen (PhAc_D) to study the isotopic effects on the vibrational spectra of complexes.

3.2 Experimental Details

Matrix isolation experiments were performed using a Sumitomo closed cycle helium compressor-cooled cryostat (HC-4E1). The cryostat along with the cold tip was housed in a vacuum chamber, where the base pressure was $\sim 10^{-6}$ torr. N₂ and Ar (Sigma Gases & Services, 99.999%) were used as the matrix gases.

C_2H_2 (Sigma Gases & Services, 99.9%), PhAc (Sigma Aldrich, 98%), Phac-D (Sigma Aldrich, 99% Atom-D) were used without further purification. PhAc was, however, subjected to several freeze-pump-thaw cycles before preparation of the sample-matrix gas mixtures. The sample-matrix gas mixture was prepared at the desired ratio, using standard manometric procedures. Sample to matrix ratios were typically varied from 0.2:1000 to 3:1000 individually for both precursors PhAc (or PhAc_D) and C_2H_2 . The matrix gas/ C_2H_2 /PhAc mixture was then deposited through an effusive nozzle onto a cold KBr substrate, mounted on a cryotip. A deposition typically lasted 1hr 30 min, at a rate of 3 mmol/h of the matrix gas, which yielded a uniform matrix film.

Infrared spectra of the matrix isolated samples were recorded over the range 4000-400 cm^{-1} , using a Bruker Tensor 27 FTIR spectrometer, operated at a resolution of 0.5 cm^{-1} . The

matrix was then warmed to an elevated temperature (27 K for N₂ matrix and 32 K for Ar matrix) to promote diffusion and complex formation; maintained at this temperature for about 1 hour and re-cooled to 12K. Spectra of the matrix, thus annealed, were again recorded. Spectra of the C₂H₂ and PhAc deposited individually in the matrix were also recorded for comparison.

3.3. Computations

Theoretical calculations were performed for the C₂H₂-PhAc complexes using the GAUSSIAN-09²⁰ suite of programs. Geometries of the precursor molecules were first optimized at the M06-2X and MP2 level of theories using 6-311++G (d,p) and aug-cc-pVDZ basis sets. Starting from the optimized monomer geometries, the geometries of the complexes were then optimized. Interaction energies were computed for the complexes, corrected separately for BSSE (basis set superposition error) using the method outlined by Boys and Bernardi²¹ and ZPE (Zero point energies). Interaction energies were also computed at the MP2/CBS and CCSD(T)/CBS limit for all the complexes. (Table 3.1)

Vibrational frequency calculations were done for the optimized geometries to enable us to characterize the nature of the stationary points and also to assign the observed frequencies in our matrix isolation experiments. The computed vibrational frequencies for the different complexes were scaled, on a mode-by-mode basis, as it is recognized that the matrix perturbs the vibrational frequencies of the trapped species, with the magnitude of perturbation depending on the vibrational frequency of the mode. We therefore consider that mode-by-mode scaling is an appropriate method to account for the varying degrees of matrix influence and helps in bringing the computational features in meaningful agreement with the experimental observations in the matrix, over the entire range of experiments. The scaling factors were obtained by comparing the strongest computed frequency, of say C₂H₂, with the strongest feature observed experimentally, in a given region. The factor that would bring the computed feature in agreement with the experimental feature was calculated for the given spectral region. The scaling factor thus obtained for uncomplexed C₂H₂, was then used to scale the computed frequencies of this submolecule in the complex for the corresponding mode.

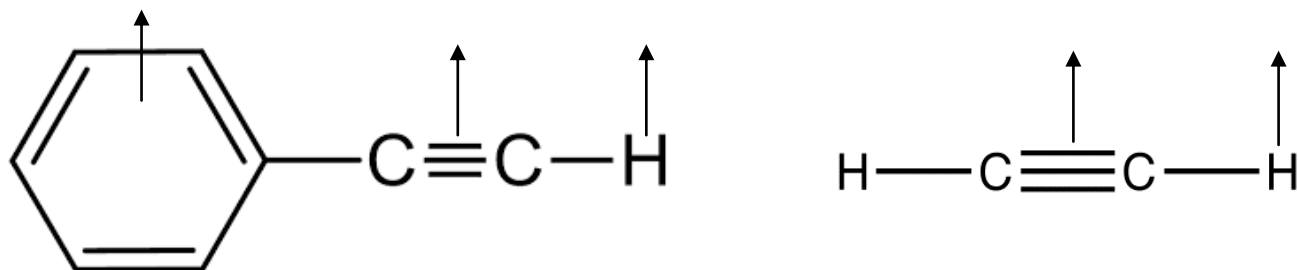


Fig.3.1. PhAc and C_2H_2 structures with the multifunctional sites depicted with an upward arrow

Table 3.1. Raw uncorrected/ZPE/BSSE interaction energies in kcal/mol for the various PhAc- C_2H_2 complexes at the M06-2X and MP2 levels of theory using 6-311++G(d,p) and aug-cc-pVDZ basis sets. The interaction energies at MP2/CBS and CCSD(T)/CBS limit are also given.

Complex	M06-2X		MP2			CCSD(T)
	6-311++G(d,p)	aug-cc-pVDZ	6-311++G(d,p)	aug-cc-pVDZ	CBS	CBS
1	-2.96/-2.45/-2.61	-3.38/-2.80/-2.36	-4.48/-3.90/-1.94	-5.90/-4.85/-2.64	-3.16	-2.38
2	-1.38/-1.01/-1.28	-1.57/-1.05/-1.31	-2.25/-1.94/-1.10	-2.63/-1.94/-1.82	-1.64	-1.49
3	-2.37/-2.01/-2.17	-2.84/-2.15/-2.37	Geom not found	-3.92/-3.17/-2.05	-2.51	-2.18
4	-2.56/-2.12/-2.18	-2.74/-2.30/-2.16	-4.05/-3.86/-1.56	-4.72/-3.72/-2.39	-2.01	-1.66

For example, the scaling factor for the C-H stretching mode of C₂H₂ monomer was computed by dividing the experimental wavenumber of the C₂H₂ monomer in the C-H stretching region, i.e. 3283.1 cm⁻¹ by the computed wavenumber in the same region at the M06-2X/aug-cc-pVDZ level of theory, i.e. 3431.6 cm⁻¹. The scaling factor thus obtained, i.e. 0.9567 was then used to scale the computed frequencies of this submolecule in the complex for the corresponding mode. Similarly, the scaling factors in the C-H stretching region of PhAc and the C-H bending region of C₂H₂ were computed.

The computed frequencies for the various modes for the PhAc-C₂H₂ complexes were simulated as a vibrational spectrum using SYNSPEC program.²² For this exercise, the scaled frequencies and intensities obtained from GAUSSIAN 09 program were used. The simulated vibrational spectra were generated assuming a Lorentzian line profile with a full width at half maximum (FWHM) of 1 cm⁻¹.

Atoms-in-molecules (AIM) analysis was done on the optimized geometries of PhAc-C₂H₂ complexes using AIM2000 (version 1.0) to explore the nature of hydrogen bonding.²³⁻²⁵ Localized Molecular Orbital Energy decomposition Analysis (LMOEDA)²⁶ was performed using GAMESS²⁷ to determine the contributions of the various components of interaction energy such as electrostatic, exchange, repulsion, polarization and dispersion towards the stabilization of the complex. NBO analysis was performed through Gaussian 09, to understand the role of the various orbital interactions in the stabilization of the complex.²⁸

3.4 Results and Discussion

3.4.1. Computational Details

The interaction energies of the different complexes at the M06-2X and MP2 levels of theory are indicated in Table 3.1. The interaction energies were also calculated at the MP2/CBS and CCSD(T)/CBS limit for all the complexes, as shown in this table.

The interaction energy (ΔE) values for the complexes were computed using the super-molecule approach:

$$\Delta E (PhAc - C_2H_2) = E (PhAc-C_2H_2) - E(PhAc) - E(C_2H_2) \dots (1)$$

The energy values computed at the complete basis set (CBS) limit were obtained using the two-point extrapolation scheme proposed by Helgaker *et al.*²⁹, and which has been outlined in Chapter 2. The estimated CCSD(T)/CBS energy was also obtained.

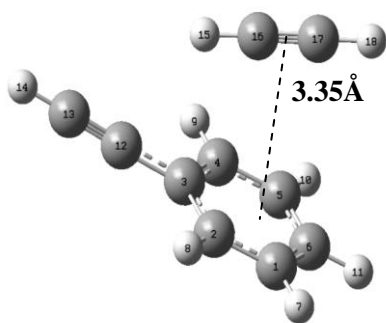
Our computations at the M06-2X/aug-cc-pVDZ level of theory indicated four structures for the PhAc-C₂H₂ complexes. Figure 3.2 shows the different optimized geometries of the PhAc-C₂H₂ complexes at the M06-2X/aug-cc-pVDZ level of theory and Table 3.2 presents the relevant molecular structural parameters for the four complexes. Complex 1 is a structure where the hydrogen of C₂H₂ interacts with the π cloud of the phenyl ring in PhAc. The C-H $\cdots\pi$ hydrogen bond distance in this complex was computed to be 2.77 Å. In complex 2, the acetylenic hydrogen in PhAc interacts with the π cloud of C₂H₂ with the C-H $\cdots\pi$ hydrogen bonded distance for this complex being 2.71 Å. In complex 3, C₂H₂ serves as the proton donor to the acetylenic π -cloud of PhAc. In this complex, the C-H $\cdots\pi$ distance was computed to be 2.62 Å; the shortest among the complexes. Complex 4 was a π stacked structure. At this level of theory, complexes 1 and 3 were nearly isoenergetic global minima. However, at the MP2/aug-cc-pVDZ level, complex 1 was found to be the global minimum, followed by complexes 4, 3 and 2. Computations were also done at the 6-311++G(d,p) level, the results of which are shown in Table 3.1.

3.4.2 Experimental

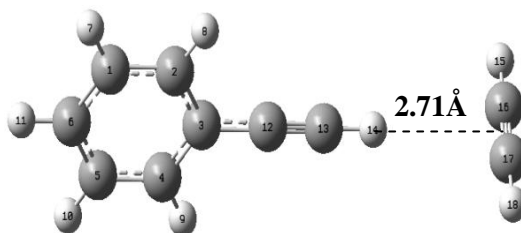
Figure 3.3 (Panel A) shows the IR spectra of PhAc and C₂H₂ in a N₂ matrix over the spectral region 3350-3200 cm⁻¹ which corresponds to \equiv C-H stretch in the two molecules. In this region, C₂H₂ showed a strong absorption at 3283.1 cm⁻¹. In addition to the feature of the C₂H₂ monomer, we also observed a feature at 3258 cm⁻¹ which has been assigned to the C₂H₂ dimer and two other features at 3218.6 and 3225.7 cm⁻¹ which are due to C₂H₂-H₂O complex.³⁰

The features due to C₂H₂-H₂O were observed even when water was not deliberately introduced, as water is an inevitable impurity in a matrix isolation experiment. Likewise, the features of matrix isolated PhAc was observed at 3323.1 cm⁻¹, with the Fermi resonance diad appearing as a site split feature at 3309.1/3310.8 cm⁻¹. The Fermi resonance has been reported to occur between the \equiv C-H stretching vibration and a combination of one quantum of C \equiv C stretch and two quanta of C \equiv C-H out-of-plane bend.³¹

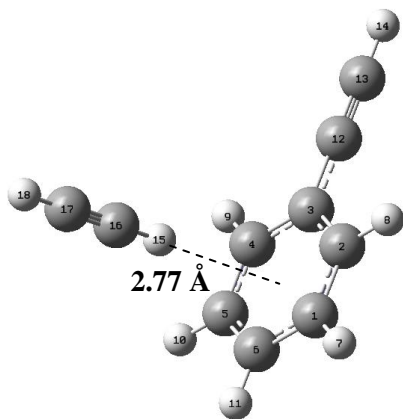
Figure 3.3 (Panel C) displays the IR spectra in the region 780-730 cm⁻¹, corresponding to the bending region of C₂H₂. The doubly degenerate bending mode of C₂H₂ in the N₂ matrix, appears as a doublet at 742.4 cm⁻¹ and 747.4 cm⁻¹. The bending mode of PhAc in the N₂ matrix appears at 758.7 cm⁻¹.



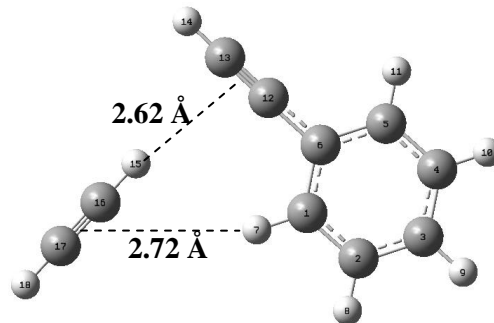
Complex 4



Complex 2



Complex 1



Complex 3

Fig.3.2. Optimized structures of PhAc-C₂H₂ complexes at M06-2X/aug-cc-pVDZ level of theory

Table 3.2. Selected geometrical parameters for the PhAc-C₂H₂ complexes at the M06-2X/aug-cc-pVDZ level of theory. The distances are given in angstroms (Å) and the angles are given in degrees (°)

Parameters	Complex 1	Complex 2	Complex 3	Complex 4
C12-C13	1.21	1.21	1.21	1.21
C16-C17	1.21	1.21	1.21	1.21
C16-H15	1.07			
H14-C16		2.71		
H14-C17		2.71		
H7-C16			2.72	
C13-H15			2.62	
H15-C13-H14			98.9	
H15-C12-C13				98.6
C17-C6-H11				111.1
C12-C3-C2-H8				1.91
H9-C4-H15	117.7			
H14-C17-H18		102.9		
C16-H15-C4-C3	118.5			
C13-H14-C17-H18		1.34		
C16-H15-C13-H14			-0.80	

When PhAc and C₂H₂ were co-deposited in a N₂ matrix and the matrix then annealed, new features were observed at 3253.1, 3315.2 and 753.7 cm⁻¹(Fig.3.3(d) Panels A, B and C). These product bands increased in intensity, when the concentration of either of the two reagents, PhAc or C₂H₂, was increased which clearly indicates that these features are due to a complex involving PhAc and C₂H₂ (Fig.3.4). Since these bands appear even at low concentrations of PhAc and C₂H₂, we believe that these bands are due to a 1:1 complex of C₂H₂ and PhAc. The assignments of these bands will be discussed later.

3.5 Vibrational assignments

Vibrational frequencies were calculated at the M06-2X/aug-cc-pVDZ level for the different complexes and compared with the experimentally observed values (Table 3.3).

3.5.1 ≡C-H asym.stretch in C₂H₂ submolecule

As mentioned earlier, in the N₂ matrix, the ≡C-H stretch for C₂H₂ appears at 3283.1 cm⁻¹ with another barely visible feature at 3311 cm⁻¹. The product band due to C₂H₂-PhAc complex at 3253.1 cm⁻¹ can be assigned to the ≡C-H asymmetric stretch of the C₂H₂ submolecule.

As can be seen from Table 3.3 and Fig.3.5, the computed shift of ~29.9 cm⁻¹ for this mode, for complex 3, is in excellent agreement with the experimentally observed shift of 30 cm⁻¹ at the M06-2X/aug-cc-pVDZ level of theory. The shifts computed for complex 1 and complex 2 are clearly different from that observed in our experiments, thereby confirming that complex 3 is clearly produced in the matrix. This complex is an H...π adduct, in which C₂H₂ is the proton donor to the π cloud of acetylenic unit in PhAc.

The shift in the ν₃ mode of the C₂H₂ submolecule is a good indicator of the nature of interaction in the complex. In complexes where C₂H₂ is the proton donor, the shifts in the ν₃ mode of C₂H₂ submolecule are usually large. For example, the ν₃ mode of C₂H₂ in the C₂H₂-H₂O and C₂H₂-C₂H₄ complex is shifted by 49 cm⁻¹ and 19.4 cm⁻¹ respectively, where C₂H₂ acts as the proton donor.^{14,18} On the other hand, in complexes where C₂H₂ acts as a proton acceptor, the shift in the ν₃ mode of C₂H₂ is much smaller. For example, in the C₂H₂-CHCl₃ complex¹⁷, where C₂H₂ is a proton acceptor, the shift in the ν₃ mode is only 4 cm⁻¹.

In the present study too, the ν₃ mode of C₂H₂ submolecule is shifted by 30.0 cm⁻¹, thus indicating that C₂H₂ is the proton donor. Experimental evidence therefore unambiguously points to C₂H₂ being the proton donor in the PhAc-C₂H₂ complex.

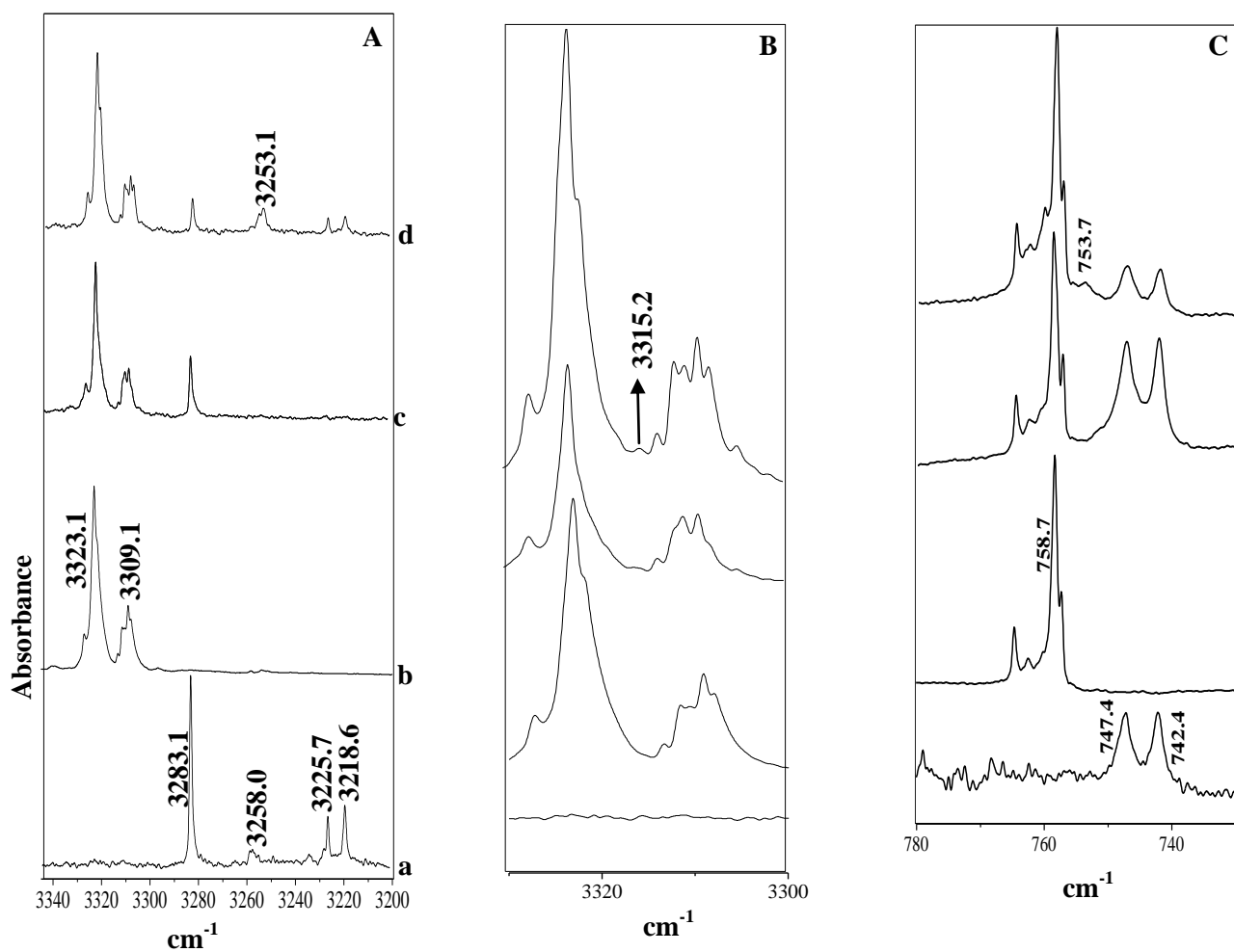


Fig.3.3. Panel A (a) $C_2H_2:N_2$ annealed (1:1000) (b) PhAc: N_2 annealed (1:1000) (c) $C_2H_2:PhAc:N_2$ (1:1:1000) at 12K (d) annealed spectrum of (c). **Panel B** (a) $C_2H_2:N_2$ annealed (1:1000) (b) PhAc: N_2 annealed (1:1000) (c) $C_2H_2:PhAc:N_2$ (1:1:1000) at 12K (d) annealed spectrum of (c). **Panel C** (a) $C_2H_2:N_2$ annealed (1:1000) (b) PhAc: N_2 annealed (1:1000) (c) $C_2H_2:PhAc:N_2$ (1:1:1000) at 12K (d) annealed spectrum of (c). **Panels A and B** show the stretching regions of C_2H_2 and PhAc, respectively. **Panel C** displays the bending region of C_2H_2 .

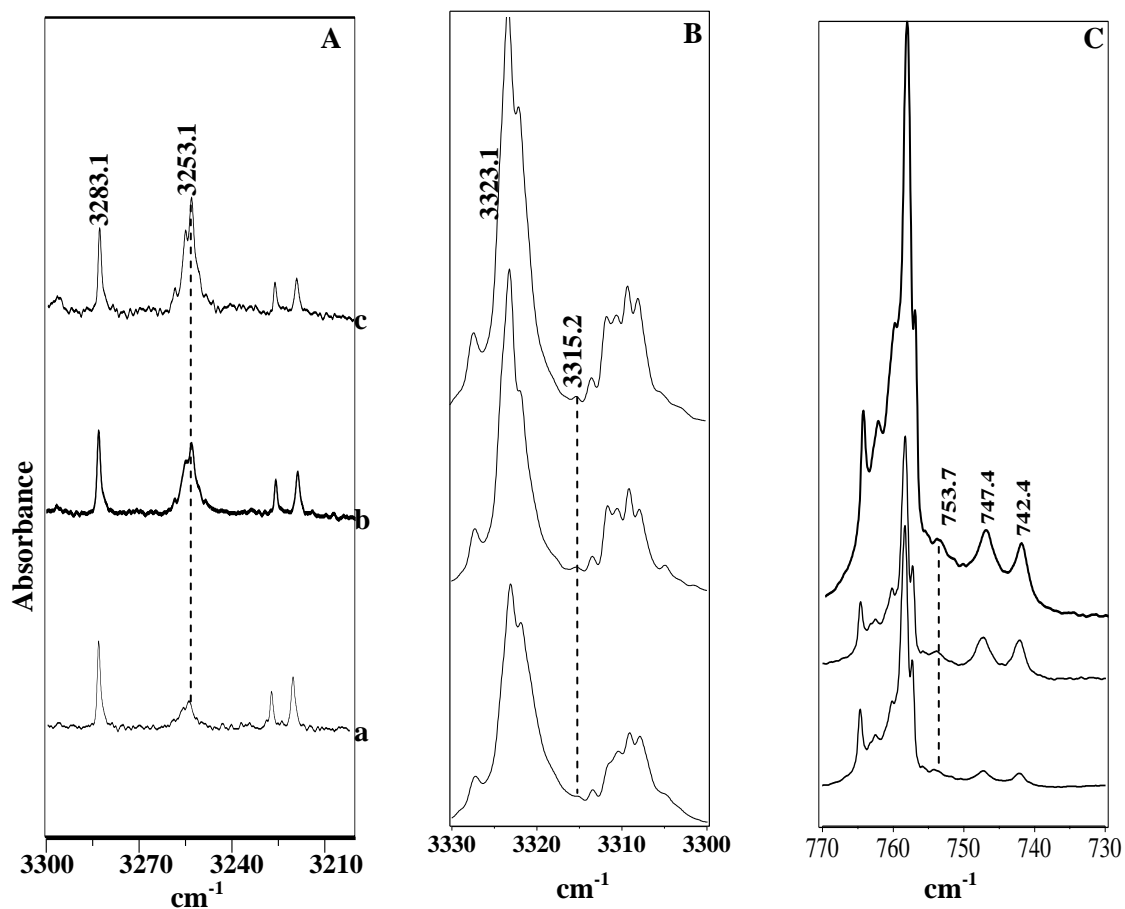


Fig.3.4. Matrix isolation infrared spectra showing the concentration dependence over the spectral region 3300-3200 cm⁻¹ **Panel A** of a) PhAc:C₂H₂:N₂ (0.25:0.1:1000), b) PhAc:C₂H₂:N₂ (0.5:0.1:1000) and c) PhAc:C₂H₂:N₂ (1:0.2:1000). **Panel B** shows the spectral region 3330-3300 cm⁻¹ of a) PhAc:C₂H₂:N₂ (1:0.25:1000), b) PhAc:C₂H₂:N₂ (3:0.25:1000) and c) PhAc:C₂H₂:N₂ (6:0.5:1000). **Panel C** shows the spectral region 770-730 cm⁻¹ of (a) PhAc:C₂H₂:N₂ (1:0.25:1000), b) PhAc:C₂H₂:N₂ (3:0.25:1000) and c) PhAc:C₂H₂:N₂ (6:0.5:1000). Sample to matrix ratio is given in parenthesis.

3.5.2 $\equiv\text{C-H}$ stretch in PhAc submolecule

The $\equiv\text{C-H}$ stretching frequency for free PhAc is observed at 3323.1 cm^{-1} which on complex formation with C_2H_2 appears as a weak feature at 3315.2 cm^{-1} . The corresponding scaled computed frequency for this mode in complex 3, occurs at 3317.0 cm^{-1} which indicates a red-shift of 6.1 cm^{-1} and which is therefore in good agreement with the experimentally observed shift of 8.0 cm^{-1} . Once again it may be observed from Table 3.3 and Fig.3.5, that complex 3 best fits with the above assignment. The small shifts observed for the C-H stretch in PhAc indicates this submolecule to be the proton acceptor, which is consistent with the structure of complex 3.

3.5.3 $\equiv\text{C-H}$ bend in C_2H_2 submolecule

The doubly degenerate bending mode of C_2H_2 in N_2 matrix appears as a doublet at 742.4 cm^{-1} and 747.4 cm^{-1} . The double degeneracy of this mode in free C_2H_2 is split in the matrix, due to the lowering of symmetry in the N_2 matrix cage. The $\equiv\text{C-H}$ bending mode of the C_2H_2 submolecule in the complex, occurs at 753.7 cm^{-1} in N_2 matrix. As can be seen from Table 3.3 and Fig.3.5, this feature matches excellently with the computed feature of 753.6 cm^{-1} assigned to complex 3.

3.5.4 $\equiv\text{C-H}$ bend in PhAc submolecule

The $\equiv\text{C-H}$ bend of PhAc in the N_2 matrix appears at 758.7 cm^{-1} . On complex formation, this mode is marginally blue shifted ($<2\text{ cm}^{-1}$); a shift so small that it is hardly discernible in the experiments. Hence we refrain from making any assignment for the $\equiv\text{C-H}$ bend of the PhAc submolecule in PhAc- C_2H_2 .

Studies on C_2H_2 -PhAc_D adduct

Experiments were performed on C_2H_2 -PhAc_D with a view to studying the effect of isotopic substitution on these complexes.

3.5.5 $\equiv\text{C-D}$ stretch in PhAc_D

Figure 3.6 (Panel A) shows the IR spectra over the region $2620\text{-}2585\text{ cm}^{-1}$, where the C-D stretch of PhAc_D is observed. The feature appears at 2600 cm^{-1} in free PhAc_D and is shifted to 2594.5 cm^{-1} in the complex. The corresponding scaled computed frequency for this feature for complex 3 occurs at 2595.4 cm^{-1} . The excellent agreement for the feature of the isotopic species lends credence to our assignment and to our conclusion that complex 3 is observed in our experiments. Panel B shows the IR spectra over the region $2620\text{-}2580\text{ cm}^{-1}$ in the Ar matrix and

the feature at 2595.4 cm^{-1} can be assigned to the $\text{PhAc}_D\text{-C}_2\text{H}_2$ adduct which also shows a concentration dependence.

The modes of the C_2H_2 submolecule in the $\text{C}_2\text{H}_2\text{-PhAc}_D$ complex show very similar shifts as were observed in the $\text{C}_2\text{H}_2\text{-PhAc}$ complex discussed above, which is depicted in Table 3.3. Hence the discussion of the modes of the C_2H_2 submolecule is not presented for the isotopic experiments.

3.6. AIM Analysis

The theory of “atoms in molecules” (AIM) is a useful tool in the interpretation of charge density. To further examine the nature of $\text{H}\cdots\pi$ interaction in $\text{C}_2\text{H}_2\text{-PhAc}$ complexes, we used the AIM theory introduced by Bader.²³⁻²⁵ Using the optimized geometry of the $\text{H}\cdots\pi$ complexes computed at M06-2X/aug-cc-pVDZ level, we searched for a (3,-1) bond critical point (BCP) (Fig.3.7).

The electron density, $\rho(r_c)$ and $\nabla^2\rho(r_c)$ (defined as sum of the Hessian eigenvalues) were analyzed at the bond critical point for all the complexes 1,2,3 and 4 (Table 3.4). The topological criteria for the existence of hydrogen bonding were proposed by Koch and Popelier.³² According to the criteria, the H-bonds should have an electron density at the H-Y(BCP) in the range 0.002-0.034 a.u. and $\nabla^2\rho(r_c)$ within 0.024-0.139 a.u. It has been observed that for closed shell interactions, as found in ionic, hydrogen bonded and van der Waals molecules, $\nabla^2\rho(r_c)$ should be positive and the charge density at the bond critical point should be low.

In all the $\text{C}_2\text{H}_2\text{-PhAc}$ complexes, the values of ρ fall in the range proposed by Koch and Popelier. It may be noted that the electron density ρ is largest for the bond critical point corresponding to the $\text{H}\cdots\pi$ interaction in complex 3, which was observed in our experiments.

An examination of $|\lambda_1/\lambda_3|$ values shows this ratio to be small, which is indicative of the fact that the charges are not accumulated between the atoms in the bonding region but more on the atoms. This observation leads to the conclusions that the $\text{C}_2\text{H}_2\text{-PhAc}$ bonding receives contributions from electrostatic interactions. Table 3.4 presents the data of the AIM analysis at M06-2X/aug-cc-pVDZ.

Table 3.3. Experimental, computed scaled^a vibrational frequencies and mode assignments for the C₂H₂-PhAc complexes in N₂ matrix at M06-2X/aug-cc-pVDZ.

Experimental		Computed				Assignment
C ₂ H ₂	Complex	Complex 1	Complex 2	Complex 3	Complex 4	
3283.1	3253.1 (-30.0)^b	3267.9 (-15.2)	3275.0 (-8.1)	3253.2 (-29.9)	3269.8 (-13.3)	≡C-H stretch in C ₂ H ₂
742.4	753.7 (11.3)	761.0 (18.6)	755.0 (12.6)	753.6 (11.2)	754.4 (12.0)	≡C-H bend in C ₂ H ₂
PhAc						
3323.1	3315.2 (-8.0)	3320.6 (-2.5)	3293.0 (-30.1)	3317.0 (-6.1)	3322.0 (-1.1)	≡C-H stretch in PhAc
758.7	-	760.1 (1.4)	759.4 (0.7)	760.0 (1.3)	759.7 (1.0)	-CH out of plane bending in benzene
PhAc _D						
2600.0	2594.5 (-5.5)	2598.2 (-1.8)	2577.3 (-22.7)	2595.4 (-4.6)	2599.1 (-0.9)	≡C-D stretch in PhAc _D

^aScaling factor in the C-H asym str. of C₂H₂=0.9567; C-H str. of PhAc=0.9499; C-D str. of PhAc_D=0.9491.

^b $\Delta\nu = \nu(\text{complex}) - \nu(\text{monomer})$ are given in parenthesis.

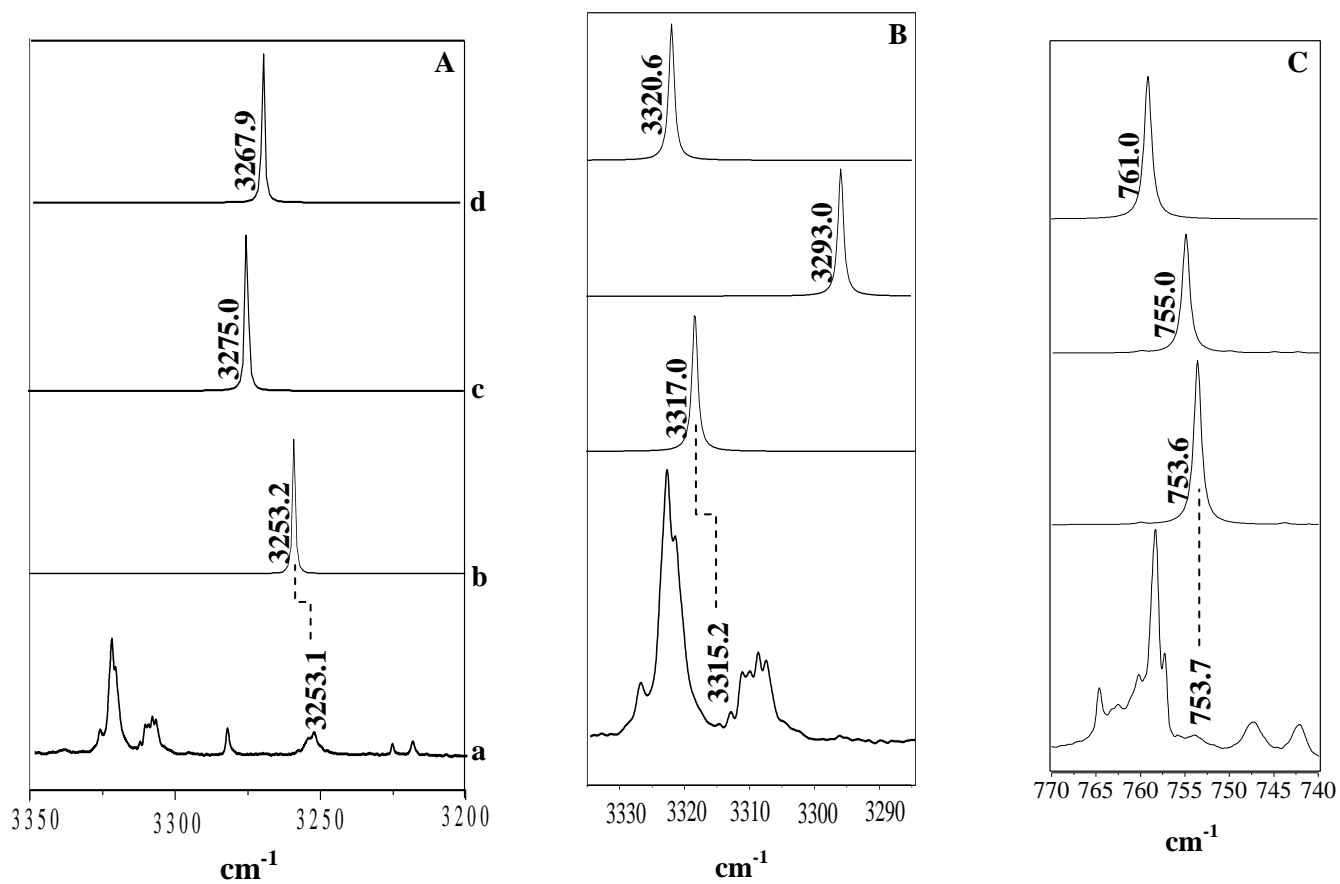


Fig. 3.5. Matrix isolation infrared annealed spectra of PhAc-C₂H₂ in a N₂ matrix over the region 3350-3200 cm⁻¹ (Panel A), 3335-3285 cm⁻¹ (Panel B) and 770-740 cm⁻¹ (Panel C). Spectra shown in (a) is experimental spectra recorded after annealing the matrix; (b), (c) and (d) show the computed spectra of complexes 3, 2 and 1 respectively.

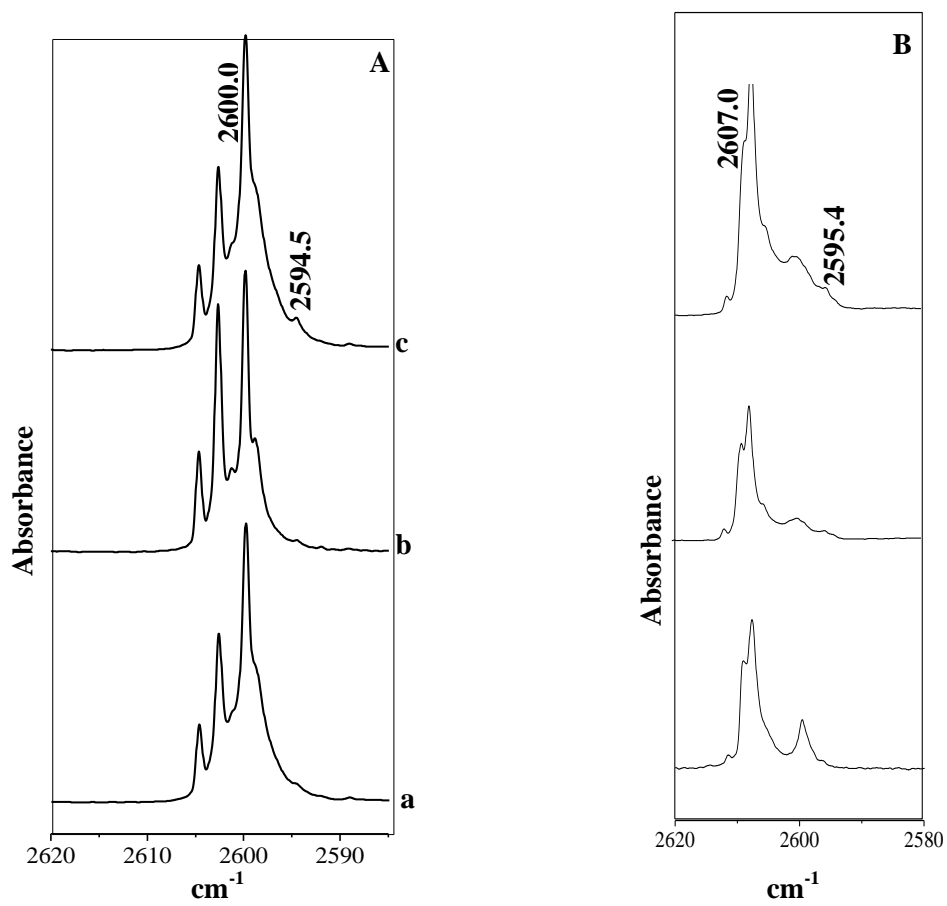


Fig.3.6. Matrix isolation infrared spectra showing the concentration dependence over the spectral region 2620-2580 cm⁻¹ (Panel A) of a) PhAc_D:C₂H₂ (0.25:0.1:1000), b) PhAc_D:C₂H₂ (0.5:0.1:1000) and c) PhAc_D:C₂H₂ (1:0.2:1000). Panels A and B show the N₂ and Ar spectra respectively.

3.7. Energy Decomposition Analysis (EDA)

Energy decomposition analysis gives the physical origin of the inter/intra-molecular interactions in a complex. EDA was done for all three complexes to understand the components of total interaction energy in terms of electrostatic energy, exchange energy, repulsion energy, polarization energy and dispersion energy. LMO-EDA scheme of analysis was employed using GAMESS.²⁷

Table 3.5 gives the partitioning of the different energy components at MP2/aug-cc-pVDZ. As shown in the table, the total interaction energy between PhAc and C₂H₂ is in the range of -2.21 to -5.87 kcal/mol. It can be seen that these complexes receive stabilization from mainly dispersion interactions. The strongest stabilizing interaction in all the complexes is dispersion followed by electrostatic interactions, as can be seen from the ratios of E_{ES}/E_{Total} and E_{Disp}/E_{Total} (Table 3.5).

That electrostatic interaction does play an important role in the stabilization of the PhAc-C₂H₂ complexes, is consistent with the small values of $|\lambda_1/\lambda_3|$ values discussed earlier through the AIM calculations. The polarization component, as can be seen from the table, makes the smallest contribution to the stabilization energy. Our conclusions are consistent with the observations of Nishio, who had pointed out that dispersion interactions play an important role in the stabilization of the C-H... π complexes, which belong to the category of soft acid-soft base interaction.³³

3.8. Natural Bond Orbital Analysis (NBO)

NBO Analysis was performed for all the complexes at M06-2X/aug-cc-pVDZ to understand the role of delocalization interactions in the stability of the complexes²⁸(Table 3.6). Second order perturbation energies of the various donor-acceptor orbital interactions were computed. These orbital interaction energies are a function of both the energy difference between the donor and acceptor orbitals and their overlap.

In case of complex 3, which was the one observed experimentally, the strongest delocalization interaction was between the acetylenic π system in PhAc and the σ^* orbital on C-H in C₂H₂, which essentially reflects the H- π interaction. This interaction had the smallest energy difference between the donor-acceptor orbitals (D-A) of 0.92 a.u. and an overlap between the two orbitals of 0.039 a.u.

Table 3.4. AIM calculations showing the electron densities $\rho(r)$ and $\nabla^2\rho(r)$ at the bond critical point for PhAc-C₂H₂ complexes at M06-2X/aug-cc-pVDZ.

M06-2X	$\rho(r_c)$	$\nabla^2\rho(r_c)$	λ_1	λ_2	λ_3	λ_1/λ_3
Complex 1	0.0077	0.0244	-0.0051	-0.0010	0.0305	0.167
Complex 2	0.0075	0.0217	-0.0058	-0.0046	0.0321	0.181
Complex 3	0.0085	0.0238	-0.0066	-0.0048	0.0352	0.188
Complex 4	0.0067	0.0218	-0.0033	-0.0011	0.0262	0.126

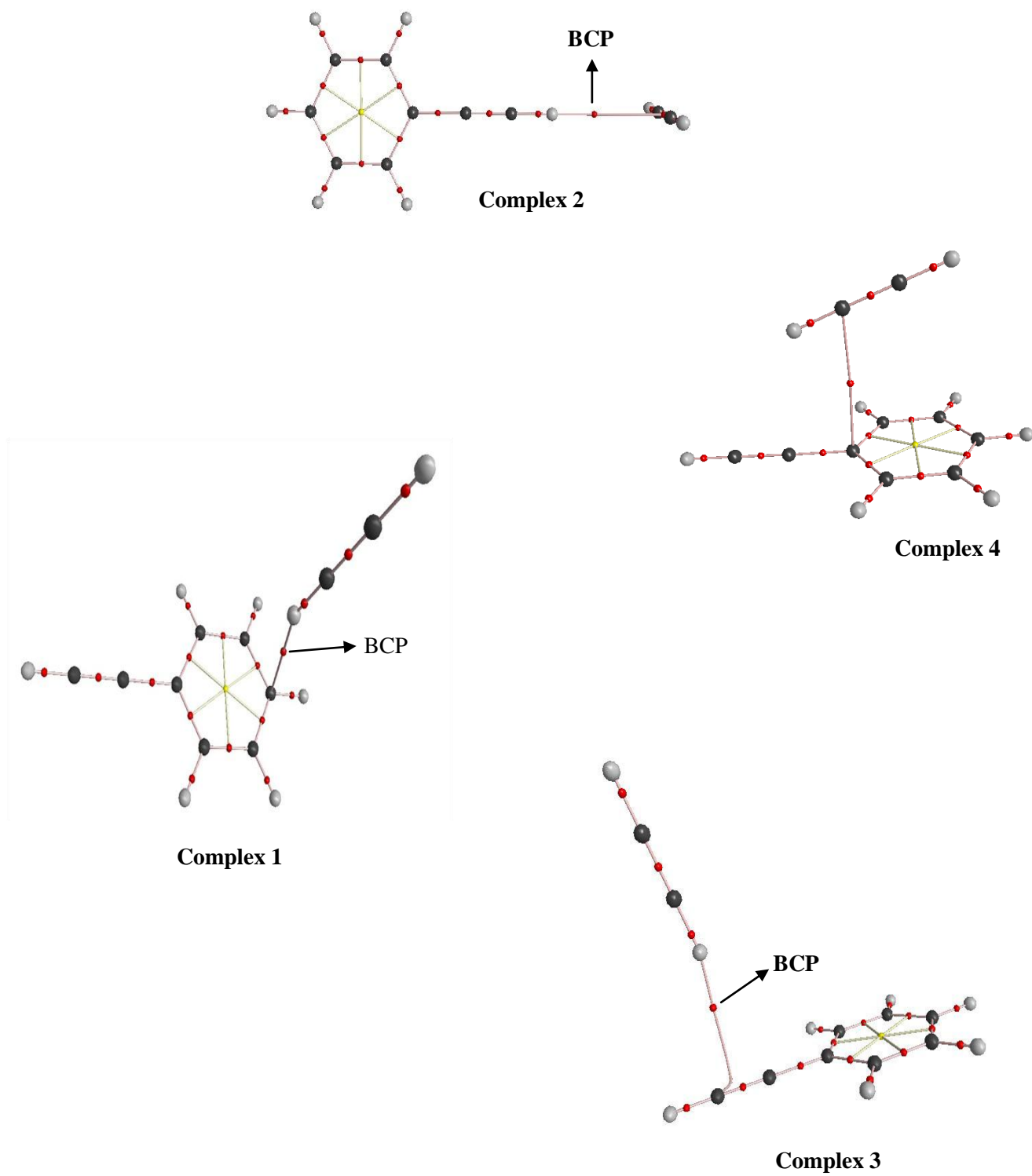


Fig.3.7. AIM analysis of the complexes at M06-2X/aug-cc-pVDZ.

It may be worthwhile mentioning that the pK_a (as reported by Bordwell *et al*)³⁴ of C_2H_2 is 25, while that of PhAc is 26.5, which is consistent with complex 3 being the global minimum, as it is in this complex that the more acidic C_2H_2 serves as the proton donor. However, if gas phase acidities are taken into account, which is what would be relevant in our matrix isolation experiments, a further explanation is warranted. The gas phase acidities for a number of molecules, have been expressed as ΔH_0 for the reaction



ΔH_0 for C_2H_2 and PhAc are 375.4 and 370.3 kcal/mol respectively³⁵, implying that in the gas phase, PhAc is more acidic than C_2H_2 , which should therefore have favoured complex 2 over complex 1 or 3. This conclusion is contrary to our experimental finding, which shows that in the complex we have observed, it is C_2H_2 that donates its proton to PhAc. It is likely that a secondary interaction between the C-H moiety of the phenyl and the π cloud of C_2H_2 renders complex 3 to be more stable than complex 2. NBO analysis also indicates a small orbital interaction between the C-H σ orbital and the π^* of the acetylenic system of C_2H_2 (Table 3.6).

In complex 4, the donor-acceptor orbital interactions are quite complicated with a number of interactions contributing to the overall stability of the complexes, hence the interaction of this complex is not shown in the table.

3.9. Conclusions

$H \cdots \pi$ complex of C_2H_2 and PhAc has been observed in our matrix isolation experiments. Our experiments provided evidence for the formation of complex 3 in the matrix, in which C_2H_2 was found to be the proton donor to the π -cloud of acetylenic group in PhAc. The formation of this complex was evidenced by shifts in the $\equiv C-H$ asymmetric stretch of C_2H_2 , $\equiv C-H$ stretch of PhAc and $\equiv C-H$ bend of C_2H_2 . In particular, the *large shift* in the vibrational frequency of the $\equiv C-H$ asymmetric stretch of C_2H_2 provided unequivocal evidence that C_2H_2 was the proton donor (complex 3). Experiments using $PhAc_D$ also confirmed, through isotopic shift data, the above observation. At the M06-2X/aug-cc-pVDZ level, both complex 1, where the C_2H_2 served as the proton donor to the π -cloud of phenyl ring and complex 3, where C_2H_2 served as the proton donor to the π -cloud of acetylenic group in PhAc were nearly isoenergetic and the lowest energy structures. The structure where PhAc acted as the proton donor to the acetylenic π -cloud was the highest energy structure at both levels. A stacked structure (complex 4) was also indicated at the

M06-2X and MP2 levels. However, no evidence was found in the matrix for complexes 1, 2 and 4. The role of secondary interactions in deciding preferences of isomers of the complexes is also apparent as has been explained. The PhAc-C₂H₂ system thus gives an insight into the C-H... π interactions occurring in a multifunctional π system.

Table 3.5. Energy Decomposition analysis of PhAc-C₂H₂ complexes at MP2/aug-cc-pVDZ^a

Complex	E_{ES}	E_{ER}	E_{Pol}	E_{Disp}	E_{Total}	E_{ES}/E_{Total}	E_{Disp}/E_{Total}	E_{Pol}/E_{Total}
Complex 1	-2.83	5.29	-2.16	-6.17	-5.87	0.48	1.05	0.37
Complex 2	-2.02	3.50	-1.50	-2.19	-2.21	0.91	0.99	0.68
Complex 3	-3.78	5.45	-1.58	-3.92	-3.83	0.99	1.02	0.41
Complex 4	-2.86	7.50	-1.63	-7.76	-4.75	0.60	1.63	0.34

^aAll energies are in kcal/mol.

Table 3.6. NBO analysis for the PhAc-C₂H₂ heterodimers, performed at M06-2X/aug-cc-pVDZ level of theory. The atom numbering indicated in the table is as shown in Fig. 2. E is the second order perturbation energy, E(j)-E(i) is the donor-acceptor energy difference and F(i,j) is the overlap between the donor and acceptor orbitals.

Complex	Orbitals involved		E (kcal/mol)	E(j)-E(i) a.u.	F(i,j) a.u.
	Donor	Acceptor			
Complex 1	C ₂ -C ₃	H ₁₅ -C ₁₆	0.93	0.88	0.028
Complex 2	C ₁₅ -C ₁₆	C ₁₃ -H ₁₄	1.73	0.94	0.036
Complex 3	C ₁₂ -C ₁₃	H ₁₅ -C ₁₆	2.03	0.92	0.039
	C ₁ -H ₇	C ₁₆ -C ₁₇	0.22	0.81	0.022

REFERENCES

- (1) Sedlak, R.; Hobza, P.; Patwari, G.N. Hydrogen-Bonded Complexes of Phenylacetylene with Water, Methanol, Ammonia, and Methylamine. The Origin of Methyl Group-Induced Hydrogen Bond Switching. *J. Phys. Chem. A* **2009**, *113*, 6620-6625.
- (2) Singh, P.C.; Patwari, G.N. IR-UV Double Resonance Spectroscopic Investigation of Phenylacetylene-Alcohol Complexes. Alkyl Group Induced Hydrogen Bond Switching. *J. Phys. Chem. A* **2008**, *112*, 5121-5125.
- (3) Maity, S.; Patwari, G.N.; Karthikeyan, S.; Kim, K.S. Binary complexes of tertiary amines with phenylacetylene. Dispersion wins over electrostatics. *Phys. Chem. Chem. Phys.* **2010**, *12*, 6150-6156.
- (4) Singh, P.C.; Bandyopadhyay, B.; Patwari, G.N. Structure of the phenylacetylene-water complex as revealed by Infrared-Ultraviolet Double Resonance Spectroscopy. *J. Phys. Chem. A* **2008**, *112*, 3360-3363.
- (5) Maity, S.; Sedlak, R.; Hobza, P.; Patwari, G.N. Infrared-Optical double resonance spectroscopic measurements and high level ab initio calculations on a binary complex between phenylacetylene and borane-trimethylamine. Understanding the role of CH \cdots π interactions. *Phys. Chem. Chem. Phys.* **2009**, *11*, 9738-9743.
- (6) Singh, P.C.; Patwari, G.N. Electronic and Vibrational Spectroscopic Investigation of Phenylacetylene-Amine Complexes: Evidence for the Diversity in the Intermolecular Structures. *J. Phys. Chem. A* **2008**, *112*, 4426-4431.
- (7) Guin, M.; Patwari, G.N.; Karthikeyan, S.; Kim, K.S. A π stacked phenylacetylene and 1,3,5-triazine heterodimer: a combined spectroscopic and *ab initio* investigation. *Phys. Chem. Chem. Phys.* **2009**, *11*, 11207-11212.
- (8) Maity, S.; Patwari, G.N.; Sedlak, R.; Hobza, P. A π -stacked phenylacetylene dimer. *Phys. Chem. Chem. Phys.* **2011**, *13*, 16706-16712.
- (9) Maity, S.; Guin, M.; Singh, P.C.; Patwari, G.N. Phenylacetylene: A hydrogen bonding chameleon. *Chem. Phys. Chem.* **2011**, *12*, 26-46.
- (10) Maity, S.; Dey, A.; Patwari, G.N.; Karthikeyan, S.; Kim, K.S. A Combined Spectroscopic and ab initio Investigation of Phenylacetylene-Methylamine Complex. Observation of σ and π Type Hydrogen Bonded Configurations and Fluorescence Quenching by Weak CH \cdots N Hydrogen

Bonding. *J. Phys. Chem. A.* **2010**, *114*, 11347-11352.

(11)Goswami, M.; Arunan, E. Microwave spectroscopic and theoretical studies on the phenylacetylene-H₂O complex: C-H \cdots O and O-H \cdots π hydrogen bonds as equal partners. *Phys. Chem. Chem. Phys.* **2011**, *13*, 14153-14162.

(12)Goswami, M.; Arunan, E. Microwave Spectrum and Structure of C₆H₅CCH \cdots H₂S complex. *J. Mol. Spec.* **2011**, *268*, 147-156.

(13)Engdahl, A.; Nelander, B. A matrix isolation study of the benzene-water interaction. *J. Phys. Chem. A* **1985**, *89*, 2860-2864.

(14)Engdahl, A.; Nelander, B. The acetylene-water complex: A matrix isolation study. *Chem.Phys.Lett.* **1983**,*100*,129-132.

(15)Sundararajan, K.; Viswanathan, K.S. A matrix isolation and *ab initio* study of the C₂H₂-MeOH complex. *J. Mol. Struct.* **2006**, *798*, 109-116.

(16)Sundararajan, K.; Viswanathan, K.S.; Jose, K.V.J.; Gadre, S.R. Effect of matrix on IR frequencies of acetylene and acetylene-methanol complex: Infrared matrix isolation and *ab initio* study. *J. Chem. Phy.* **2007**, *127*, 104501-104505.

(17)Jemmis, E.D.; Giju, K.T.; Sundararajan, K.; Sankaran, K.; Vidya, V.; Viswanathan, K.S.; Leszczynski, J. An *ab initio* and matrix isolation infrared study of the 1:1 C₂H₂-CHCl₃ adduct. *J. Mol. Str.* **1999**, *510*, 59-68.

(18) Sankaran, K.; Viswanathan, K.S.; Kulkarni, A.D.; Gadre, S.R. H \cdots π complexes of acetylene-ethylene: A matrix isolation and computational study. *J. Phys. Chem. A.* **2002**, *106*, 1504-1510.

(19)Sundararajan, K.; Viswanathan, K.S.; Kulkarni, A.D.; Gadre, S.R. H \cdots π complexes of acetylene-benzene: a matrix isolation and computational study. *J. Mol. Struct.* **2002**, *613*, 209-222.

(20)M.J.Frisch, G.W.Trucks, H.B.Schlegel, G.E.Scuseria, M.A.Robb, J.R.Cheeseman, G. Scalmani, V.Barone, B.Mennucci, G.A.Petersson, H.Nakatsuji, M.Caricato, X.Li, H.P. Hratchian, A.F. Izmaylov, J. Bloino, G. Zheng, J.L. Sonnenberg, M.Hada, M.Ehara, K.Toyota, R.Fukuda, J.Hasegawa, M.Ishida, T.Nakajima, Y.Honda, O.Kitao, H.Nakai, T.Vreven, J.J.A. Montgomery, J.E.Peralta, F.Ogliaro, M.Bearpark, J.J.Heyd, E.Brothers, K.N. Kudin, V.N. Staroverov, R.Kobayashi, J.Normand, K.Raghavachari, A.Rendell, J.C.Burant, S.S. Iyengar, J. Tomasi, M.Cossi, N.Regga, J.M.Millam, M.Klene, J.E.Knox, J.B. Cross, V.Bakken, C.Adamo,

J.Jaramillo, R.Gomperts, R.E.Stratmann, O.Yazyev, A.J.Austin, R.Cammi, C.Pomelli, J.W.Ochterski, R.L.Martin, K.Morokuma, V.G.Zakrzewski, G.A.Voth, P.Salvador, J.J. Dannenberg, S.Dapprich, A.D.Daniels, O.Farkas, J.B.Foresman, J.V.Ortiz, J.Cioslowski, D.J. Fox, Gaussian 09 Revision A.1, Gaussian Inc. Wallingford CT,2009.

(21) Boys, S.B.; Bernardi, F. The calculation of small molecular interactions by the differences of separate total energies. Some procedures with reduced errors. *Mol.Phys.* **1970**, *19*, 553-566.

(22) The spectra were simulated using SYNSPEC made available by K. Irikura, National Institute of Standards and Technology, Gaithersburg, MD 20899, USA, **1995**.

(23) Bader, R.F.W. Atoms in Molecules. A Quantum Theory (Clarendon Press, Oxford, 1994).

(24) Bone, R.G.A.; Bader, R.F.W. *J. Phys.Chem.* **1996**, *100*, 10892-10911.

(25) F.Bieger-König, D.Bayles, and J.Schönbohn, AIM2000 (Version 1.0); Chemical Adviser: R.F.W.Bader.

(26) Su, P.F.; Li, H. Energy Decomposition Analysis of Covalent Bonds and Intermolecular Interactions. *J. Chem. Phys.* **2009**, *131*, 014102-014115.

(27) Schmidt, M.W. et. al. *J. Comp. Chem.* **1993**, *14*, 1347-1363.

(28) Glendening, E.D.; Reed, A. E.; Carpenter, J.E.; Weinhold, F. NBO Version 3.1.

(29)Helgaker, T.; Klopper, W.; Koch, H.; Noga, J. Basis set convergence of correlated calculations on water. *J. Chem. Phys.* **1997**,*106*, 9639-9646.

(30)Jose, K.V.; Gadre, S.R.; Sundararajan, K.; Viswanathan, K.S. Effect of Matrix on IR Frequencies of acetylene and acetylene-methanol complex: Infrared Matrix Isolation and ab initio Study. *J. Chem. Phys.* **2007**,*127*,104501-104505.

(31)Stearns, J.A.; Zwier, T.S. Infrared and Ultraviolet Spectroscopy of Jet-Cooled ortho-, meta- and para- Diethynylbenzene. *J. Phys. Chem. A.* **2003**, *107*, 10717-10724.

(32)Koch, U.; Popelier, P.L.A. Characterization of CH \cdots O hydrogen bonds on the basis of charge density. *J. Phys. Chem.* **1995**, *99*, 9747-9754.

(33)Nishio, M. The CH/ π hydrogen bond in chemistry. Conformation, supramolecules, optical resolution and interactions involving carbohydrates. *Phys. Chem. Chem. Phys.* **2011**, *13*, 13873-13900.

(34) Bordwell, F.G.; Matthews, W.S. Equilibrium acidities of carbon acids II. Hydrocarbon Indicators, Phenylacetylene and Other Carbon Acids in the 20-27 pK Region. *J. Am. Chem. Soc.*, **1974**, *96*, 1214–1216.

(35) Bartmess, J.E.; Scott, J.A.; McIver, R.T. Scale of Acidities in the Gas Phase from Methanol to Phenol. *J. Am. Chem. Soc.* **1979**, *101*, 6046-6056.

CHAPTER 4: STUDY OF HYDROGEN BONDED INTERACTIONS IN BORAZINE ACETYLENE

4.1. Introduction

Borazine ($B_3N_3H_6$) or *s*-triazaborane, is an inorganic compound isoelectronic with benzene (C_6H_6), obtained by substituting each C-C linkage in the latter, by a B-N linkage. In contrast to C_6H_6 , in which the π electrons are delocalized around the six carbon atoms, the electrons tend to be localized around nitrogen atoms in $B_3N_3H_6$. $B_3N_3H_6$ has both electron rich *p* orbitals centered on nitrogen and electron deficient *p* orbitals centered on boron. Therefore, it behaves as an amphoteric π electron system. $B_3N_3H_6$, unlike its organic counterpart, is soluble in polar solvents. It is an important industrial compound, serving as a starting material for some ceramics and as a precursor for growing boron nitride thin films.¹⁻²

The similarities and differences between the organic and inorganic counterparts have attracted comparisons, resulting in many theoretical and experimental studies on these systems. Kartha *et al* studied the infrared spectra of $B_3N_3H_6$ and its isotopic variants.³ Niedenzu *et al* reported an extensive gas phase infrared and liquid Raman spectroscopic studies of various isotopically labelled forms of $B_3N_3H_6$.⁴ They confirmed the findings of Kartha *et al* and assigned all the active fundamentals. Perhaps the first matrix isolation study on $B_3N_3H_6$ was done by Kaldor and Porter when they recorded the infrared spectra of $B_3N_3H_6$ in an Ar matrix.⁵ Recently, we reported the interaction of $B_3N_3H_6$ with H_2O and compared this system with the $C_6H_6-H_2O$ system.⁶ While the $C_6H_6-H_2O$ system manifested an $H\cdots\pi$ complex as the global minimum, the most stable complex in the $B_3N_3H_6-H_2O$ system showed an $N-H\cdots O$ interaction. A major challenge in handling $B_3N_3H_6$ is its rather poor stability in ambient conditions, being extremely sensitive to moisture and decomposing fairly rapidly in the presence of water.

With $B_3N_3H_6$ and C_6H_6 displaying such interesting differences, it was appealing to compare the $B_3N_3H_6-C_2H_2$ system with the well studied $C_6H_6-C_2H_2$ system, which has been shown to display a $C-H\cdots\pi$ interaction. A number of studies are available in the literature involving $C-H\cdots\pi$ interactions, and they primarily involve the π cloud of C_2H_4 , C_2H_2 and aromatic ring systems.⁷⁻¹⁰ In the case of $C_2H_4-C_2H_2$, the C-H group of both C_2H_2 and C_2H_4 act as the proton donors and both types of structures were observed in the matrix isolation

experiments.⁷ C₆H₆-C₂H₂ has also been well studied, both computationally and experimentally, and matrix isolation experiments show the presence of the C-H... π complex, where the C-H of C₂H₂ serves as a proton donor to the π cloud of C₆H₆.⁸⁻⁹ B₃N₃H₆ and C₂H₂, both being capable of serving as proton donors or acceptors, the nature of the hydrogen bonded complexes formed, depends upon the competition between these interaction sites. B₃N₃H₆ has two possible sites for the formation of a hydrogen bond with C₂H₂. One is the N-H bond, which can serve as a proton donor to C₂H₂, forming an N-H... π bond. Alternatively, the π system in B₃N₃H₆ can act as a proton acceptor for the hydrogen in C₂H₂, with the formation of a C-H... π bond, much like the C₂H₄-C₂H₂ and C₆H₆-C₂H₂ systems.⁷⁻⁹ The relative preference of these possible sites and comparing the potential energy landscape of this system with that of the C-H... π systems prompted our study of the B₃N₃H₆-C₂H₂ system.

4.2. Experimental details

4.2.1 Synthesis of B₃N₃H₆

B₃N₃H₆ was prepared using the procedure of Li *et al*¹¹ which was suitably modified. A two necked 500 mL Schlenk flask, taken inside a glove box was charged with powdered (NH₄)₂SO₄ (Merck, $\geq 99\%$) (50 g, 378 mmol) and AlCl₃ (Sigma Aldrich, 99.99%) (1g, 7.5mmol). NaBH₄ (Sigma Aldrich, 98%) (20g, 529mmol) was placed in an addition funnel (250 mL) that was fixed on one neck of the Schlenk flask. A reflux condenser was attached to the other neck of the Schlenk flask. The entire set-up was mounted in an oil bath placed on a magnetic stirrer. Dry tetraglyme (Sigma Aldrich $\geq 99\%$) (250 mL) was added to the addition funnel and the solution of NaBH₄ so obtained, was added drop wise, to the mixture of (NH₄)₂SO₄ and AlCl₃. During the addition, the temperature of the reaction flask was kept below 50°C. After complete addition of the solution, the contents of the Schlenk flask were stirred for three hours (between 40-45°C). This was followed by filtration of the mixture to yield a clear solution. The solution of B₃N₃H₆ in tetraglyme was used as such for the matrix isolation experiments, without distilling off the solvent, the reasons for which will be explained below.

While pure B₃N₃H₆ could have been isolated from the tetraglyme by distillation, the reactivity of B₃N₃H₆ towards moisture precluded such a strategy. B₃N₃H₆ in tetraglyme, on the other hand, was stable as it did not get into contact with water and hence could be used without concern of it decomposing. Hence the B₃N₃H₆ that was prepared was retained in the tetraglyme

and used as such. As abundant caution, the $B_3N_3H_6$ in tetraglyme was stored inside an Ar atmosphere glove box. The vapor pressure of tetraglyme being extremely low (<0.01 mm Hg at $20^\circ C$) relative to that of $B_3N_3H_6$ (259 mm Hg at $20^\circ C$), the vapor phase over the $B_3N_3H_6$ -tetraglyme system consisted entirely of $B_3N_3H_6$, which was used in preparing matrix isolated $B_3N_3H_6$.

4.2.2 Matrix isolation IR experiments

Details of the experimental procedure followed are given in Chapter 3. C_2H_2 (Sigma Gases & Services, 99.9%) was mixed with the matrix gas in a 1-L mixing chamber, at the desired matrix to sample ratio, using standard manometric procedures. The matrix gas/ C_2H_2 mixture was then deposited onto a KBr substrate, through one nozzle of a double jet deposition assembly, using a fine flow needle valve (Model: EVN 116, Pfeiffer vacuum). Typical deposition rates were ~ 2.5 mmol/hr of the matrix gas.

$B_3N_3H_6$ in tetraglyme was taken in a glass container attached to the second nozzle of the double jet assembly. $B_3N_3H_6$ /tetraglyme was subjected to several freeze-pump-thaw cycles before use. The temperature of the $B_3N_3H_6$ /tetraglyme sample was maintained at an appropriate temperature (typically $-60^\circ C$) to ensure isolation of $B_3N_3H_6$ in the matrix. At the temperature at which the $B_3N_3H_6$ /tetraglyme sample was maintained, only $B_3N_3H_6$ had sufficient vapor pressure to be deposited in the matrix, and not the less volatile tetraglyme.

After co-deposition of $B_3N_3H_6$ and the C_2H_2 /matrix gas mixture, the spectrum of the matrix isolated species was recorded using a Bruker Tensor 27 FTIR spectrometer operated at a resolution of 0.5 cm^{-1} . After a spectrum was recorded, the matrix was then warmed to a temperature of ~ 27 K, using the temperature controller unit (Lakeshore Instruments). The matrix was maintained at this temperature for about 30 minutes and then re-cooled to 12 K. The spectra of the matrix, thus annealed, were then recorded. Spectra of the $B_3N_3H_6$ and C_2H_2 deposited individually in the matrix were also recorded for comparison.

Since $B_3N_3H_6$ was taken in tetraglyme in which its concentration was not estimated, it was not possible to determine the exact matrix-to-sample ratios for $B_3N_3H_6$. However, since the variation of the vapor pressure of $B_3N_3H_6$ with temperature was known, it was possible to estimate the relative changes in the $B_3N_3H_6$ concentration in the matrix in the various experiments performed.

Typically the $B_3N_3H_6$ /tetraglyme solutions were maintained at $-60^\circ C$. Variation in the temperature around these values did not produce any change in the spectra, indicating that the sample was isolated in the matrix and no dimer or larger oligomers of $B_3N_3H_6$ were produced.

4.3. Computations

Theoretical calculations were performed for the $B_3N_3H_6-C_2H_2$ complexes using the GAUSSIAN-09¹² suite of programs. Interaction energies were computed for the complexes, corrected separately for BSSE (basis set superposition error) using the method proposed by Boys and Bernardi¹³ and ZPE (Zero point energies). The single point interaction energies were also calculated at the MP2/CBS and CCSD(T)/CBS limit for all the complexes, as shown in table 4.1.

The geometry of $B_3N_3H_6$, C_2H_2 and their hetero-dimers, shown in Fig. 4.1, was optimized using the MP2/aug-cc-pVDZ method without imposing any symmetry constraints. The resultant geometry was used in subsequent single-point energy calculations at MP2/aug-cc-pVTZ, MP2/aug-cc-pVQZ and CCSD(T)/CBS levels of theory. The core electrons were kept frozen in all the atoms. The procedure and equations used for the CBS extrapolation are described in Chapter 3. Table 4.2 shows selected structural parameters for the various $B_3N_3H_6-C_2H_2$ complexes at MP2/aug-cc-pVDZ level.

Vibrational frequencies of the complexes were computed, to assign the observed frequencies in the experiments and also to ensure that the computed geometries correspond to a minimum on the potential surface by checking that no imaginary frequencies were indicated. The computed frequencies of the monomer were scaled according to a mode by mode scaling procedure, already described in details in Chapter 3.

Atoms-in-molecules analysis (AIM) was performed using the AIM2000 package to explore the electron density (ρ) and laplacian ($\nabla^2\rho$) of electron density at the (3,-1) bond critical point.¹⁴⁻¹⁶ Localized Molecular Orbital Energy decomposition Analysis (LMOEDA)¹⁷ was performed using GAMESS¹⁸ to determine the contributions of the various components of interaction energy such as electrostatic, exchange, repulsion, polarization and dispersion towards the stabilization of the complex. Natural Bond Orbital (NBO) analysis (Version 3.1) which was implemented using Gaussian 09, helped in determining the role of various delocalization interactions in all the complexes.¹⁹

Table 4.1. Interaction energy values (ΔE in kcal/mol) obtained using the M06-2X, MP2 and CCSD(T) methods for different isomers of $B_3N_3H_6-C_2H_2$. The single point interaction energies at the MP2/CBS and CCSD(T)/CBS limit are also given for $B_3N_3H_6-C_2H_2$ and $C_6H_6-C_2H_2$ dimers.

Complex	M06-2X		MP2			CCSD(T)
	6-311++G(d,p)	aug-cc-pVDZ	6-311++G(d,p)	aug-cc-pVDZ	CBS	CBS
Stacked	-1.44/-1.15/-1.27	-1.58/-1.38/-1.16	-1.51/-1.06/-0.49	-2.59/-2.40/-0.97	-1.48	-1.14
T_{ac}	-1.98/-1.49/-1.81	-2.36/-1.90/-1.62	-2.02/-0.91/-0.58	-3.61/-3.04/-1.65	-1.97	-1.78
Bent CH\cdotsN	-2.14/-1.52/-1.12	-2.42/-1.95/-1.78	SP(-14.3)	-3.50/-2.82/-1.63	-2.07	-1.84
Bent NH\cdotsC	-2.06/-1.57/-1.90	-2.36/-1.91/-1.93	-2.08/-1.70/-0.90	-3.40/-2.89/-2.03	-2.50	-2.34
C₆H₆^{π}-C₂H₂^{π}	-	-	-	-	-1.87	-0.58
C₆H₆^{π}-C₂H₂^{CH}	-	-	-	-	-3.36	-2.72
C₆H₆^{CH}-C₂H₂^{π}	-	-	-	-	-0.96	-0.81

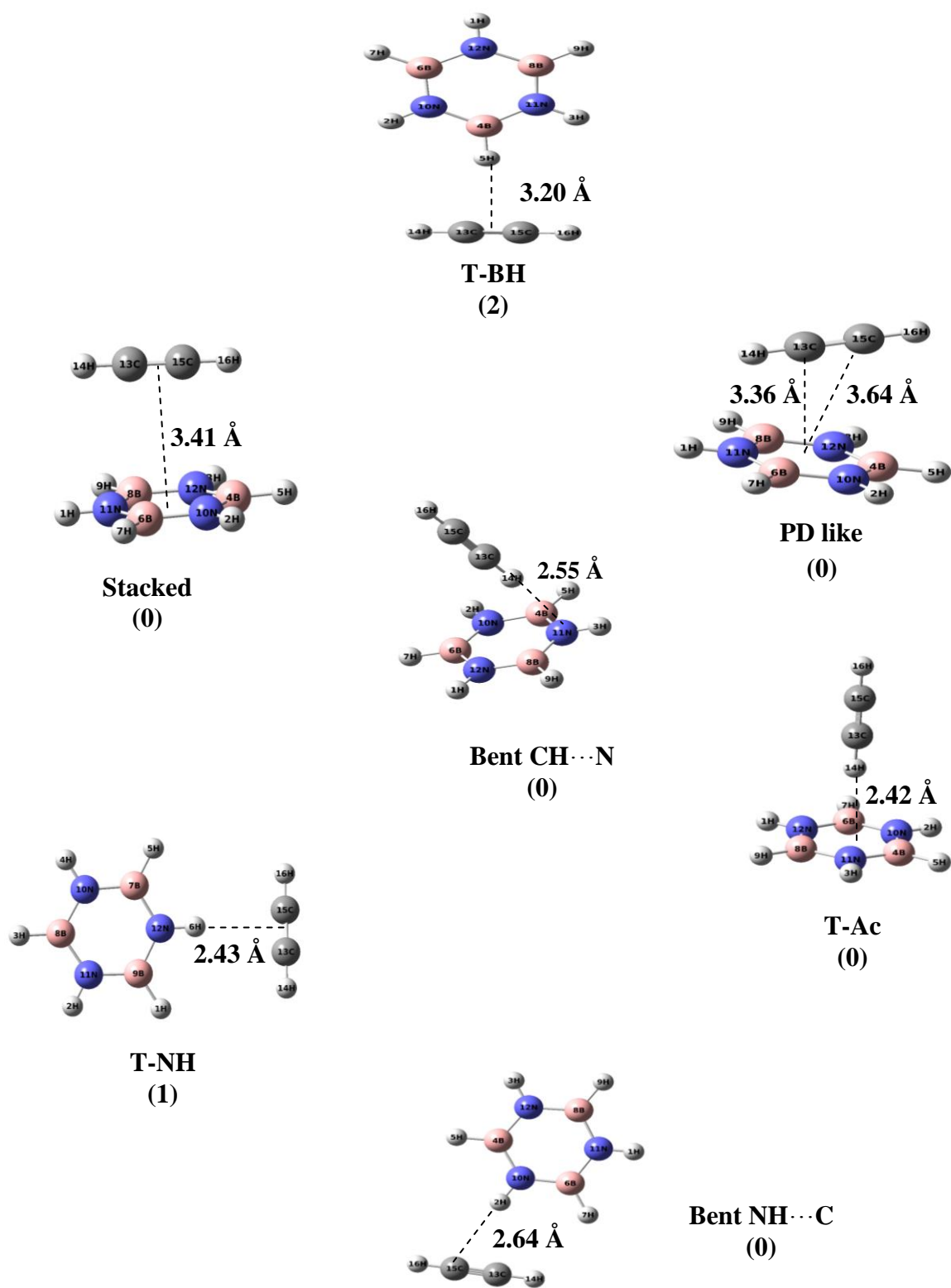


Fig.4.1. Possible geometries of the $B_3N_3H_6-C_2H_2$ complexes at MP2/aug-cc-pVDZ. The number of imaginary frequencies are given in parenthesis.

Table 4.2. Selected structural parameters for the B₃N₃H₆-C₂H₂ complexes at the MP2/aug-cc-pVDZ level of theory. The distances are given in angstroms (Å) and the angles are given in degrees (°) The atom numbering is as given in figure 4.1.

Bent NH...C	
C ₁₅ -H ₂	2.64 Å
N ₁₀ -C ₁₅ -C ₁₃	68.2°
N ₁₀ -H ₂ -C ₁₅	174.5°
N ₁₀ -H ₂ -C ₁₅ -C ₁₃	3.9°
Bent CH...N	
H ₁₄ -N ₁₁	2.55 Å
H ₁₄ -N ₁₁ -H ₃	104.1°
C ₁₃ -H ₁₄ -N ₁₁ -H ₃	-167.6°
T-Ac	
H ₁₄ -N ₁₀	2.80 Å
H ₁₄ -N ₁₁	2.80 Å
H ₁₄ -N ₁₂	2.80 Å
H ₁₄ -N ₁₁ -H ₃	120.4°
H ₁₄ -N ₁₀ -H ₂	120.4°
Stacked	
C ₁₃ -N ₁₁	3.51 Å
H ₁₆ -B ₄ -H ₅	87.1°
C ₁₃ -C ₁₅ -B ₄	108.4°
H ₁ -N ₁₁ -B ₆ -H ₇	-0.39°

4.4. RESULTS AND DISCUSSION

4.4.1 Computational

The optimized geometry of different $B_3N_3H_6-C_2H_2$ dimers is illustrated in Figure 4.1. As can be seen from Table 4.1, the global minimum corresponded to the isomer where the N-H bond of $B_3N_3H_6$ was directed toward one of the two carbon atoms of C_2H_2 , which is labeled as the **bent NH...C** structure. The interaction energy for the **bent NH...C** was found to be -2.34 kcal/mol at the CCSD(T)/CBS limit. The next most stable isomer corresponds to a geometry in which a C-H bond of C_2H_2 forms a weak hydrogen bond with a nitrogen atom of the $B_3N_3H_6$ molecule, which we have labeled as **bent CH...N**.

T-Shaped Geometry

The optimized geometry of the T-shaped $B_3N_3H_6-C_2H_2$ dimer is shown in Figure 4.1. The **T-Ac** geometry, in which C_2H_2 acts as the proton donor was found to be a stable minimum with an interaction energy of -1.78 kcal/mol, estimated at the CCSD(T)/CBS limit.

There are at least two other isomers possible in which $B_3N_3H_6$ acts as a proton donor. One is **T-BH**, in which a BH bond of $B_3N_3H_6$ interacts with the π -electron cloud of C_2H_2 and it is found to be a second order saddle point with frequencies $41.73i\text{ cm}^{-1}$ (A') and $19.00i\text{ cm}^{-1}$ (A''). Energetically, **T-BH** is the least stable structure of all the geometries considered in this study. The other conformer is **T-NH**, in which a NH bond of $B_3N_3H_6$ interacts with the π -electron cloud of C_2H_2 . It is a first order saddle point ($26.21i\text{ cm}^{-1}$).

Stacked and Parallel displaced Geometries

The optimized geometries for the stacked and the parallel displaced isomer at the MP2/aug-cc-pVDZ level of theory are shown in figure 4.1. The stacked geometry corresponded to the one where the π cloud of C_2H_2 was exactly on top of the partially delocalized π cloud of $B_3N_3H_6$, whereas in the parallel displaced geometry (PD like) geometry, the C_2H_2 is slightly displaced. In this structure, the distance between the center of the $B_3N_3H_6$ molecule and the two carbon atoms of the C_2H_2 molecule is found to be different. This indicates that the carbon atom of C_2H_2 does not prefer to sit on any nitrogen atom of $B_3N_3H_6$.

4.4.2 Experimental

Panels A, B and C in fig. 4.2 show the infrared spectra over the regions 3500-3400, 3300-3200 and 760-730 cm^{-1} , respectively. Trace 'a' in the figure shows the infrared spectrum of

matrix isolated $B_3N_3H_6$ in a N_2 matrix. Strong absorptions are observed at 3476.7 cm^{-1} and 3472.0 cm^{-1} , corresponding to the antisymmetric stretch of $B_3N_3H_6$ (**Panel A**). This is a doubly degenerate mode, split due to the matrix site effects. The bending mode of $B_3N_3H_6$ is observed at 735.3 cm^{-1} (**Panel C**). Trace ‘b’ shows the features due to the antisymmetric C-H stretch of C_2H_2 in N_2 matrix, with a strong feature at 3283 cm^{-1} (**Panel B**). In addition to the feature of the C_2H_2 monomer, we also observed a feature at 3257.6 cm^{-1} , which is due to the C_2H_2 dimer and two other features at 3218.6 and 3225.7 cm^{-1} , due to $C_2H_2\text{-H}_2O$ complex.²⁰ The bending modes of C_2H_2 are observed at 742.4 and 747.4 cm^{-1} (**Panel C**).

When $B_3N_3H_6$ and C_2H_2 were co-deposited, and the matrix then annealed, new product features were observed at 3443.6 cm^{-1} , 3263.0 cm^{-1} , 3271.3 cm^{-1} and 753.3 cm^{-1} (Traces ‘d’ and ‘e’). The product features mentioned above increased in intensity when the concentration of either of the two precursors, $B_3N_3H_6$ or C_2H_2 , was increased, thereby confirming that they were due to the $B_3N_3H_6\text{-C}_2H_2$ adducts.

4.5. Vibrational assignments

The experimentally observed product bands in the $B_3N_3H_6\text{-C}_2H_2$ co-deposition experiments were assigned based on the computed wavenumber values obtained at the MP2/aug-cc-pVDZ level of theory. As explained earlier, the computed frequencies for the complexes were scaled using scaling factors that were obtained by comparing the computed and experimental features of the monomer precursors. The mode assignments are given in Table 4.3 and the computed spectra of the various $B_3N_3H_6\text{-C}_2H_2$ complexes are given in Figure 4.3.

4.5.1 N-H stretch in $B_3N_3H_6$

As shown in trace ‘e’ (Fig. 4.2, Panel ‘A’), the doubly degenerate antisymmetric N-H stretch of $B_3N_3H_6$ appears at 3472.0 cm^{-1} and 3476.7 cm^{-1} . The product feature due to $C_2H_2\text{-B}_3N_3H_6$ complex at 3443.6 cm^{-1} can be assigned to the N-H stretch in $B_3N_3H_6$, thus showing a *red* shift of 28.4 cm^{-1} in N_2 matrix. As can be seen from Table 4.3 and Figure 4.3, the computed shift of 30 cm^{-1} for this mode in the **bent** $NH\cdots C$ complex, is in good agreement with the experimentally observed shift of $\sim 28\text{ cm}^{-1}$. The shifts computed for the other complexes are clearly different from that observed in our experiments, thus indicating that the 3443.6 cm^{-1} feature can unambiguously be assigned to the bent $NH\cdots C$ complex formed in the matrix.

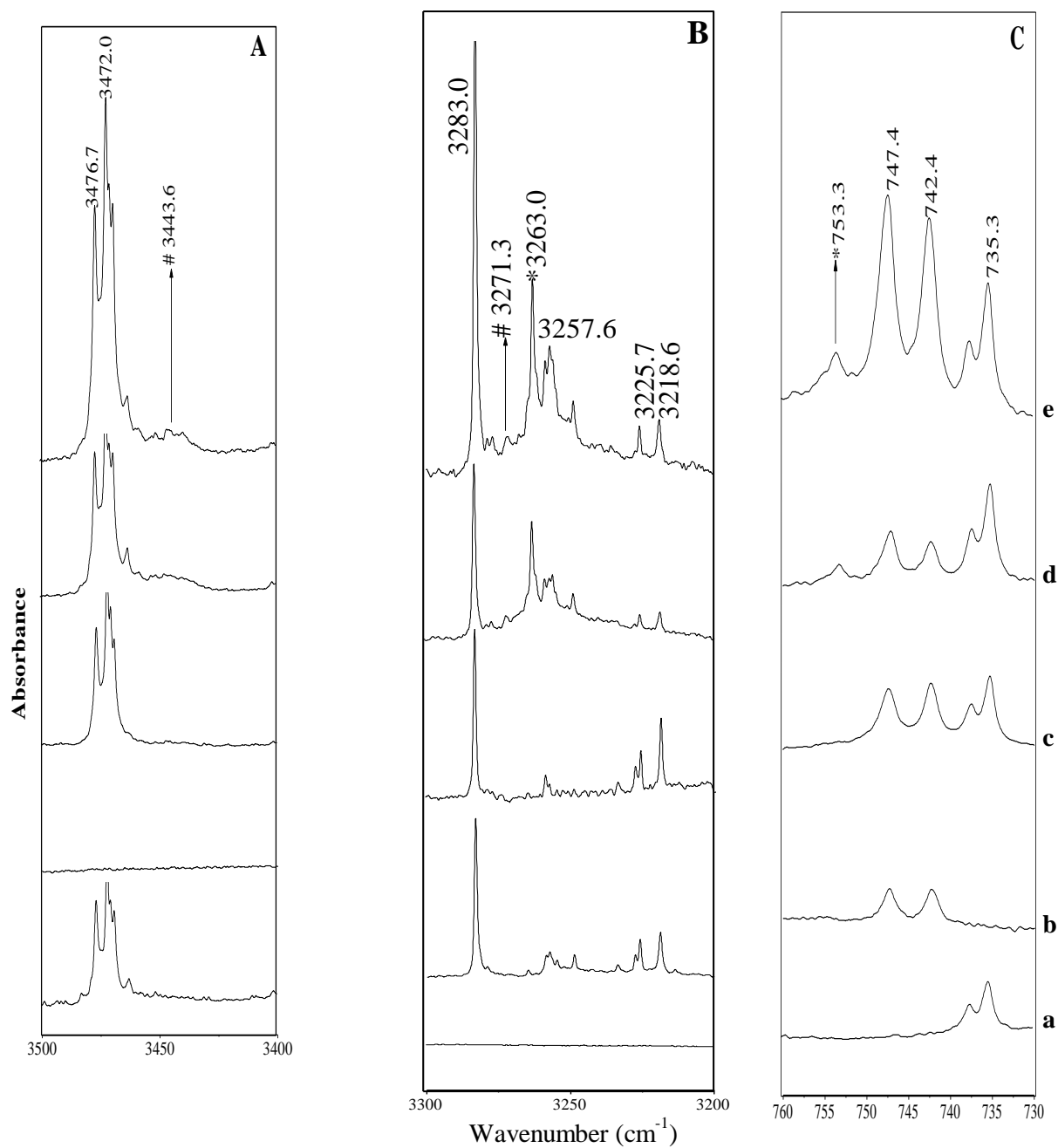


Fig.4.2. Infrared spectrum of (a) $B_3N_3H_6:N_2$ (x:1000) (b) $C_2H_2:N_2$ (1:1000) (c) $B_3N_3H_6:C_2H_2:N_2$ (x:1:1000) at 12K (d) spectrum of (c) annealed at 27K, (e) $B_3N_3H_6:C_2H_2:N_2$ (x:2:1000) annealed at 27 K. Panels A, B and C show the regions 3500-3400, 3300-3200 and 760-730 cm^{-1} respectively.

4.5.2 C-H asymmetric stretch in C₂H₂

In the N₂ matrix, the \equiv C-H stretch for C₂H₂ appears at 3283.0 cm⁻¹. Two product bands due to the \equiv C-H asymmetric stretch of the C₂H₂ submolecule in C₂H₂-B₃N₃H₆ complex were observed at 3271.3 and 3263.0 cm⁻¹ (Fig.4.2, trace 'e', Panel B), with the latter feature being considerably more intense than the former. This assignment implies that following complex formation, the \equiv C-H asymmetric stretch of the C₂H₂ submolecule is *red* shifted by 11.7 and 20 cm⁻¹ respectively, in the N₂ matrix. The computed shift of 8 cm⁻¹ for the **bent NH...C** is in good agreement with the observed shift of 11.7 cm⁻¹ (Table 4.3 and Figure 4.3). This complex was already identified in the matrix based on the perturbations observed for the N-H stretch in B₃N₃H₆, discussed in the last section. The corresponding perturbation observed for \equiv C-H asymmetric stretch in C₂H₂, therefore further corroborates the identification of this complex.

In addition, we also observed another feature *red* shifted by 20 cm⁻¹, which is in good agreement with the computed red shift of 23.6 cm⁻¹ of this mode for the **bent CH...N** complex. We therefore assign the 3263.0 cm⁻¹ feature to the **bent CH...N** complex. It may be noted that perturbations in the N-H stretch of B₃N₃H₆ for this complex was not observed, as the shift in this mode was computed to be just 2.7 cm⁻¹, which cannot be resolved from the feature of uncomplexed B₃N₃H₆.

The computed intensity of C-H asymmetric stretch of C₂H₂ for the **bent CH...N** (215 km/mol) is more than twice that computed for the **bent NH...C** complex (97 km/mol). This result is consistent with the stronger intensity observed for the 3263.0 cm⁻¹ feature compared with that for the 3271.3 cm⁻¹ feature, as pointed out earlier.

4.5.3 C-H bend in C₂H₂

The doubly degenerate bending mode of C₂H₂ in the N₂ matrix occurs as a doublet at 742.4 and 747.4 cm⁻¹, split due to the reduced symmetry in the N₂ matrix cage. The product band due to C₂H₂-B₃N₃H₆ complex at 753.3 cm⁻¹ (Fig. 4.2e, Panel C) is *blue* shifted by 10.9 cm⁻¹ from the monomer C₂H₂ feature, which is in excellent agreement with the computed shift of 11.9 cm⁻¹ in the **bent NH...C** complex (Table 4.3). The corresponding product feature in the bent CH...N complex could not be observed as it was computed to manifest a very small shift of 0.9 cm⁻¹.

Experimental observation of the perturbations in the antisymmetric stretches of N-H of $B_3N_3H_6$, the C-H antisymmetric stretch and the bend of C_2H_2 clearly indicate that we were trapping both the **bent** $NH\cdots C$ and the **bent** $CH\cdots N$ complexes of $B_3N_3H_6-C_2H_2$ in the matrix. None of the other vibrational modes of $B_3N_3H_6$ or C_2H_2 showed any substantial perturbations in their vibrational frequencies of the complex to serve as signatures for complex formation.

4.6. AIM analysis

Wavefunctions generated from optimized geometries of $B_3N_3H_6-C_2H_2$ complexes at MP2/aug-cc-pVDZ level of theory were used to locate (3, -1) bond critical points (BCP).¹⁴⁻¹⁶ The computed electron density $\rho(r_c)$ and $\nabla^2\rho(r_c)$ (defined as the sum of the Hessian eigenvalues, λ_1 , λ_2 and λ_3) were examined at the bond critical point for the complexes. According to Koch and Popelier, the H-bonds have an electron density at the BCP in the range 0.002-0.034 a.u. and $\nabla^2\rho(r_c)$, within the range 0.024-0.139 a.u.²¹ A positive sign of $\nabla^2\rho(r_c)$ is indicative of closed shell interaction, where electronic charge is locally depleted between a pair of atoms.

We have also computed the interaction energy values for the different complexes, using the topological parameters, $\rho(\mathbf{r}_{CP})$ and $\nabla^2\rho(\mathbf{r}_{CP})$, by evaluating the local kinetic energy density, $G(\mathbf{r}_{CP})$ and the local potential energy density, $V(\mathbf{r}_{CP})$ ²². While the actual values of the interaction energy computed using this method (Table 4.4) are somewhat different from those shown in Table 4.1, it can be seen that this analysis also yields the bent $N-H\cdots C$ complex to be the most stable, while the T-Ac and the bent $CH\cdots N$ are isoenergetic and less stable than the global minimum.

4.7. Energy Decomposition Analysis

Individual contributions towards the total interaction energy obtained for the different geometries of $B_3N_3H_6-C_2H_2$ using the Localized Molecular Orbital-Energy Decomposition Analysis (LMO-EDA)¹⁷ are listed in Table 4.5. The contributions are electrostatic, exchange-repulsion, polarisation and dispersion interactions. The stacked geometry is dominated by the dispersion interaction, but significant contributions come from electrostatic interactions. On the other hand, there is an increase in the electrostatic contribution and a decrease in the dispersion interaction in going from the stacked to the T-shaped geometry. The **bent** geometries have nearly similar contributions from electrostatic, polarisation and dispersion interactions, a characteristic of a hydrogen bond.

Table 4.3. Experimental (N_2 matrix) and scaled^a computed vibrational wavenumbers (in cm^{-1}) and mode assignments for the $B_3N_3H_6-C_2H_2$ complexes. Computations were performed at the MP2/aug-cc-pVDZ level of theory.

Experimental		Computed				Mode Assignment
Monomer	Complex	Bent NH...C	Bent CH...N	T-Ac	Stacked	
$B_3N_3H_6$ 3472.0	3443.6 (-28.4)^b	3441.8 (-30.2)	3469.3 (-2.7)	3467.6 (-4.4)	3471.7 (-0.3)	N-H asym. str. in $B_3N_3H_6$
C_2H_2 3283.0	3263.0 (-20.0)	-	3259.4 (-23.6)	3277.8 (-5.2)	3282.2 (-0.8)	
	3271.3 (-11.7)	3275.5 (-8.0)	-	3277.8 (-5.2)	3282.2 (-0.8)	
C_2H_2 742.4	753.3 (10.9)	754.3 (11.9)	743.3 (0.9)	763.6 (21.2)	732.6 (-9.8)	C-H bend in C_2H_2

^[a] Scale factors are: 0.9522 for the N-H stretch in $B_3N_3H_6$; 0.9569 for the C-H stretch in C_2H_2 ; 1.055 for the C-H bend in C_2H_2 .

^[b] Values in parentheses are $\Delta\nu$, defined as $[\nu(\text{complex}) - \nu(\text{monomer})]$.

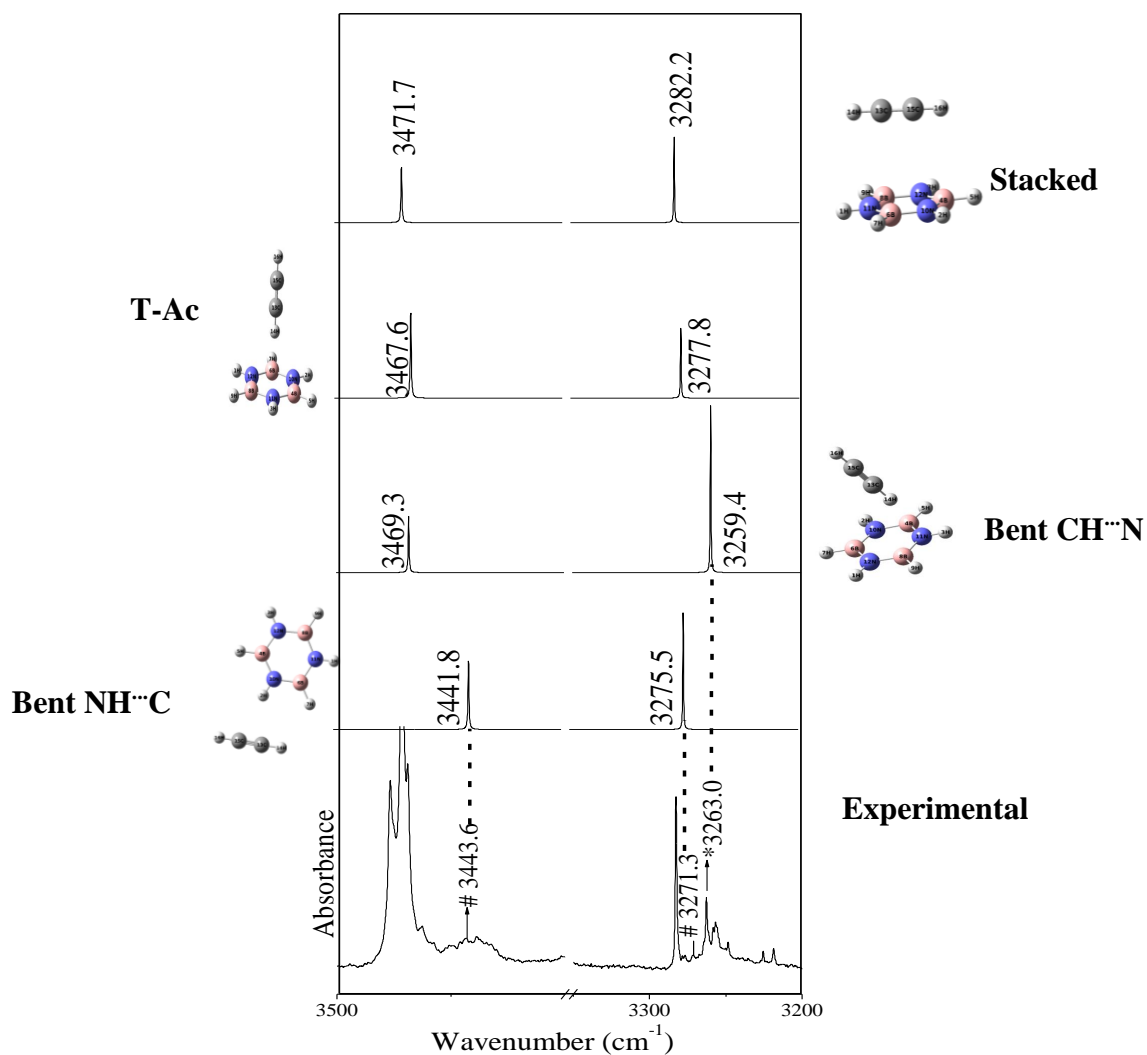


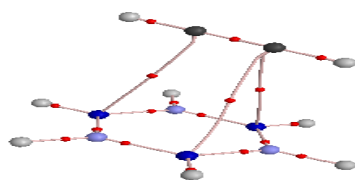
Fig.4.3. Comparison of experimental and computed spectra of the various $B_3N_3H_6-C_2H_2$ complexes. The structure of the complex is given alongside each computed spectrum.

Table 4.4. AIM calculations showing the values of the electron density $\rho(r_c)$ and its Laplacian $\nabla^2\rho(r_c)$, λ_1/λ_3 at the bond critical point, local kinetic energy density $G(r_{CP})$, local electronic potential energy density $V(r_{CP})$ and the interaction energy ΔE , for the $B_3N_3H_6-C_2H_2$ complexes, computed at MP2/aug-cc-pVDZ level of theory. The values of $\rho(r_c)$, $\nabla^2\rho(r_c)$, $G(r_{CP})$ and $V(r_{CP})$ are in atomic units and ΔE in kcal/mol.

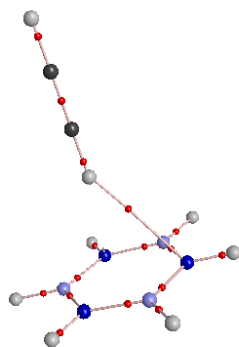
Isomer	$\rho(r_c)$	$\nabla^2\rho(r_c)$	λ_1/λ_3	$G(r_{CP})$	$V(r_{CP})$	ΔE
Stacked	0.0045	0.0124	0.139	0.00241	-0.00172	-0.54
T-Ac	0.0062	0.0216	0.146	0.00421	-0.00301	-0.94
Bent CH \cdots N	0.0061	0.0215	0.146	0.00418	-0.00299	-0.94
Bent NH \cdots C	0.0105	0.0290	0.195	0.00628	-0.00531	-1.67

Table 4.5. Energy decomposition analysis of the $B_3N_3H_6-C_2H_2$ complexes at the MP2/aug-cc-pVDZ level of theory.

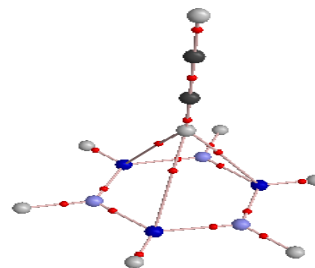
Complex	E_{ES}	E_{ER}	E_{Pol}	E_{Disp}	E_{Total}	E_{ES}/E_{Total}	E_{Disp}/E_{Total}	E_{Pol}/E_{Total}
Stacked	-1.22	4.23	-0.80	-4.82	-2.61	0.47	1.85	0.31
T-Ac	-1.40	3.05	-1.38	-3.92	-3.65	0.38	1.07	0.38
Bent CH \cdots N	-2.24	4.42	-1.63	-4.05	-3.50	0.64	1.16	0.47
Bent NH \cdots C	-3.24	4.35	-1.17	-3.37	-3.43	0.94	0.98	0.34



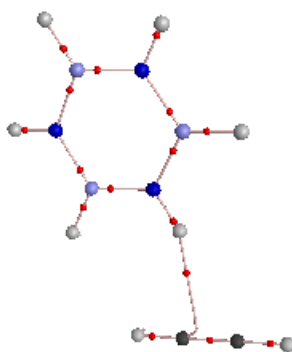
Stacked



Bent CH...N



T-Ac



Bent NH...C

Fig.4.4. AIM analysis for the stable $B_3N_3H_6-C_2H_2$ complexes at MP2/aug-cc-pVDZ level of theory. (Nitrogen: Dark Blue, Boron: Light Blue, Carbon: Black, Hydrogen: White, Bond critical point: Red)

4.8. Natural Bond Orbital Analysis (NBO)

NBO was carried out using NBO 3.1 version implemented using Gaussian 09.¹⁹ For the bent $\text{NH}\cdots\text{C}$ complex, which was the global minimum, the strongest delocalization interaction was between the bonding orbitals $\text{C}_{13}\text{-C}_{15}$ and the antibonding orbitals $\text{H}_2\text{-N}_{10}$. In the bent $\text{CH}\cdots\text{N}$ geometry, the interaction was found to be between the bonding orbitals of $\text{B}_4\text{-N}_{11}$ and the antibonding orbitals of $\text{C}_{13}\text{-H}_{14}$. The second order perturbation energies for both the complexes formed in the matrix, i.e. bent $\text{NH}\cdots\text{C}$ and the bent $\text{CH}\cdots\text{N}$ geometries were almost equal. (Table 4.6)

4.9. Comparison Between $\text{C}_6\text{H}_6\text{-C}_2\text{H}_2$ and $\text{B}_3\text{N}_3\text{H}_6\text{-C}_2\text{H}_2$ Dimers

It is interesting to study how the interaction in a $\text{C}_6\text{H}_6\text{-C}_2\text{H}_2$ dimer gets modified when the C-C linkages in C_6H_6 are replaced by B-N linkages in $\text{B}_3\text{N}_3\text{H}_6$. Clearly the global minima in the two systems manifest a major difference, in that while C_2H_2 is the proton donor to C_6H_6 in the $\text{C}_6\text{H}_6\text{-C}_2\text{H}_2$ system, $\text{B}_3\text{N}_3\text{H}_6$ is the proton donor in the $\text{B}_3\text{N}_3\text{H}_6\text{-C}_2\text{H}_2$ system.

The computed interaction energy values for the different conformers of $\text{C}_6\text{H}_6\text{-C}_2\text{H}_2$ and $\text{B}_3\text{N}_3\text{H}_6\text{-C}_2\text{H}_2$ dimers at the MP2/CBS and the CCSD(T)/CBS limit are compared in Table 4.1. The intermolecular contact distances are smaller for the $\text{C}_6\text{H}_6\text{-C}_2\text{H}_2$ dimer⁹ than for the $\text{B}_3\text{N}_3\text{H}_6\text{-C}_2\text{H}_2$ dimer, as shown in Figure 4.1. The sandwich geometry is the least stable conformer for $\text{C}_6\text{H}_6\text{-C}_2\text{H}_2$, but it becomes stable for $\text{B}_3\text{N}_3\text{H}_6\text{-C}_2\text{H}_2$. The repulsion between the π -electron cloud of C_6H_6 and that of C_2H_2 becomes less dominant in going from C_6H_6 to $\text{B}_3\text{N}_3\text{H}_6$. This is due to the charge transfer interaction in $\text{B}_3\text{N}_3\text{H}_6\text{-C}_2\text{H}_2$. The T-shaped isomers in which the acetylenic C-H bond interacts with the π -electron cloud of C_6H_6 and $\text{B}_3\text{N}_3\text{H}_6$ are stable minima for both systems. However, this structure is more stable in the C_6H_6 system than in the $\text{B}_3\text{N}_3\text{H}_6$ system. The zero point energy corrected binding energy is reduced by a factor of two in going from $\text{C}_6\text{H}_6\text{-C}_2\text{H}_2$ dimer to $\text{B}_3\text{N}_3\text{H}_6\text{-C}_2\text{H}_2$ dimer. It must be noted that, unlike the $\text{C}_6\text{H}_6\text{-C}_2\text{H}_2$ dimer, where the $\text{C-H}\cdots\pi$ structure is the global minimum, in the $\text{B}_3\text{N}_3\text{H}_6\text{-C}_2\text{H}_2$ dimer, the structure with the $\text{N-H}\cdots\text{C}$ interaction is the most stable structure which clearly reveals the different interactions manifested by the two systems.

Table 4.6. NBO analysis for the $B_3N_3H_6-C_2H_2$ dimers, performed at MP2/aug-cc-pVDZ level of theory. The atom numbering indicated in the table is as shown in Fig. 4.1. E is the second order perturbation energy, $E(j)-E(i)$ is the donor-acceptor energy difference and $F(i,j)$ is the overlap between the donor and acceptor orbitals.

Complex	Orbitals involved		E (kcal/mol)	E(j)-E(i) a.u.	F(i,j) a.u.
	Donor	Acceptor			
Stacked	$C_{13}-C_{15}$	B_6-N_{10}	0.46	0.66	0.016
T_{ac}	B_6	$C_{13}-H_{14}$	0.34	0.63	0.035
	B_8	$C_{13}-H_{14}$	0.34	0.63	0.035
	B_{10}	$C_{13}-H_{14}$	0.34	0.63	0.035
Bent CH\cdotsN	B_4-N_{11}	$C_{13}-H_{14}$	3.02	1.18	0.055
Bent NH\cdotsC	$C_{13}-C_{15}$	H_2-N_{10}	2.99	1.17	0.053

4.10. Conclusions

This chapter describes a computational and experimental study of the interactions between $B_3N_3H_6$ and C_2H_2 . The global minimum was found to be the bent $NH\cdots C$ complex, in which the N-H of $B_3N_3H_6$ was found to be the proton donor to C_2H_2 , which was different from the global minimum structure observed for the $C_6H_6-C_2H_2$ dimer. The formation of the bent $NH\cdots C$ complex in $B_3N_3H_6-C_2H_2$ dimer was evidenced by shifts in the N-H stretch of $B_3N_3H_6$, $\equiv C-H$ asymmetric stretch of C_2H_2 and $\equiv C-H$ bend of C_2H_2 . Located higher in energy relative to this structure, was an isomer with a bent $CH\cdots N$ geometry, where the C-H of C_2H_2 was the proton donor to the nitrogen of $B_3N_3H_6$. This structure was also observed in our experiments, as indicated by the shift in the $\equiv C-H$ asymmetric stretch of C_2H_2 . This structure of the $B_3N_3H_6-C_2H_2$ dimer closely resembles the minimum energy structure observed in the $C_6H_6-C_2H_2$ dimer. AIM calculations for this system reveals hydrogen bonding interactions between the two precursors, $B_3N_3H_6$ and C_2H_2 , in their most stable structures. π -stacked structures were also indicated though with much smaller interaction energies. Unlike in the $C_6H_6-C_2H_2$ dimer, the π -stacked structure in the $B_3N_3H_6-C_2H_2$ dimer turns out to be a stable minimum. Energy Decomposition Analysis showed that the electrostatic and dispersion interactions play an important role in stabilizing the global minimum in $B_3N_3H_6-C_2H_2$, in contrast to the $C-H\cdots\pi$ interaction in $C_6H_6-C_2H_2$, where the dispersion interaction played a major role. The N-H hydrogen bonded systems as observed in $B_3N_3H_6$ complexes thus present an interesting case study for hydrogen bonding interactions.

REFERENCES

- (1)Fazen, P.J.; Beck, J.S.; Lynch, A.T.; Remsen, E.E.; Sneddon, L.G. Thermally induced Borazine Dehydropolymerization Reactions. Synthesis and Ceramic Conversion Reactions of a New High- Yield Polymeric Precursor to Boron Nitride. *Chem. Mater.* **1990**, *2*, 96-97.
- (2)Lourie, O.R.; Jones, C.R.; Bartlett, B.M.; Gibbons, P.C.; Ruoff, R.S.; Buhro, W.E. CVD growth of Boron Nitride Nanotubes. *Chem. Mater.* **2000**, *12*, 1808-1810.
- (3)Karthi, V.B.; Krishnamachari, S.L.N.G.; Subramaniam, C.R. The infrared spectra of borazine and its isotopic species. Assignment of the a_2'' fundamental modes. *J.Mol.Spec.***1967**, *23*, 149-157.
- (4)Niedenzu, K.; Sawodny, W.; Watanabe, H.; Dawson, J.; Totani, T.; Weber, W. The vibrational spectrum of borazine. *Inorg.Chem.* **1967**, *6*, 1453-1461.
- (5)Kaldor, A.; Porter, R.F. Matrix Isolation study of borazine and boroxine. Vibrational Analysis. *Inorg. Chem.* **1971**, *10*, 775-785.
- (6)Mishra, P.; Verma, K.; Bawari, D.; Viswanathan, K.S. Does borazine-water behave like benzene-water? A matrix isolation infrared and *ab initio* study. *J. Chem. Phys.* **2016**, *144*, 234307-16.
- (7)Sankaran, K.; Viswanathan, K. S.; Kulkarni, A. D.; Gadre, S. R. H- π Complexes of Acetylene-Ethylene: A Matrix Isolation and Computational Study. *J. Phys. Chem. A.* **2002**, *106*, 1504-1510.
- (8)Majumder, M.; Mishra, B.K.; Sathyamurthy, N. CH $\cdots\pi$ and $\pi\cdots\pi$ interaction in benzene-acetylene clusters *Chem. Phys. Lett.* **2013**, *557*, 59-65.
- (9)Sundararajan, K.; Viswanathan, K. S.; Kulkarni, A. D.; Gadre, S. R. H- π Complexes of Acetylene–Benzene: A Matrix-Isolation and Computational Study. *J. Mol. Struct.* **2002**, *613*, 209-222.
- (10)Sundararajan, K.; Sankaran, K; Viswanathan, K.S. A Matrix Isolation and *ab initio* study of the Hydrogen Bonded Complexes of Acetylene with Pyridine. *J. Mol .Struct.* **2005**, *733*, 187-192.
- (11)Li, J.; Zhang, C.R.; Li, B.; Cao, F.; Wang, S. An Improved Synthesis of Borazine with Aluminium Chloride as Catalyst *Eur. J. Inorg. Chem.* **2010**, *2010*, 1763-1766.

-
- (12)M.J.Frisch, G.W.Trucks, H.B.Schlegel, G.E.Scuseria, M.A.Robb, J.R.Cheeseman, G. Scalmani, V.Barone, B.Mennucci, G.A.Petersson, H.Nakatsuji, M.Caricato, X.Li, H.P. Hratchian, A.F. Izmaylov, J. Bloino, G. Zheng, J.L. Sonnenberg, M.Hada, M.Ehara, K.Toyota, R.Fukuda, J.Hasegawa, M.Ishida, T.Nakajima, Y.Honda, O.Kitao, H.Nakai, T.Vreven, J.J.A. Montgomery, J.E.Peralta, F.Ogliaro, M.Bearpark, J.J.Heyd, E.Brothers, K.N. Kudin, V.N. Staroverov, R.Kobayashi, J.Normand, K.Raghavachari, A.Rendell, J.C.Burant, S.S. Iyengar, J. Tomasi, M.Cossi, N.Regga, J.M.Millam, M.Klene, J.E.Knox, J.B. Cross, V.Bakken, C.Adamo, J.Jaramillo, R.Gomperts, R.E.Stratmann, O.Yazyev, A.J.Austin, R.Cammi, C.Pomelli, J.W.Ochterski, R.L.Martin, K.Morokuma, V.G.Zakrzewski, G.A.Voth, P.Salvador, J.J. Dannenberg, S.Dapprich, A.D.Daniels, O.Farkas, J.B.Foresman, J.V.Ortiz, J.Cioslowski, D.J. Fox, Gaussian 09 Revision A.1, Gaussian Inc. Wallingford CT,2009.
- (13)Boys, S.F.; Bernardi, F. The calculation of small molecular interactions by the differences of separate total energies. Some procedures with reduced errors. *Mol. Phys.*, **1970**, *19*, 553-566.
- (14)Bader, R.F.W. Atoms in Molecules. A Quantum Theory (Clarendon Press, Oxford, 1994).
- (15)Bone, R.G.A.; Bader, R.F.W. Identifying and Analysing Intermolecular Bonding Interactions in van der Waals Molecules. *J. Phys. Chem.* **1996**, *100*, 10892-10911.
- (16)F. Bieger-König, D. Bayles, and J. Schönbohn, AIM2000 (Version 1.0); Chemical Adviser: R. F. W. Bader.
- (17)Su, P.F.; Li, H. Energy Decomposition Analysis of Covalent Bonds and Intermolecular Interactions. *J. Chem. Phys.* **2009**, *131*, 014102-014115.
- (18) Schmidt, M.W. et. al., General atomic and molecular electronic structure system. *J. Comp. Chem.* **1993**, *14*, 1347-1363.
- (19)Glendening, E.D.; Reed, A. E.; Carpenter, J.E.; Weinhold, F. NBO Version 3.1.
- (20)Engdahl, A.; Nelander, B. The acetylene-water complex: A matrix isolation study. *Chem. Phys. Lett.*, **1983**, *100*, 129-132.
- (21)Koch, U.; Popelier, P.L.A. Characterization of CH \cdots O hydrogen bonds on the basis of charge density. *J. Phys. Chem.* **1995**, *99*, 9747-9754.
- (22)Espinosa, E.; Molins, E.; Lecomte, C. Hydrogen bond strengths revealed by topological analyses of experimentally observed electron densities. *Chem.Phys.Lett.* **1998**, *285*, 170-173.

CHAPTER 5: BORAZINE DIMER

5.1. Introduction

A comparison of the dimers of $B_3N_3H_6$ with that of C_6H_6 is expected to present an interesting case study. Kawahara *et al.* studied the various conformations of $B_3N_3H_6$ dimer using the second order Moller Plesset perturbation theory (MP2) and reported the gauche parallel stacked structure with the B atoms of one $B_3N_3H_6$ molecule aligned above the N atoms of the other $B_3N_3H_6$ moiety to be the most stable geometry.¹ We call this as the aligned stacked (AS) structure. In addition, $B_3N_3H_6$ dimer also displays the parallel displaced (PD) stacked structure, as was indicated by the computations in the case of the C_6H_6 dimer. In $B_3N_3H_6$ dimer where the charge transfer plays an important role, it was found for the gauche geometry that electron correlation was also important.¹ Bettinger *et al.* studied the various $B_3N_3H_6$ homodimers using *ab initio* calculations and concluded that the AS structure was the most stable followed by the PD and the T_N structure (where the N-H of one $B_3N_3H_6$ interacted with the N of the second $B_3N_3H_6$) at the MP2/QZVPP level of theory.² Interestingly, our computations showed that there exists one more structure for the $B_3N_3H_6$ dimer, where the H attached to the nitrogen atom of $B_3N_3H_6$ (of an N-H group) interacts with the H attached to the boron atom (of a B-H group) of another $B_3N_3H_6$, thus constituting a *dihydrogen* bond. Dihydrogen bonds have received enormous attention lately.³⁻¹⁵ Transition metals and boron are classic examples of elements that can accommodate the hydridic hydrogen, leading to the formation of such dihydrogen bonds and hence, these types of bonds have been most commonly observed in such systems. Borane-amine complexes, in particular, have been discussed in many studies addressing this type of interaction, manifesting N-H...H-B contacts.⁵⁻¹³ Theoretical studies on these dihydrogen complexes reveal that these exhibit short H...H distances.⁴ Matrix isolation studies on ammonia borane were carried out by Smith *et al.* in 1973, but there was no discussion on the experimental evidence of a dihydrogen bond.¹⁶ There are many experimental studies in literature on transition metal hydrides, showing the presence of bis-dihydrogen bonds.¹⁷ The first explicit evidence for the formation of a dihydrogen bond in a metal hydride was given separately by Crabtree *et al.*¹⁸ and Morris *et al.*¹⁹. Since then, most of the experimental work on dihydrogen bond has been focused on metal hydrides. Other than the metal hydride systems, very few examples can be found in the literature on systems exhibiting dihydrogen bonds. Crystal structure and high pressure studies on

ammonia-borane clusters have been reported to show such interactions.^{12,20} A recent excellent review has discussed the various facets of the dihydrogen bond with special reference to the reactions of metal hydrides.²¹ As we will show in this work, there exists an isomer of a $B_3N_3H_6$ dimer that displays two dihydrogen contacts operating cooperatively, and is probably one of the few examples of a dihydrogen bond in a 1:1 complex. Furthermore, to the best of our knowledge, no experimental study exists on the dimers of $B_3N_3H_6$, and this report is therefore the first experimental study on this dimer. This study also begs a comparison between the C_6H_6 dimers and the $B_3N_3H_6$ dimers, which is presented.

5.2. Experimental details

5.2.1 Synthesis

The method of synthesis of $B_3N_3H_6$ has been described in Chapter 4.

5.2.2 Matrix isolation IR experiments

The experimental setup has been described in detail in Chapter 3.

5.3. Computational details

The geometries, energies and vibrational frequencies were computed at the MP2 and the M06-2X levels of theory in conjunction with 6-311++G(d,p) and aug-cc-pVDZ basis sets for the $B_3N_3H_6$ dimers using the Gaussian 09 suite of program.²² The optimized structures of the $B_3N_3H_6$ dimers at the MP2/aug-cc-pVDZ level of theory are shown in Fig.5.1. The interaction energies of the complexes, were then computed and corrected separately for zero point energy (ZPE) and basis set superposition error (BSSE) by Boys and Bernardi²³ (Table 5.1). The single point interaction energies for the various $B_3N_3H_6$ dimers were also computed at the MP2/CBS and CCSD(T)/CBS method and are given in table 5.1. Table 5.2 gives the selected structural parameters for the $B_3N_3H_6$ dimers at MP2/aug-cc-pVDZ level of theory.

Vibrational frequencies of all the $B_3N_3H_6$ dimers were computed both to assign the observed frequencies in the matrix isolation experiments and also to ensure that the computed geometries did indeed correspond to a minimum on the potential surface by checking that no imaginary frequencies were indicated. Scaling of the computed frequencies was performed using the mode by mode scaling procedure, already described in Chapter 3.

Atoms-in-molecules (AIM) theory by Bader, implemented through AIM2000 (Version 1.0), was used to understand the nature of the interactions by computing electron density $\rho(\mathbf{r}_c)$ and $\nabla^2 \rho(\mathbf{r}_c)$ (defined as the sum of the Hessian eigenvalues, λ_1 , λ_2 and λ_3) at the bond critical points (BCP) corresponding to the hydrogen bonding interactions.²⁴⁻²⁶ Energy Decomposition Analysis (EDA) was also used to carry out the partitioning of the total energy of the complexes into various fractions. LMO-EDA²⁷ scheme of analysis was employed using GAMESS²⁸. Natural Bond Orbital (NBO) analysis was performed through Gaussian 09, to further understand the role of various orbital interactions in the stabilization of the dimers.

5.4. RESULTS AND DISCUSSION

5.4.1 Computational

Fig. 5.1 gives the optimized structures of the $B_3N_3H_6$ homodimers at the MP2/aug-cc-pVDZ level of theory. At this level of theory, four structures, AS, PD, T_N and $H \cdots H$ were obtained as minima on the potential energy surface for the $B_3N_3H_6$ dimers. There were two types of stacked structures; one of which is labeled as the aligned stacked (AS) dimer and the other is a parallel displaced (PD) stacked dimer. In the AS structure, the two $B_3N_3H_6$ units lie with all N and B atoms of one $B_3N_3H_6$ located exactly above the B and N, respectively, of the second unit. In the PD structure, one $B_3N_3H_6$ unit is slightly displaced relative to the other, much like in the C_6H_6 parallel displaced dimer. Both these structures were nearly isoenergetic and represent the global minima. The next structure was one where the N-H of one $B_3N_3H_6$ unit interacted with the N atom of the second $B_3N_3H_6$, which we have labeled as the T_N structure, which is much like the T-shaped dimer in C_6H_6 . In addition to the above three structures which were also reported by Bettinger², we located a fourth minimum, for the first time, where hydrogen of the N-H group of one $B_3N_3H_6$ interacts with the hydrogen attached to B-H group of the second $B_3N_3H_6$, thus constituting a dihydrogen bond. The distance between the two hydrogens in this complex was found to be 2.13 Å at the MP2/aug-cc-pVDZ level, which is typical of distances observed for dihydrogen bonds⁴ and close to values observed in the weak classical hydrogen bonds. The dihydrogen bonded structure was the least bound of the four $B_3N_3H_6$ dimers at all levels of theory, though only marginally so. At the MP2/6-311++G(d,p) level, the dihydrogen bonded structure was computed to be slightly more stable than the T_N structure. AIM, EDA and NBO analysis were also done on the various homodimers of $B_3N_3H_6$.

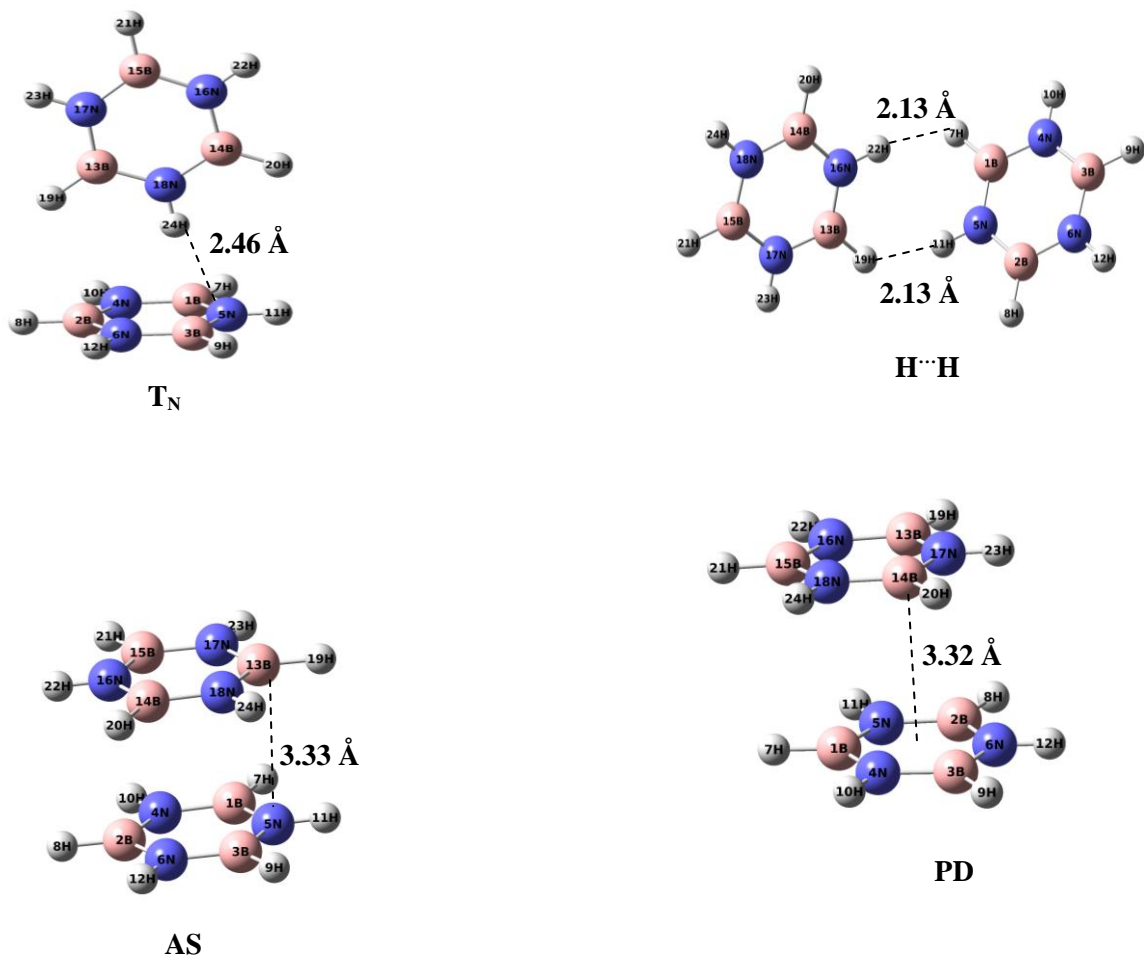


Fig.5.1. Optimized geometries of the $B_3N_3H_6$ homodimers computed at the MP2/aug-cc-pVDZ level of theory.

Table 5.1. Interaction energies of the various complexes of $B_3N_3H_6$ dimer given as uncorrected/ZPE corrected/BSSE corrected energies (kcal/mol) using the MP2 and M06-2X methods and 6-311++G(d,p) and aug-cc-pVDZ basis sets. Single point interaction energies at CCSD(T)/CBS level are also given.

Dimer	MP2		M06-2X		MP2	CCSD(T)
	6-311++G(d,p)	aug-cc-pVDZ	6-311++G(d,p)	aug-cc-pVDZ	CBS	CBS
AS	-4.93/-4.39/-2.00	-6.82/-6.68/-2.65	-4.51/-4.41/-4.14	-5.26/-5.00/-3.98	-4.42	-4.36
PD	-4.50/-3.81/-1.67	-6.40/-6.09/-2.34	-4.17/-3.54/-3.80	-4.77/-4.47/-3.50	-3.98	-3.94
T_N	-3.14/-2.71/-1.11	-5.26/-4.84/-2.27	-2.89/-2.45/-2.68	-3.47/-3.19/-2.48	-3.57	-3.41
H...H	-2.33/-1.90/-1.40	-3.62/-3.09/-1.66	-1.93/-1.56/-1.81	-2.49/-2.17/-1.72	-2.61	-2.41

Table 5.2. Selected structural parameters for the B₃N₃H₆ dimers at the MP2/aug-cc-pVDZ level of theory. The distances are given in angstroms (Å) and the angles are given in degrees (°). The atom numbering is as shown in figure 5.1.

AS	
B ₁₃ -N ₅	3.34 Å
N ₁₆ -B ₂	3.33 Å
H ₁₉ -B ₁₃ -N ₅	121.0°
PD	
N ₁₇ -N ₆	3.68 Å
B ₁₅ -B ₁	3.57 Å
T_N	
H ₂₄ -N ₅	2.46 Å
H ₂₄ -N ₆	2.85 Å
H ₂₄ -N ₄	2.85 Å
N ₁₈ -H ₂₄ -N ₅	165.4°
H···H	
H ₂₂ -H ₇	2.13 Å
H ₁₉ -H ₁₁	2.13 Å
N ₁₆ -H ₂₂ -H ₇	159.0°
B ₁₃ -H ₁₉ -H ₁₁	110.2°

5.4.2 Experimental

Experiments were performed in both N₂ and Ar matrices, however, the results obtained using both the matrixes being similar, we present only the results of our experiments using the N₂ matrix to avoid a repetitive display of data and discussions.

Figure 5.2 (Panel A) displays the infrared spectrum in the region 3490-3450 cm⁻¹ of matrix isolated B₃N₃H₆ in the N₂ matrix, which shows strong absorptions at 3476.7 cm⁻¹ and 3472.0 cm⁻¹ corresponding to the antisymmetric N-H stretches in B₃N₃H₆. Panel B shows the spectrum in the region 925-910 cm⁻¹ corresponding to the bending region of B₃N₃H₆, which shows a strong absorption at 917.4 cm⁻¹. When the matrix was annealed, new product features were observed at 3462.8 cm⁻¹ and 3458.0 cm⁻¹ in the N-H stretching region of B₃N₃H₆ and at 921.4 cm⁻¹ in the bending region. (Fig 5.2c Panels A and B). Trace 'd' shows a subtraction of the as-deposited spectrum from that of the annealed spectrum, in which the down going peaks were product features formed during annealing. The above mentioned product features can be clearly seen in the difference spectrum. The product features mentioned above were only seen at high concentrations of B₃N₃H₆, thereby confirming that they were due to the dimers of B₃N₃H₆.

Since B₃N₃H₆ was taken in tetraglyme in which its concentration was not estimated, it was not possible to determine the exact matrix to sample ratios for B₃N₃H₆. However, since its variation of vapor pressure with temperature was known, it was possible to estimate the relative changes in the B₃N₃H₆ concentration in the matrix in the various experiments performed. For example, an increase in temperature from -30°C to -20°C of B₃N₃H₆, doubles the vapor pressure.

5.5. Vibrational Assignments

5.5.1 N-H stretch in B₃N₃H₆

The product feature obtained at 3462.8 cm⁻¹ is red shifted by 9.2 cm⁻¹ from the monomer B₃N₃H₆ feature at 3472.0 cm⁻¹. This red shift agrees with the computed red shift of 5.5 cm⁻¹ for the proton acceptor B₃N₃H₆ submolecule in the T_N dimer (Table 5.3 and Fig.5.3, Panel A). The proton donating B₃N₃H₆ submolecule in this dimer, is computed to show a red shift of 16 cm⁻¹, which agrees well with the product feature at 3458.0 cm⁻¹, which works out to an experimental red shift of 14 cm⁻¹. These product features therefore confirm the presence of the T_N dimer in the matrix.

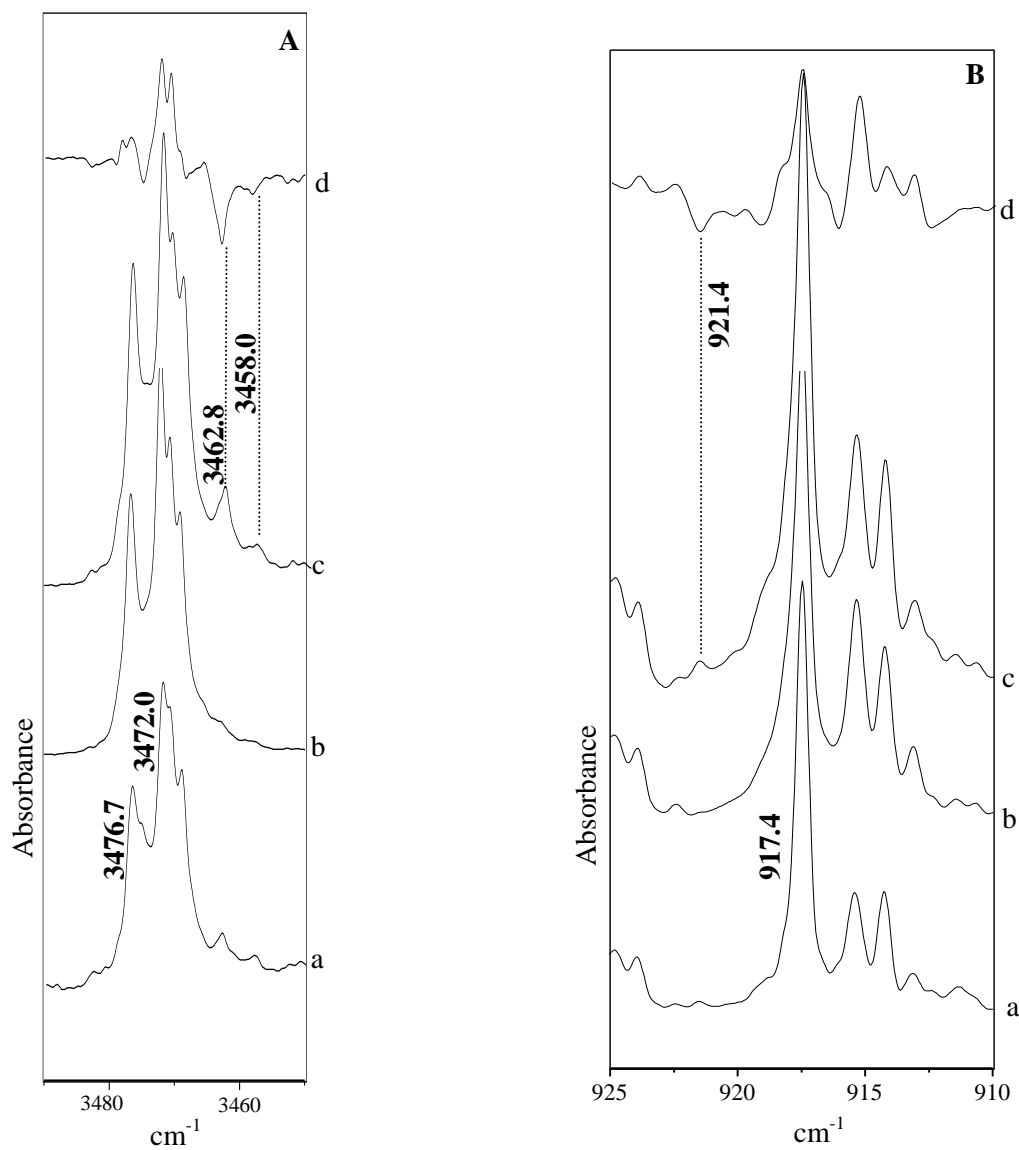


Fig.5.2. Matrix isolation IR spectra of (a) $B_3N_3H_6:N_2$ (0.5x:1000) annealed at 27 K (b) $B_3N_3H_6:N_2$ (x:1000) deposited at 12 K. (c) Spectrum of sample in 'b' annealed at 27 K, (d) Spectrum 'b' subtracted from 'c'. Negative going peaks are product peaks formed during annealing. Panels A and B show features in the N-H stretch region and bending region, respectively.

Table 5.3. Experimental wavenumbers (cm^{-1}) in N_2 matrix and scaled computed wavenumbers^a for the $\text{B}_3\text{N}_3\text{H}_6$ dimers, together with mode assignments. Computations were performed at the MP2/aug-cc-pVDZ level.

Experimental		Computed				Mode Assignment
Monomer	Dimer	AS	PD	T_N	$\text{H}\cdots\text{H}$	
3472.0	3462.8 (-9.2)	3468.3 (-3.7)	3469.3 (-2.7)	3466.5 ^b (-5.5)	-	N-H stretch
	3458.0 (-14.0)	3467.2 (-4.8)	3468.0 (-4.0)	3456.0 ^c (-16.0)	3458.5 (-13.5)	
917.4	921.4 (4.0)	904.3 (-13.1)	907.0 (-10.4)	913.4 (-4.0)	920.0 (2.6)	Ring bend

^aScale factor for N-H stretching region=0.9522, Scale factor for bending region= 0.9989

^bN-H stretch of $\text{B}_3\text{N}_3\text{H}_6$ serving as the proton acceptor

^cN-H stretch of $\text{B}_3\text{N}_3\text{H}_6$ serving as the proton donor

The 3458.0 cm^{-1} feature also occurs at just the position computed for the dihydrogen complex, which was computed to show a red shift of 13.5 cm^{-1} (Table 5.3 and Fig.5.3, Panel A). The 3458.0 cm^{-1} feature can therefore be also considered as a strong candidate for a feature of the dihydrogen bonded dimer; thus raising the possibility that this feature could be assigned for both the T_N and the dihydrogen bonded dimer. As will be shown later, the dual assignment of this feature for both the T_N and the dihydrogen bonded structure is in fact tenable and we believe that the dihydrogen bonded dimer is actually produced in the annealing process. The stacked structures may well have been formed in the matrix, but their infrared signatures show shifts that are too small to be discerned and we do not find any evidence for their formation.

5.5.2. Ring bending mode in $B_3N_3H_6$

The new product feature in the bending region of $B_3N_3H_6$ was observed at 921.4 cm^{-1} , which showed a *blue* shift of 4.0 cm^{-1} from the uncomplexed $B_3N_3H_6$. From Table 5.3 and Fig.5.3 (Panel B), it can be seen that this experimentally observed shift agrees well with the computed *blue* shift of 2.6 cm^{-1} for this mode for the dihydrogen bonded complex. All other dimers show a red shift for this mode and it is only the dihydrogen dimer that shows a blue shift. The observation of the blue shifted bending feature is unambiguous evidence for the presence of the dihydrogen bonded complex in the matrix. Taken together with this evidence, the double assignment of the 3458.0 cm^{-1} feature mentioned earlier for both the T_N and dihydrogen dimer is therefore tenable. The corresponding mode for the T_N geometry was found to be red shifted by 4 cm^{-1} , in our calculations at the MP2/aug-cc-pVDZ level. However, this feature could not be discerned in our experiments due to spectral interferences.

5.6. AIM analysis

To further examine the nature of the interaction in $B_3N_3H_6$ homodimers, we used the AIM theory.²⁴⁻²⁶ Using the optimized geometry of the complexes computed at the MP2/aug-cc-pVDZ level, we searched for a (3,-1) bond critical point (BCP). The electron density, $\rho(r_c)$ and $\nabla^2\rho(r_c)$ (defined as sum of the Hessian eigenvalues) were analyzed at the bond critical point for all the complexes. The topological criteria for the existence of hydrogen bonding were proposed by Koch and Popelier.²⁹ The characterization of dihydrogen bonds on the basis of electron density has also been studied by Popelier.¹³

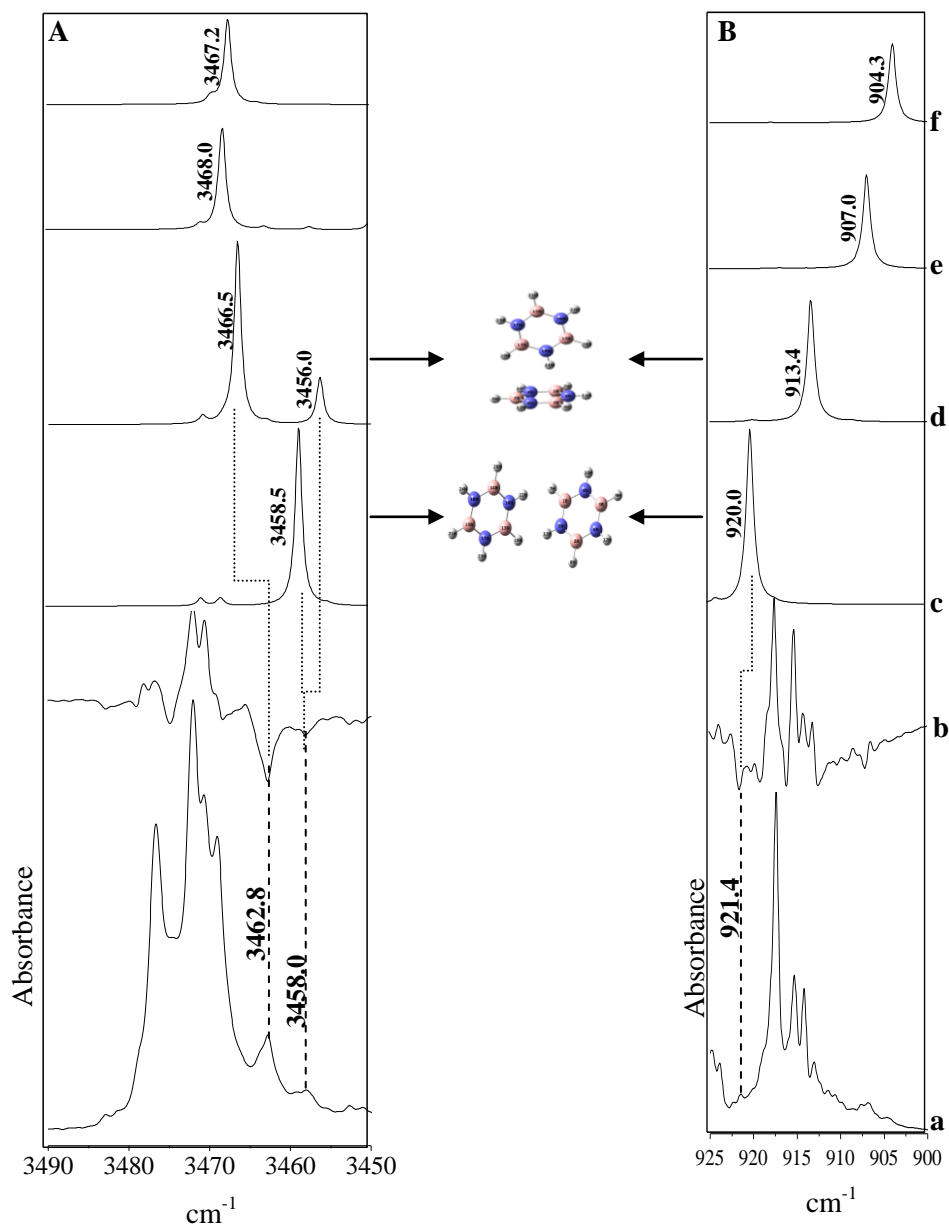


Fig.5.3. (a) Experimental spectrum of the $B_3N_3H_6$ dimer in N_2 matrix (x:1000) (b) Subtracted spectrum; computed spectrum for the (c) $H^{\cdots}H$ complex (d) T_N complex (e) PD complex, (f) AS complex. Panels A and B show features in the N-H stretching and bending region, respectively.

As it is clear from Table 5.4, all the $B_3N_3H_6$ dimers fall into the range given by Koch and Popelier. It was found that at the MP2/aug-cc-pVDZ level of theory, the electron density at the bond critical point was found to be maximum for the dimer corresponding to the T_N geometry closely followed by the dihydrogen bonded geometry. The $\nabla^2\rho(\mathbf{r}_C)$ were found to be nearly equal for both the T_N and the dihydrogen bonded geometry (Table 5.4). In order to calculate the interaction energy of each dihydrogen bond in our structure, we computed the interaction energy for the dihydrogen bonded geometry, using the topological parameters, $\rho(\mathbf{r}_{CP})$ and $\nabla^2\rho(\mathbf{r}_{CP})$, by evaluating the local kinetic energy density, $G(\mathbf{r}_{CP})$ and the local potential energy density, $V(\mathbf{r}_{CP})$, as described by Espinosa et al.³⁰ It was found that the interaction energy for each dihydrogen bond was -1.4 kcal/mol and thus, the total interaction energy for two dihydrogen bonds was -2.8 kcal/mol (E_{stb} for dihydrogen dimer at MP2/aug-cc-pVDZ= 3.62 kcal/mol). It is therefore concluded that the two dihydrogen bonds in the $B_3N_3H_6$ dimer act in cooperation, and it is the total strength of these two dihydrogen bonds that makes it possible for us to observe this complex in our matrix isolation experiments.

5.7. EDA Analysis

Energy decomposition analysis using the LMO-EDA method was done on the various homodimers of $B_3N_3H_6$ at the MP2/aug-cc-pVDZ level of theory using GAMESS.²⁸ It was found that in all the dimers, the dispersion interaction played a major role followed by electrostatic interactions. While in all the cases, the electrostatic contribution was the second most dominant contributor, it was relatively more important in the stacked (AS) geometries than in the other isomers; a conclusion which is in agreement with Bettinger *et al.*² The large electrostatic contribution in the aligned stacked geometry could be explained in terms of the polarity of the B-N bonds (Table 5.5).

5.8. NBO Analysis

NBO analysis was performed at the MP2/aug-cc-pVDZ to understand the role of delocalization interactions in the stability of the dimers. Second order perturbation energies of the various donor-acceptor orbital interactions were computed, which are shown in Table 5.6.

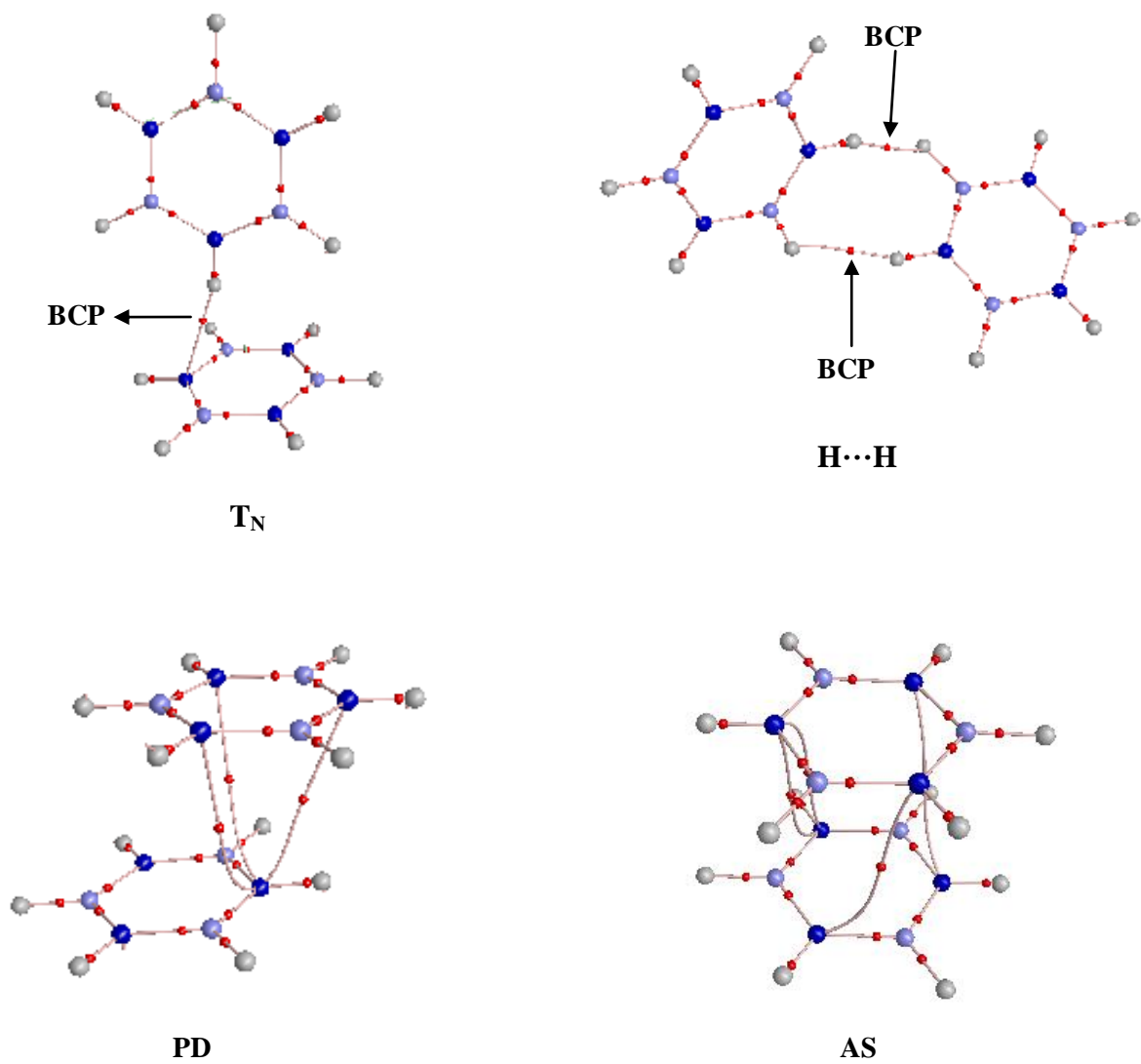


Fig.5.4. AIM analysis for the $B_3N_3H_6$ dimers at the MP2/aug-cc-pVDZ level of theory. The atom labels in this figure are those shown in Fig. 1.

Table 5.6. NBO analysis for the B₃N₃H₆ dimers, performed at MP2/aug-cc-pVDZ level of theory. The atom numbering indicated in the table is as shown in Fig. 1. E is the second order perturbation energy, E(j)-E(i) is the donor-acceptor energy difference and F(i,j) is the overlap between the donor and acceptor orbitals.

Complex	Orbitals involved		E (kcal/mol)	E(j)-E(i) a.u.	F(i,j) a.u.
	Donor	Acceptor			
AS	B ₃ -N ₅	B ₁₃ -N ₁₈	1.94	0.63	0.031
PD	B ₁₃ -N ₁₆	N ₅ -B ₂	2.66	0.63	0.037
T _N	B ₃ -N ₅	N ₁₈ -H ₂₄	2.03	1.17	0.045
H··H	B ₁₃ -H ₁₉	H ₁₁ -N ₅	1.01	1.32	0.033
	B ₁ -H ₇	H ₂₂ -N ₁₆	1.03	1.32	0.033

In the T_N complex, the strongest delocalization interaction was between the N-H antibonding orbital and the B-N bonding orbitals. The dihydrogen bonded isomer, showed two strong delocalization interactions; one was between the bonding orbitals of $B_{13}-H_{19}$ and the antibonding orbitals of $H_{11}-N_5$ and the second between the bonding orbitals of B_1-H_7 and the antibonding orbitals of $H_{22}-N_{16}$.

5.9. Conclusions

This work for the first time, reports a matrix isolation study of the $B_3N_3H_6$ dimers. While our computations agree with an earlier study of Bettinger *et al.*, we see an additional dihydrogen bonded dimer not reported earlier. The aligned and parallel displaced stacked structures were found to be almost isoenergetic for the $B_3N_3H_6$ dimer at the MP2/aug-cc-pVDZ level of theory. However these isomers could not be seen in our matrix isolation experiments due to the small shifts in the infrared frequencies of the precursor. Experimentally, two isomeric forms of the $B_3N_3H_6$ dimers were observed in our matrix. One was the T_N structure, where the N-H of one $B_3N_3H_6$ molecule pointed towards the nitrogen atom of the second $B_3N_3H_6$ molecule; a structure that was similar to the T-shaped C_6H_6 dimer. In addition to this structure, we also observed a dihydrogen bonded structure, both computationally and experimentally. In this structure, *two* dihydrogen bonds were in operation, probably cooperatively, which therefore placed it in terms of stability, behind the classical hydrogen bonded T_N dimer, by just about 0.5 kcal/mol. This is one of few examples of an experimental report of a dihydrogen bond not involving a metal hydride.

References

- (1) Kawahara, S.-I.; Tsuzuki, S.; Uchimaru, T. Ab initio calculation of interaction nature of borazine ($B_3N_3H_6$) dimer. *J. Chem. Phys.* **2003**, *119*, 10081-10087.
- (2) Bettinger, H.F.; Kar, T.; Garcia, E. Borazine and Benzene Homo- and Heterodimers. *J. Phys. Chem. A* **2009**, *113*, 3353-3359.
- (3) Lipkowski, P.; Grabowski, S.J.; Robinson, T. L.; Leszczynski, J. Properties of the C-H \cdots H Dihydrogen Bond: An ab initio and Topological Analysis. *J. Phys. Chem. A* **2004**, *108*, 10865-10872.
- (4) Alkorta, I.; Elguero, J.; Mo', O.; Yanez, M.; Del Bene, J.E. Ab Initio Study of the Structural, Energetic, Bonding and IR Spectroscopic Properties of Complexes with Dihydrogen Bonds. *J. Phys. Chem. A* **2002**, *106*, 9325-9330.
- (5) Staubitz, A.; Robertson, A. P. M.; Manners, I. Ammonia-Borane and Related Compounds as Dihydrogen Sources. *Chem. Rev.* **2010**, *110*, 4079-4124.
- (6) Vijayalakshmi, K. P.; Suresh, C.H. Ammonia Borane Clusters: Energetics of Dihydrogen Bonding, Cooperativity, and the Role of Electrostatics. *J. Phys. Chem. A* **2017**, *121*, 2704-2714.
- (7) Stephens, F.H.; Pons, V.; Baker, R.T. Ammonia-borane: the hydrogen source par excellence? *Dalton Trans* **2007**, *25*, 2613-2626.
- (8) Singh, P.C.; Patwari, G. N. The C-H \cdots H-B dihydrogen bonded borane-trimethylamine dimer: A computational study. *Chem. Phys. Lett.* **2006**, *419*, 265-268.
- (9) Singh, P.C.; Patwari, G. N. Theoretical investigation of C-H \cdots H-B dihydrogen bonded complexes of acetylenes with borane-trimethylamine. *Chem. Phys. Lett.* **2006**, *419*, 5-9.
- (10) Patwari, G.N. Proton affinities of borane-amines: consequences on dihydrogen bonding. *J. Phys. Chem. A* **2005**, *109*, 2035-2038.
- (11) Patwari, G. N.; Ebata, T.; Mikami, N. Gas phase dihydrogen bonding: clusters of borane amines with phenol and aniline. *Chem. Phys.* **2002**, *283*, 193-207.
- (12) Klooster, W.T.; Koetzle, T. F.; Siegbahn, P. E. M.; Richardson, T. B.; Crabtree, R. H. *J. Am. Chem. Soc.* **1999**, *121*, 6337-6343.
- (13) Popelier, P. L. A. Characterization of a Dihydrogen Bond on the Basis of the Electron Density. *J. Phys. Chem. A* **1998**, *102*, 1873-1878.

-
- (14) Kulkarni, S. A. Dihydrogen Bonding in Main Group Elements: An ab Initio Study. *J. Phys. Chem. A* **1998**, *102*, 7704-7711.
- (15) Kulkarni, S. A.; Srivastava, A.K. Dihydrogen Bonding in Main Group Elements: A Case Study of Complexes of LiH, BH₃ and AlH₃ with Third-Row Hydrides. *J. Phys. Chem. A* **1999**, *103*, 2836-2842.
- (16) Smith, J.; Seshadri, K.S.; White, D. Infrared Spectra of Matrix Isolated BH₃-NH₃, BD₃-ND₃, and BH₃-ND₃. *J. Mol. Spec.* **1973**, *45*, 327-337.
- (17) Bakhmutova, E.V.; Bakhmutov, V.I.; Belkova, N.V.; Besora, M.; Epstein, L.M.; Lledós, A.; Nikonov, G. I.; Shubina, E. S.; Tomás, J.; Vorontsov, E.V. *Chem. Eur. J.* **2004**, *10*, 661-671.
- (18) Peris, E.; Lee, J. C.; Rambo, J. R.; Eisenstein, O.; Crabtree, R.H. Factors affecting the strength of X-H \cdots H-M Hydrogen Bonds. *J. Am. Chem. Soc.* **1995**, *117*, 3485-3491.
- (19) Lough, A. J.; Park, S.; Ramachandran, R.; Morris, R.H. *J. Am. Chem. Soc.* **1994**, *116*, 8356-8357.
- (20) Trudel, S.; Gilson, D. F. R. High-Pressure Raman Spectroscopic Study of the Ammonia-Borane Complex. Evidence for the Dihydrogen Bond. *Inorg. Chem.* **2003**, *42*, 2814-2816.
- (21) Belkova, N. V.; Epstein, L.M.; Filippov, O. A.; Shubina, E.S. Hydrogen and dihydrogen bonds in the reactions of metal hydrides. *Chem. Rev.* **2016**, *116*, 8545-8587.
- (22) M.J. Frisch et al, *Gaussian 09*, Gaussian, Inc., Wallingford CT, 2010.
- (23) Boys, S.F.; Bernardi, F. The calculation of small molecular interactions by the differences of separate total energies. Some procedures with reduced errors. *Mol. Phys.* **1970**, *19*, 553-566.
- (24) Bader, R.F.W. *Atoms in Molecules, A Quantum Theory*, Clarendon Press, Oxford, 1994.
- (25) Bone, R.G.A.; Bader, R.F.W. Identifying and Analyzing Intermolecular Bonding Interactions in van der Waals Molecules. *J. Phys. Chem.* **1996**, *100*, 10892-10911.
- (26) Bieger-König, F.; Bayles, D.; Schönbohn, J. AIM2000 (Version 1.0); Chemical Adviser: R. F. W. Bader.
- (27) Su, P. F.; Li, H.; Energy Decomposition Analysis of Covalent Bonds and Intermolecular Interactions. *J. Chem. Phys.* **2009**, *131*, 014102-014115.
- (28) Schmidt, M.W. ; Baldrige, K.K; Boatz, J.A.; Elbert, S.T.; Gordon, M.S.; Jensen, J.H.; Koseki, S; Matsunaga, N. Nguyen, K.A.; Su, S. *et. al.* General Atomic and Molecular Electronic Structure System. *J. Comp. Chem.* **1993**, *14*, 1347-1363.

(29) Koch, U.; Popelier, P.L.A. Characterization of CH \cdots O hydrogen bonds on the basis of charge density. *J. Phys. Chem.* **1995**, *99*, 9747-9754.

(30) Espinosa, E.; Molins, E.; Lecomte, C. Hydrogen bond strengths revealed by topological analyses of experimentally observed electron densities. *Chem. Phys. Lett.* **1998**, *285*, 170-173.

CHAPTER 6: BORAZINE-BENZENE AND BORAZINE-PHENYLACETYLENE COMPLEXES

6.1. Introduction

In this work, we have studied the hydrogen bonded complexes of $B_3N_3H_6$ with two further π systems; C_6H_6 and PhAc.

In our previous studies, we found interesting differences between the complexes of $B_3N_3H_6-H_2O$ ¹, $B_3N_3H_6-C_2H_2$ ² and the $B_3N_3H_6$ dimer³ and the corresponding complexes involving the organic counterpart, C_6H_6 . Therefore, it was interesting to study the interactions in the complex formed between, $B_3N_3H_6$ and C_6H_6 . Bettinger *et al* studied the $B_3N_3H_6-C_6H_6$ complexes using high level *ab initio* calculations at the MP2/aug-cc-pVQZ level and concluded that the T-NH geometry, where the N-H of $B_3N_3H_6$ interacted with the π cloud of C_6H_6 , and the parallel displaced geometry, where the C_6H_6 and $B_3N_3H_6$ rings were slightly displaced relative to each other were nearly isoenergetic structures and were the global minima.⁴ No experimental study on this system have been reported so far. We also studied the $B_3N_3H_6$ -PhAc system both computationally and experimentally, as PhAc has components of both C_2H_2 and C_6H_6 and is also expected to show non-covalent interactions, with a multitude of isomers. $B_3N_3H_6$ has two possible sites for the formation of a hydrogen bond with PhAc. One is the N-H bond, which can serve as a proton donor to the phenyl ring, forming an N-H $\cdots\pi$ bond, alternatively, the partially delocalised π system in $B_3N_3H_6$ can act as a proton acceptor from the hydrogen in C_2H_2 , with the formation of a C-H $\cdots\pi$ bond. PhAc also has multifunctional sites for hydrogen bonding. The π cloud of phenyl ring and that of acetylene in PhAc which can act as proton acceptor sites and the C-H of phenyl and acetylenic ring can act as the proton donor sites. The relative preference of these possible sites therefore opens interesting possibilities that prompted our study of the $B_3N_3H_6$ -PhAc system. Our previous studies on the PhAc-Ac heterodimer showed C_2H_2 to be the proton donor to the acetylenic π cloud of in PhAc. It was therefore interesting to see the interactions involving PhAc, with an N-H system like $B_3N_3H_6$.

6.2. Experimental details

6.2.1 Synthesis

$B_3N_3H_6$ was synthesised by the method already described in Chapter 4 where $B_3N_3H_6-C_2H_2$ complexes were discussed.

6.2.2 Matrix isolation IR experiments

The experimental setup was the same as described in Chapter 3. C_6H_6 (Sigma Aldrich, 99%), PhAc (Sigma Aldrich, 98%) and PhAc_D (Sigma Aldrich, 99%), were co-deposited with $B_3N_3H_6$, to study the $B_3N_3H_6-C_6H_6$ and $B_3N_3H_6-PhAc$ complexes.

Section I: $B_3N_3H_6-C_6H_6$

6.3. Computational details

The geometries, energies and vibrational frequencies of the precursor molecules, $B_3N_3H_6$ and C_6H_6 were computed using the Gaussian 09 suite of program.⁵ MP2 and M06-2X methods were employed in conjunction with 6-311++G(d,p) and aug-cc-pVDZ basis sets. Using the monomer geometries, the geometries of the $B_3N_3H_6-C_6H_6$ complexes were then computed, which are shown in Fig. 6.1. The interaction energies of the $B_3N_3H_6-C_6H_6$ complexes, were then computed and were corrected separately for zero point energy (ZPE) and basis set superposition error (BSSE) by Boys and Bernardi⁶ (Table 6.1). The single point interaction energies values computed at the MP2/CBS limit and the CCSD(T)/CBS limit were also computed, which are shown in this table. Table 6.2 gives the selected structural parameters for the $B_3N_3H_6-C_6H_6$ geometries at the MP2/aug-cc-pVDZ level of theory.

The computed frequencies and intensities of the various vibrational modes of the complexes, obtained from GAUSSIAN 09, were used to simulate a vibrational spectrum using the SYNSPEC program.⁷ The simulated vibrational spectra were generated assuming a Lorentzian line profile with a full width at half maximum (FWHM) of 1 cm^{-1} .

Atoms in molecules analysis (AIM) was used to understand the nature of the interactions by computing electron density (ρ) and $\nabla^2\rho$ at the bond critical points (BCP) corresponding to the hydrogen bonding interactions.⁸⁻¹⁰ Localized Molecular Orbital Energy Decomposition analysis (LMOEDA) was also performed using GAMESS to partition the total interaction energy of all the $B_3N_3H_6-C_6H_6$ and $B_3N_3H_6-PhAc$ complexes into various fractions.¹¹ Natural Bond Orbital analysis implemented using Gaussian 09 helped in exploring the various delocalization interactions in all the $B_3N_3H_6-C_6H_6$ and $B_3N_3H_6-PhAc$ complexes.¹²

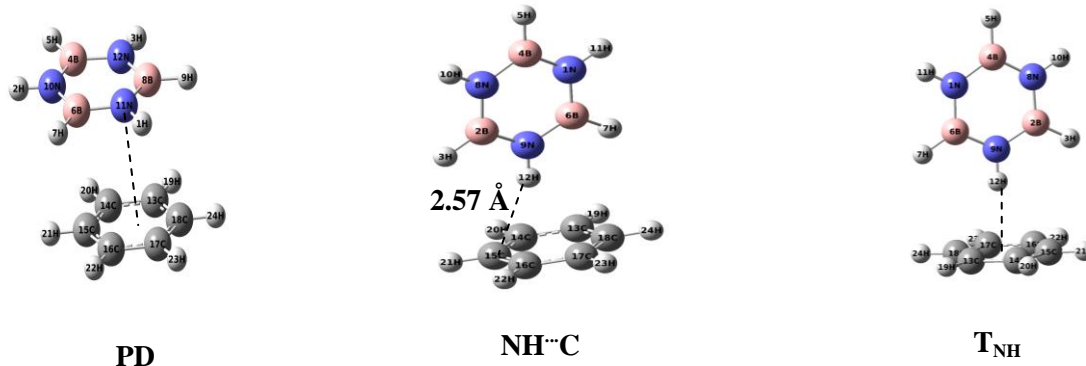


Fig.6.1. Optimised structures of the B₃N₃H₆-C₆H₆ complexes at MP2/aug-cc-pVDZ level of theory

Table 6.1. Interaction energies, in kcal/mol, of the various complexes of B₃N₃H₆-C₆H₆ heterodimers given as Uncorrected/ZPE corrected/BSSE corrected energies (kcal mol⁻¹) at MP2 and M06-2X levels of theory using the 6-311++G(d,p) and aug-cc-pVDZ basis sets.

Complex	MP2	M06-2X		CBS	
	aug-cc-pVDZ	6-311++G(d,p)	aug-cc-pVDZ	MP2	CCSD(T)
T-NH	-7.51/-6.73/-3.62	-3.97/-3.60/ -1.67	-4.55/-4.17/-2.25	-5.21	-4.50
NH...C	-7.41/-6.65/-3.63	Geom. not found	-3.50/-3.14/-2.17	-5.15	-4.48
PD	-8.35/-7.64/-3.38	-4.54/-4.08/ -3.91	-4.95/-4.78/-2.49	-5.01	-3.78

Table 6.2. Selected structural parameters for the B₃N₃H₆-C₆H₆ complexes at the MP2/aug-cc-pVDZ level of theory. The distances are given in angstroms (Å) and the angles are given in degrees (°)

T-NH	
H ₁₂ -C ₁₅	2.63 Å
H ₁₂ -C ₁₇ -H ₂₃	121.0°
N ₉ -H ₁₂ -C ₁₇ -H ₂₃	-0.57°
NH...C	
H ₁₂ -C ₁₅	2.57 Å
H ₁₂ -C ₁₅ -H ₂₁	118.7°
N ₉ -H ₁₂ -C ₁₅ -H ₂₁	-0.02°
PD	
N ₁₁ -C ₁₈	3.45 Å
N ₁₀ -C ₁₅	3.46 Å
N ₁₁ -H ₁ -C ₁₈	91.5°
N ₁₁ -H ₁ -C ₁₈ -H ₂₄	120.6°

6.4. RESULTS AND DISCUSSION

6.4.1 Computational

The interaction energies of the different $B_3N_3H_6-C_6H_6$ complexes at the M06-2X and MP2 methods using aug-cc-pVDZ and 6-311++G(d,p) basis sets are shown in Table 6.1. The interaction energies were also calculated at the MP2/CBS and CCSD(T)/CBS limit for all the complexes, as shown in this table.

Our computations at the MP2/aug-cc-pVDZ level of theory indicated three structures for the $B_3N_3H_6-C_6H_6$ complexes. The first structure was the parallel displaced structure (PD), in which the C_6H_6 and $B_3N_3H_6$ rings were slightly displaced relative to each other. The second structure was the one where the N-H of $B_3N_3H_6$ interacted with the carbon atom of C_6H_6 (which we have labelled as the $NH\cdots C$ structure) and the third structure was the T-NH structure, where the N-H of $B_3N_3H_6$ pointed to the centre of the C_6H_6 ring. The energies of these structures are given in Table 6.1.

As can be seen from table 6.1, at the MP2/aug-cc-pVDZ level, the T-NH and the $NH\cdots C$ structures were found to be almost isoenergetic and the lowest in energy, followed by the PD structure.

6.4.2 Experimental

Figure 6.2(a) in Panel A shows the matrix isolation spectrum of C_6H_6 . Figure 6.2(b) shows the infrared spectrum of matrix isolated $B_3N_3H_6$ in N_2 matrix with strong absorptions at 3476.7 cm^{-1} and 3472.0 cm^{-1} corresponding to the antisymmetric N-H stretches in $B_3N_3H_6$. Trace (c) shows the spectrum when both $B_3N_3H_6$ and C_6H_6 were deposited at 12 K. Traces (d) and (e) show the infrared spectra when the matrix was annealed 27 K. On annealing the matrix, new product features were observed, at 3437.6 cm^{-1} and a weaker feature 3452.7 cm^{-1} .

Fig. 6.2 Panel B shows the spectra over the region $910-925\text{ cm}^{-1}$, which corresponds to the bending region of $B_3N_3H_6$. As seen from the spectra (d) and (e), the product band observed at 916.2 cm^{-1} can be unambiguously assigned to the $B_3N_3H_6-C_6H_6$ complex as this feature could be discerned only in the annealed spectrum and also only when both precursors were co-deposited.

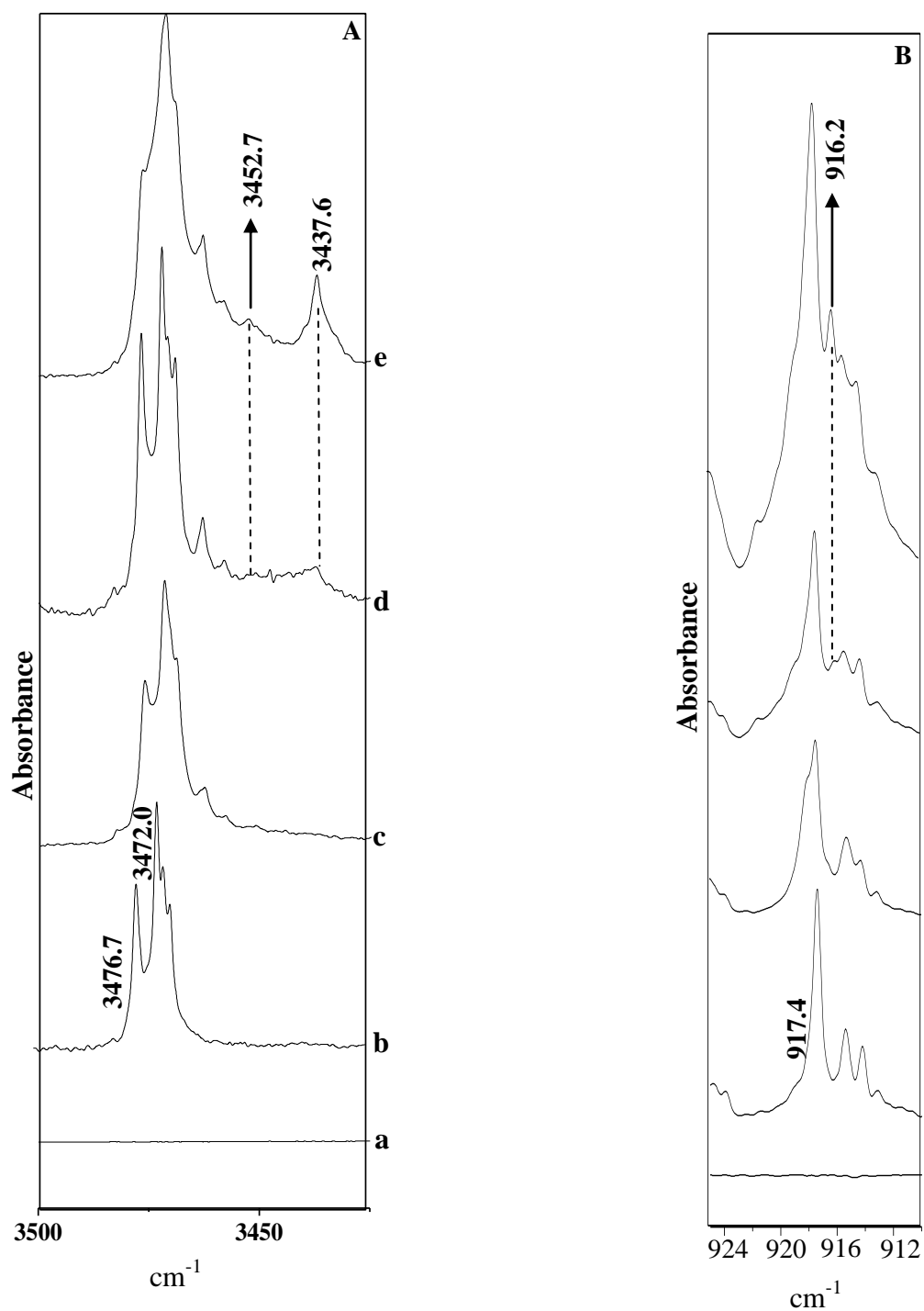


Fig.6.2. Panel A shows matrix isolation IR spectra from 3500-3425 cm⁻¹. (a) C₆H₆: N₂ (3:1000) (b) B₃N₃H₆:N₂ (x:1000) (c) B₃N₃H₆:C₆H₆:N₂ (x:3:1000) at 12K (d) B₃N₃H₆:C₆H₆: N₂ (x:3:1000) annealed at 27K (e) B₃N₃H₆:C₆H₆:N₂ (x:6:1000) annealed at 27K. Panel B shows the bending region of B₃N₃H₆ from 925-910 cm⁻¹. (a) C₆H₆:N₂ (3:1000) (b) B₃N₃H₆:N₂ (x:1000) (c)B₃N₃H₆:C₆H₆:N₂ (x:3:1000) at 12K (d) B₃N₃H₆:C₆H₆:N₂ (x:3:1000) annealed at 27K (e) B₃N₃H₆:C₆H₆:N₂ (x:6:1000) annealed at 27K.

6.5. Vibrational Assignments

6.5.1. N-H stretch in $B_3N_3H_6$

The new product feature at 3437.6 cm^{-1} , which is a red shift of 34.4 cm^{-1} , agrees well with the computed red shift for the N-H stretch in $B_3N_3H_6$, of 32.7 cm^{-1} for the $NH\cdots C$ complex. This complex, together with the T-NH structure, constitute the two nearly degenerate lowest energy isomers of the complex. The weak feature at 3452.7 cm^{-1} feature, which is a red shift of 19.3 cm^{-1} , can be assigned to the N-H stretch in the T-NH complex, which shows a computed red shift of 18.0 cm^{-1} . Our experiments therefore identified both the lowest energy, $NH\cdots C$ and T-NH structures, in both of which $B_3N_3H_6$ serves as the proton donor to C_6H_6 . (Table 6.3 and figure 6.3).

6.5.2. Ring bending mode in $B_3N_3H_6$

The new product feature in the bending region was found to occur at 916.2 cm^{-1} . This feature is in good agreement with the computed feature for the same mode at 916.1 for the $NH\cdots C$ isomer. The shift in the T-NH structure is too small ($\sim 0.2\text{ cm}^{-1}$) to be experimentally identified (Table 6.3 and fig.6.3).

Section II. $B_3N_3H_6$ -PhAc complexes

6.6. Computational Details

In case of the $B_3N_3H_6$ -PhAc complexes, our computations at the MP2/aug-cc-pVDZ level of theory, revealed three complexes, which were minima on the potential energy surface. One was the bent $NH\cdots C$ complex, where the N-H of $B_3N_3H_6$ interacted with one of the carbon atoms of C_2H_2 in PhAc. This complex was similar to the bent $NH\cdots C$ complex obtained in our studies on the $B_3N_3H_6$ - C_2H_2 complexes.² The second structure was the stacked geometry, where both the partially delocalized π electron cloud of $B_3N_3H_6$ and phenyl π cloud in PhAc were stacked above one other. The third structure was a T-NH structure, where the N-H of $B_3N_3H_6$ interacts with the π cloud of the phenyl ring in PhAc. The interaction energies of all the optimized structures at the M06-2X and MP2 methods in conjunction with the 6-311++G(d,p) and the aug-cc-pVDZ basis sets are shown in Table 6.4. The single point interaction energies values computed at the MP2/CBS limit and the CCSD(T)/CBS limit were also computed, which are also shown table 6.4. Table 6.5 gives the selected structural parameters for the $B_3N_3H_6$ -PhAc complexes at the MP2/aug-cc-pVDZ level of theory.

Table 6.3. Experimental (N_2 matrix), scaled computed vibrational wavenumbers (in cm^{-1}) and mode assignments for $B_3N_3H_6-C_6H_6$ complexes. Computations were performed at MP2/aug-cc-pVDZ level.

Experimental		Computed			Mode
Monomer	Complex	NH \cdots C	T-NH	PD	
$B_3N_3H_6$ 3472.0	3437.6 (-34.4)	3439.3 (-32.7)	3454.0 (-18.0)	3465.5 (-6.5)	N-H stretch in $B_3N_3H_6$
	3452.7 (-19.3)	3439.3 (-32.7)	3454.0 (-18.0)	3465.5 (-6.5)	
917.4	916.2 (-1.2)	916.1 (-1.3)	917.2 (-0.2)	912.2 (-5.2)	Ring deformation

^[a] Scale factors are: 0.9522 for the N-H stretch in $B_3N_3H_6$; 0.9989 for the N-H bend in $B_3N_3H_6$.

^[b] Values in parentheses are $\Delta\nu$, defined as $[\nu(\text{complex}) - \nu(\text{monomer})]$.

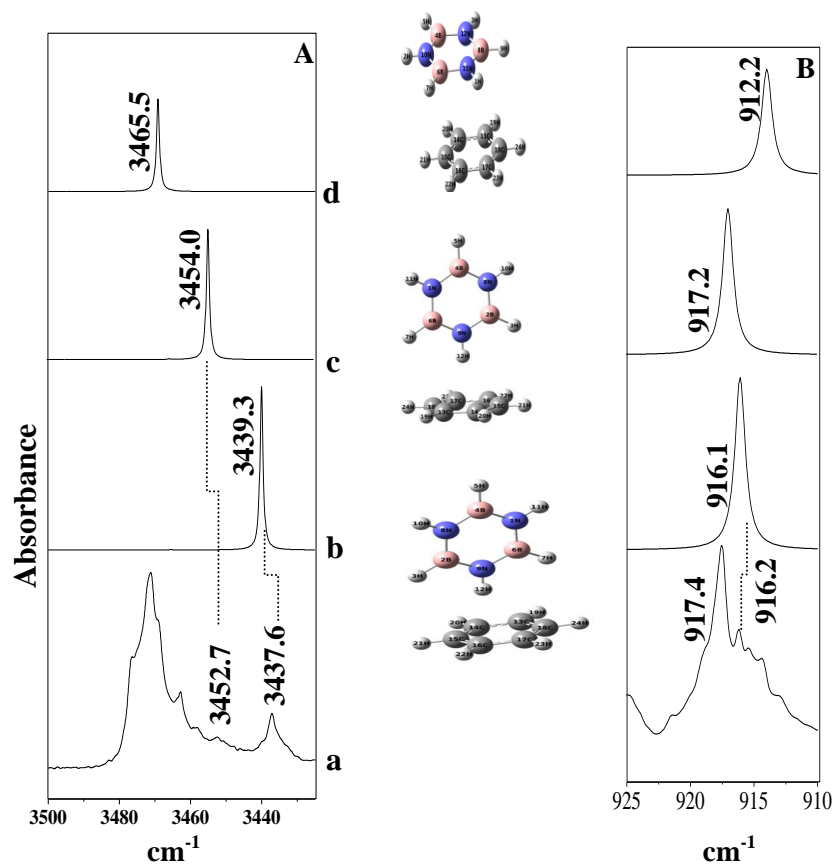


Fig.6.3. Panel A showing (a) experimental spectrum of $\text{B}_3\text{N}_3\text{H}_6:\text{C}_6\text{H}_6:\text{N}_2$ annealed at 27K (x:6:1000) (b) Computed spectrum of bent $\text{NH}\cdots\text{C}$ complex(c) Computed spectrum of T-NH complex (d) Computed spectrum of PD complex

6.7. Results and Discussion

6.7.1 Computational

The interaction energies of the different $B_3N_3H_6$ -PhAc complexes at the M06-2X and MP2 methods using aug-cc-pVDZ and 6-311++G** basis sets are shown in Table 6.4. The interaction energies were also calculated at the MP2/CBS and CCSD(T)/CBS limit for all the complexes, as shown in this table.

Our computations at the MP2/aug-cc-pVDZ level of theory indicated three structures for the $B_3N_3H_6$ -PhAc complexes. The first structure was the stacked structure, in which the electron cloud of PhAc and $B_3N_3H_6$ rings were stacked above each other. The second structure was the one where the N-H of $B_3N_3H_6$ interacted with the carbon atom of C_2H_2 in PhAc (which we have labelled as the bent $NH\cdots C$ structure) and the third structure was the T-NH structure, where the N-H of $B_3N_3H_6$ pointed to the centre of the phenyl ring in PhAc.

As can be seen from table 6.4, at the MP2/aug-cc-pVDZ level, the stacked structure was found to be the lowest in energy, followed by the T-NH and the bent $NH\cdots C$ structures.

6.7.2. Experimental

Panels A, B and C in Fig. 6.5 show the infrared spectra, spanning the regions 3550-3400, 3340-3300 and 2610-2590 cm^{-1} , respectively. Trace 'a' in the figure shows the infrared spectrum of matrix isolated PhAc in a N_2 matrix. Strong absorptions are observed at 3323.1 cm^{-1} and 3309 cm^{-1} , corresponding to the Fermi diad of PhAc (Panel B). Trace 'b' shows the infrared spectrum of matrix isolated $B_3N_3H_6$ in a N_2 matrix. Strong absorptions are observed at 3476.7 cm^{-1} and 3472.0 cm^{-1} , corresponding to the antisymmetric stretch of $B_3N_3H_6$ (Panel A). This is a doubly degenerate mode, split due to the matrix site effects.

When $B_3N_3H_6$ and PhAc were co-deposited, and the matrix then annealed, new product features were observed at 3433.4 cm^{-1} and 3315.5 cm^{-1} (Trace 'd' Panels A and B). The product features mentioned above increased in intensity when the concentration of either of the two precursors, $B_3N_3H_6$ or PhAc, was increased, thereby confirming that they were due to the $B_3N_3H_6$ -PhAc adducts. Furthermore, they were not observed when only one of the two precursors were deposited.

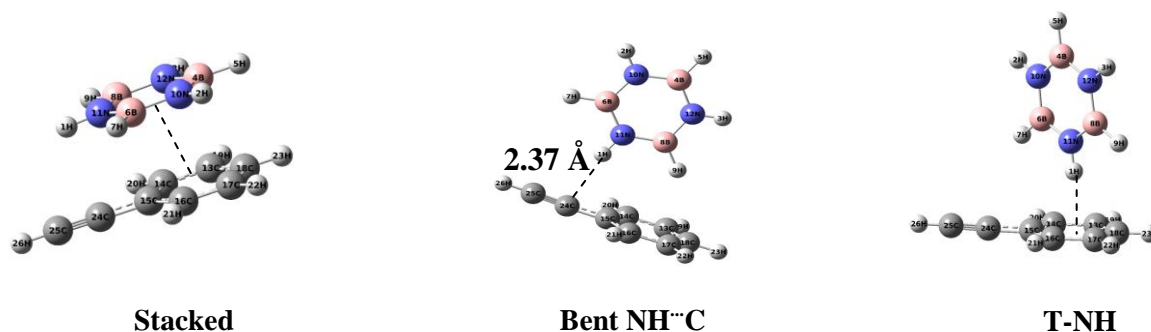


Fig. 6.4. Optimized structures of $B_3N_3H_6$ -PhAc complexes at MP2/aug-cc-pVDZ level of theory

Table 6.4. Interaction energies, in kcal mol^{-1} , of the various complexes of $B_3N_3H_6$ -PhAc, given as uncorrected/ZPE corrected/BSSE corrected energies (kcal mol^{-1}) at M06-2X and MP2 levels of theory using 6-311++G(d,p) and aug-cc-pVDZ basis sets.

Complex	M06-2X		MP2		CBS	CCSD(T)
	6-311++G(d,p)	aug-cc-pVDZ	6-311++G(d,p)	aug-cc-pVDZ		
Stacked	-5.59/-5.10/-4.83	-6.13/-5.65/-4.64	-8.17/-7.82/-3.11	-10.25/-9.70/-4.33	-6.19	-4.54
T-NH	-4.03/-3.53/-3.49	-4.44/-4.24/-2.16	Geom. Not found	-7.57/-7.09/-3.70	-5.30	-4.77
Bent NH...C	-3.75/-3.33/-3.26	-4.16/-3.77/-3.15	-5.54/-5.11/-2.28	-7.24/-6.54/-3.37	-4.88	-4.07

Table 6.5. Selected structural parameters for the various B₃N₃H₆-PhAc complexes at the MP2/aug-cc-pVDZ level of theory.

Stacked	
N ₁₁ -C ₁₅	3.46 Å
B ₄ -C ₁₈	3.66 Å
C ₂₅ -N ₁₁ -H ₁	54.7°
N ₁₀ -H ₂ -C ₁₈	56.5°
C ₂₄ -C ₁₅ -C ₁₆ -H ₂₁	-0.35°
T-NH	
H ₁ -C ₁₃	2.74 Å
N ₁₁ -H ₁ -C ₁₈	156.0°
N ₁₁ -H ₁ -C ₁₈ -H ₂₃	22.2°
Bent NH...C	
H ₁ -C ₂₄	2.37 Å
H ₁ -C ₂₅	2.77 Å
N ₁₁ -H ₁ -C ₂₄	168.5°
N ₁₁ -H ₁ -C ₂₄ -C ₂₅	-179.9°

6.8. Vibrational assignments

The experimentally observed product bands in the $B_3N_3H_6$ -PhAc co-deposition experiments were assigned based on the computed wavenumbers obtained at MP2/aug-cc-pVDZ. As explained before, the computed frequencies for the complexes were scaled using scaling factors that were computed by comparing the computed and experimental features of the monomer precursors, as described in Chapter 3. The mode assignments for the different vibrations in the $B_3N_3H_6$ -PhAc complexes are given in table 6.6. Figure 6.6 (Panels A and B) show the computed plots of all the complexes using SYNSPEC program and compares with the experimental spectrum. The simulated vibrational spectra were generated assuming a Lorentzian line profile with a full width at half maximum (FWHM) of 1 cm^{-1} .

6.8.1. N-H stretch in $B_3N_3H_6$

Fig. 6.5(b) shows the spectrum of $B_3N_3H_6$, with a strong absorption at 3472.0 cm^{-1} and 3476.7 cm^{-1} , that corresponds to the antisymmetric stretch of $B_3N_3H_6$. The product feature due to PhAc- $B_3N_3H_6$ complex at 3433.4 cm^{-1} can be assigned to the N-H stretch in $B_3N_3H_6$, thus showing a red shift of 39 cm^{-1} in the N_2 matrix. As can be seen from table 6.6, the computed shift of this mode was 29 cm^{-1} which is in close agreement with those obtained for the structure where the N-H of $B_3N_3H_6$ acts as a proton donor to the carbon atom of C_2H_2 in PhAc. The shifts computed for the other complexes are clearly different from that observed in our experiments, thus indicating that we were observing the bent $NH\cdots C$ complex in our matrix isolation experiments. It must be noted that in the study of the $B_3N_3H_6$ - C_6H_6 complexes, the T-NH structure was also observed along with the $NH\cdots C$ structure. However, the intensity of the T-NH structure was less as compared to the $NH\cdots C$ structure. In case of the $B_3N_3H_6$ -PhAc complexes, the T-NH structure could not be discerned in our experiments. It would be worthwhile to mention here that in our study on the $B_3N_3H_6$ - C_2H_2 complexes, the bent $NH\cdots C$ structure was the one observed in our matrix isolation experiments. In some ways, the $B_3N_3H_6$ -PhAc system was mimicking the $B_3N_3H_6$ - C_2H_2 system.

6.8.2. C-H symmetric stretch in PhAc

In the N_2 matrix, PhAc shows a strong absorption at 3323.1 cm^{-1} with a Fermi resonance diad appearing as a site split feature at $3309.2/3310.8\text{ cm}^{-1}$. The Fermi resonance has been reported to occur between the C-H stretching vibration and a combination of one quantum of C-C stretch and two quanta of C-C-H out of plane bend¹³. The C-H stretch in PhAc was observed at

3315.5 cm^{-1} which showed an experimental shift of 7.6 cm^{-1} which is in excellent agreement with the computational shift of 5.0 cm^{-1} for the bent $\text{NH}\cdots\text{C}$ complex.

PhAc_D-Borazine Experiments

6.8.3. C-D stretch in PhAc_D

Experiments were also done with PhAc_D to explore the complex feature in the C-D region of PhAc_D (Fig.6.5, Panel C). Since the C-D region of PhAc_D does not show any Fermi resonance, we were able to discern the C-D stretch in PhAc_D at 2595.0 cm^{-1} which agreed well with the computationally scaled wavenumber of 2594.3 cm^{-1} for the bent $\text{NH}\cdots\text{C}$ complex. Hence, the excellent agreement for the feature of the isotopic species lends credence to our assignment and to our conclusion that the bent $\text{NH}\cdots\text{C}$ is observed in our experiments.

As can be seen from table 6.6, the computed feature for the bent $\text{NH}\cdots\text{C}$ complex in the C-D stretching region of PhAc_D at 2594.3 cm^{-1} , which shows a red shift of 5.7 cm^{-1} , matches excellently with the experimental feature of this complex at 2595.0 cm^{-1} , showing a red shift of 5 cm^{-1} .

6.9. Atoms-in-molecules analysis

AIM analysis was carried out for all the complexes to explore the nature of interactions. In all the $\text{B}_3\text{N}_3\text{H}_6\text{-C}_6\text{H}_6$ and $\text{B}_3\text{N}_3\text{H}_6\text{-PhAc}$ complexes, the values of ρ fall in the range proposed by Koch and Popelier for hydrogen bonded systems.¹⁴ The electron density at the intramolecular bond critical point was found to be almost same in the T-NH and the $\text{NH}\cdots\text{C}$ complex in case of the $\text{B}_3\text{N}_3\text{H}_6\text{-C}_6\text{H}_6$ complexes.

In the case of the $\text{B}_3\text{N}_3\text{H}_6\text{-PhAc}$ complexes too, the electron density at the bond critical point corresponding to the hydrogen bond was found to be nearly the same for the bent $\text{NH}\cdots\text{C}$ complex and the T-NH complex. An examination of $|\lambda_1/\lambda_3|$ values shows this ratio to be small for the stacked geometries in both systems, which is indicative of the fact that the charges are not accumulated between the atoms in the bonding region but more on the atoms. Tables 6.7 and 6.8 present the data of the AIM analysis at MP2/aug-cc-pVDZ for the various $\text{B}_3\text{N}_3\text{H}_6\text{-C}_6\text{H}_6$ and $\text{B}_3\text{N}_3\text{H}_6\text{-PhAc}$ complexes, respectively while figures 6.7 and 6.8 show the various intramolecular bond critical points of the complexes.

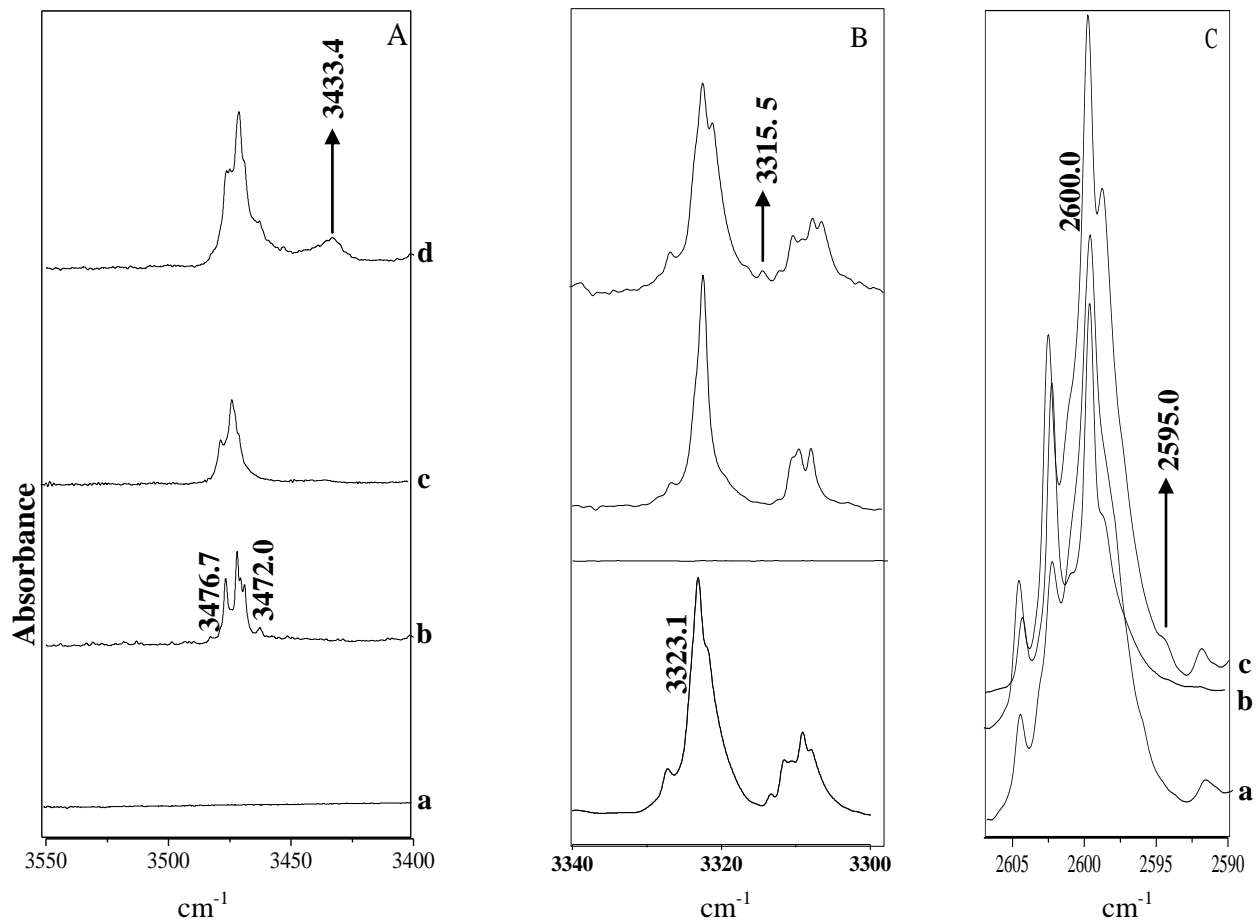


Fig.6.5. Panels A and B represent infrared spectrum of (a) PhAc:N₂ (1:1000) (b) B₃N₃H₆:N₂ (x:1000) (c) B₃N₃H₆: PhAc:N₂ (x:1:1000) at 12 K (d) spectrum of (c) annealed at 27 K. Panel C (a) PhAc_D:N₂ (1:1000) (b) B₃N₃H₆:PhAc_D:N₂ (x:1:1000) at 12 K (c) B₃N₃H₆:PhAc_D:N₂ (x:1:1000) annealed at 27 K. Panels A, B and C show the regions 3550-3400, 3340-3300 and 2610-2590 cm^{-1} respectively.

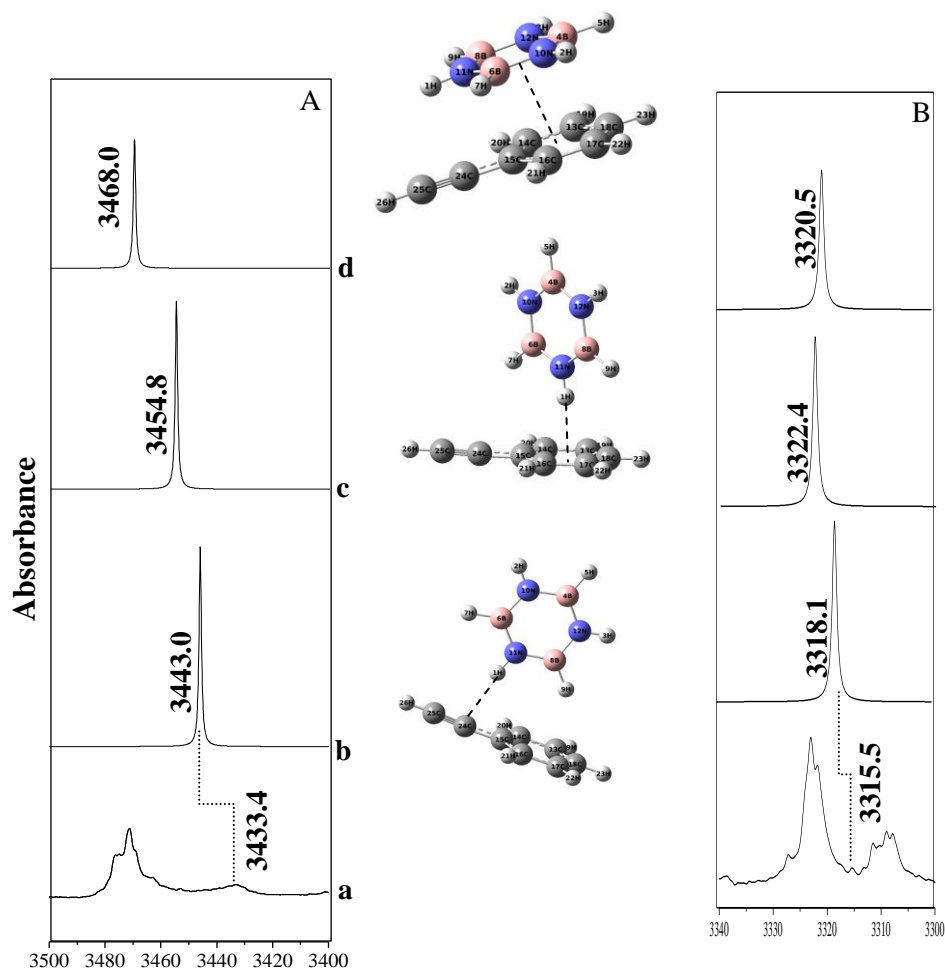


Fig.6.6. Panel A showing the (a) Experimental spectrum of $B_3N_3H_6:PhAc:N_2$ (x:1:1000) annealed at 27K (b) Computed spectrum of Bent $NH...C$ complex (c) T-NH complex (d) Stacked complex.

Table 6.6. Experimental (N_2 matrix), scaled^a computed vibrational wavenumbers (in cm^{-1}) and mode assignments for $B_3N_3H_6$ -PhAc and $B_3N_3H_6$ -PhAc_D complexes at MP2/aug-cc-pVDZ level

Experimental		Computed			Mode
Monomer	Complex	Bent NH...C	T-NH	Stacked	
$B_3N_3H_6$ 3472.0	3433.4 (-38.6)^b	3443.0 (-29.0)	3454.8 (-17.2)	3468.0 (-4.0)	N-H asym. str. in $B_3N_3H_6$
PhAc 3323.1	3315.5 (-7.6)	3318.1 (-5.0)	3322.4 (-0.7)	3320.5 (-2.6)	C-H str. in PhAc
PhAc_D 2600.0	2595.0 (-5.0)	2594.3 (-5.7)	2598.9 (-1.1)	2612.5 (12.5)	C-D str. in PhAc _D

^[a] Scale factors are: 0.9522 for the N-H stretch in $B_3N_3H_6$; 0.9546 for the C-H stretch in PhAc and 0.9712 for the C-D stretch in PhAc_D

^[b] Values in parentheses are $\Delta\nu$, defined as $[\nu(\text{complex}) - \nu(\text{monomer})]$.

6.10. Energy Decomposition Analysis

LMO-EDA¹¹ computations were performed for the B₃N₃H₆-C₆H₆ and B₃N₃H₆-PhAc complexes, to understand the components of total interaction energy, in terms of electrostatic energy, exchange energy, repulsion energy, polarization energy and dispersion energy. As can be seen from the tables 6.9 and 6.10, the dispersion interaction is the major contributor towards the total interaction energy followed by electrostatic for all the B₃N₃H₆-C₆H₆ and B₃N₃H₆-PhAc complexes. The polarisation component is the least significant contributor among all the complexes.

6.11. Natural Bond Orbital Analysis

NBO was performed for the B₃N₃H₆-C₆H₆ and B₃N₃H₆-PhAc complexes at the MP2/aug-cc-pVDZ level.

In the case of B₃N₃H₆-C₆H₆, it was observed that in the NH[⋯]C complex, which was observed in our experiments, there was a preferential interaction of B₃N₃H₆ with one side of the benzene ring (C₁₅), as indicated by the NBO analysis (Table 6.11). In the T-NH complex, the interaction of B₃N₃H₆ was more symmetric, with the interaction being nearly the same with all the carbons of C₆H₆, indicating the N-H of B₃N₃H₆ was pointing to the centre of the C₆H₆ ring.

In case of the B₃N₃H₆-PhAc complexes, the bent NH[⋯]C complex, which was the one observed in the matrix, the strongest delocalisation interaction was present between the bonding orbitals of C₂₄-C₂₅ and the antibonding orbitals of N₁₁-H₁. It must be noted that in the T-NH complex, the lower symmetry of PhAc compared with C₆H₆, causes the N-H to be asymmetrically disposed, and hence B₃N₃H₆ is tilted towards one side of the PhAc, which is indicated by the pattern of interaction revealed by our NBO calculations. (Table 6.12)

6.12. Phenylacetylene-Benzene Complexes

In addition to studying the B₃N₃H₆-C₆H₆ and B₃N₃H₆-PhAc complexes, we also explored the PhAc-C₆H₆ complexes. For this complex, two structures were found as minima on the potential energy surface at the M06-2X and MP2 levels of theory. The stacked structure was found to be the global minimum having a BSSE corrected interaction energy of -5.88 kcal/mol at the MP2/aug-cc-pVDZ level of theory, followed by the H[⋯]π complex, where the C-H of PhAc was acting as a proton donor to the π cloud of C₆H₆, having a BSSE corrected interaction energy of -2.92 kcal/mol. Matrix isolation experiments were done both in N₂ and Ar experiments.

However, we were not observe product features that could be unambiguously assigned to any of the complexes and hence, not been discussed.

6.13. Conclusions

This work reports a matrix isolation study of the interactions between $B_3N_3H_6$ with C_6H_6 and PhAc. The computational studies on the $B_3N_3H_6$ - C_6H_6 complexes carried out by Bettinger *et al* revealed the T-NH structure and the parallel displaced structure to be nearly isoenergetic and the global minima at the MP2/aug-cc-pVQZ level of theory. Our computations at the M06-2X and the MP2 levels indicates an additional structure where the N-H of $B_3N_3H_6$ interacted with one of the carbon atoms of C_6H_6 , which we label as the $NH\cdots C$ complex. We were able to observe this complex along with the T-NH complex, where the N-H of $B_3N_3H_6$ interacts with the π cloud of C_6H_6 .

The computations, at the MP2 and M06-2X levels on the $B_3N_3H_6$ -PhAc system yielded three minima; the stacked structure, the bent NH-C and T-NH structure. Of these, we observed the bent NH-C structure in the matrix. This observation was also corroborated by experiments where we used PhAc_D, where the features due to C-D stretch in PhAc_D confirms the presence of the bent $NH\cdots C$ complex in our experiments.

AIM calculations were done to determine the nature of bonding in these complexes. Energy decomposition analysis was also done on the various complexes to explore the nature of interactions. The stacked structures, despite being the global minima structures in case of the PhAc- $B_3N_3H_6$ and PhAc- C_6H_6 complexes, could not be observed in our matrix isolation experiments, since they do not present strong signatures in the infrared experiment. This work gives an insight into the various hydrogen bonding interactions occurring between an N-H system like $B_3N_3H_6$ and π systems like C_6H_6 and PhAc.

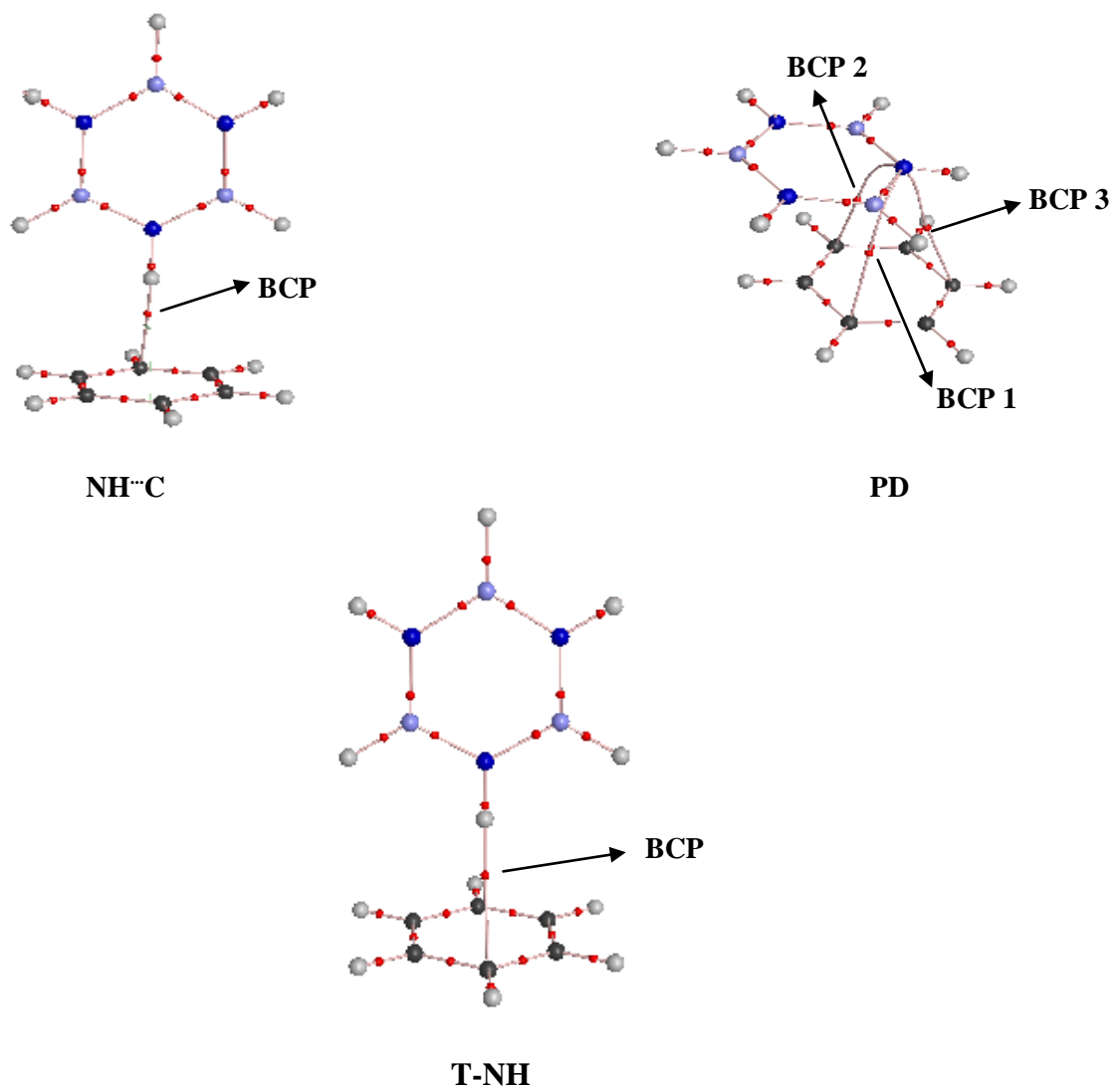


Fig 6.7. AIM analysis of $B_3N_3H_6-C_6H_6$ complexes at MP2/aug-cc-pVDZ

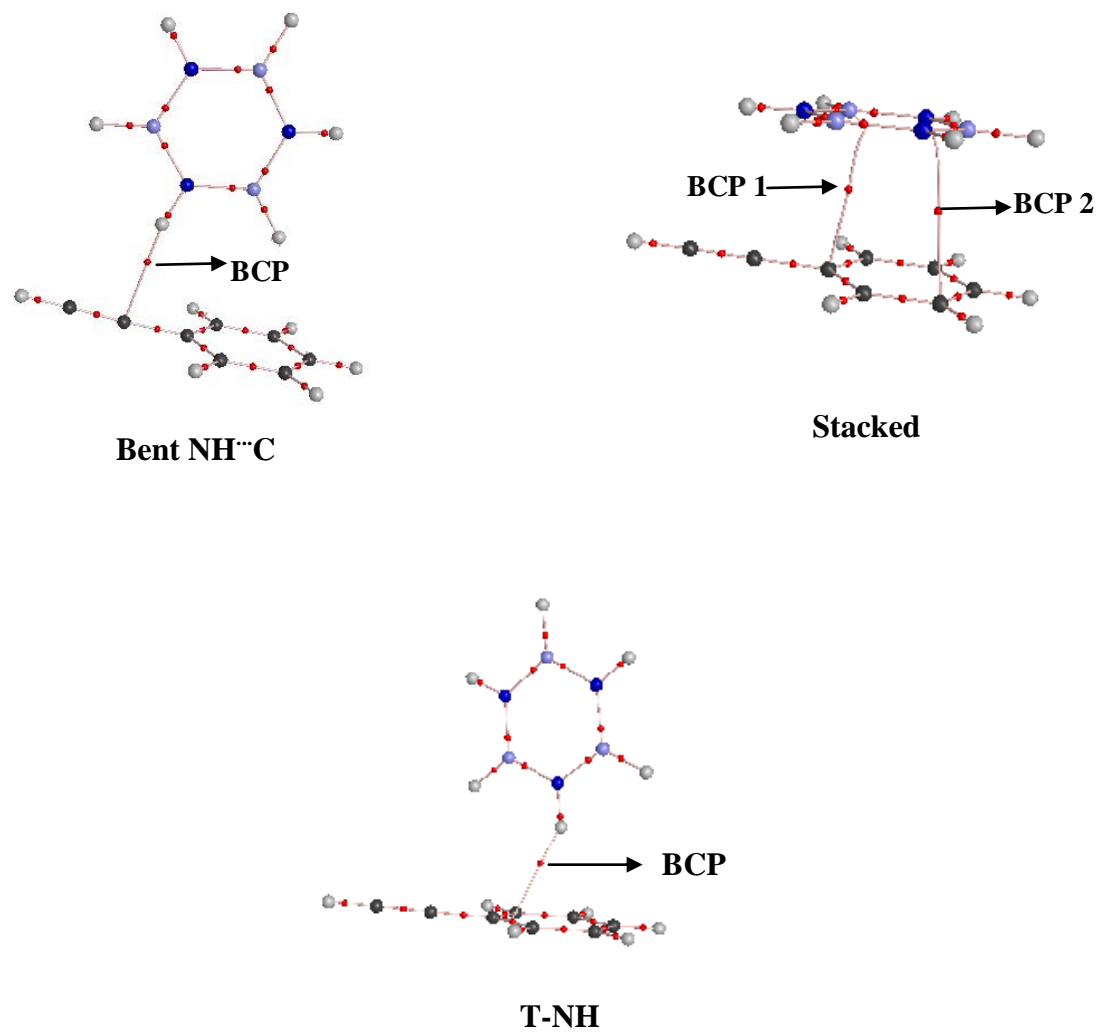


Fig.6.8. AIM analysis of $B_3N_3H_6$ -PhAc complexes at MP2/aug-cc-pVDZ

Table 6.7. AIM calculations showing the values of the electron density $\rho(r_c)$ and its Laplacian $\nabla^2\rho(r_c)$, λ_1/λ_3 at the bond critical point for the $B_3N_3H_6-C_6H_6$ complexes computed at MP2/aug-cc-pVDZ level of theory. The values of $\rho(r)$, $\nabla^2\rho(r)$ are in atomic units.

Complex	$\rho(r_c)$	λ_1	λ_2	λ_3	$\nabla^2\rho(r)$	λ_1/λ_3
PD ^a	0.0074	-0.0021	-0.0019	0.0249	0.021	0.083
	0.0074	-0.0020	-0.0018	0.0249	0.021	0.082
	0.0058	-0.0019	-0.0002	0.0194	0.017	0.101
NH\cdotsC	0.0095	-0.0064	-0.0006	0.0380	0.031	0.168
T-NH	0.0096	-0.0065	-0.0009	0.0385	0.031	0.169

^aValues of electron density and Laplacian at BCP 1,2 and 3 indicated.

Table 6.8. AIM calculations showing the values of the electron density $\rho(r_c)$ and its Laplacian $\nabla^2\rho(r_c)$, λ_1/λ_3 at the bond critical point for the $B_3N_3H_6-PhAc$ complexes computed at MP2/aug-cc-pVDZ level of theory. The values of $\rho(r)$, $\nabla^2\rho(r)$ are in atomic units.

Complex	$\rho(r_c)$	λ_1	λ_2	λ_3	$\nabla^2\rho(r)$	λ_1/λ_3
Stacked ^a	0.0079	-0.0023	-0.0010	0.0270	0.024	0.085
	0.0071	-0.0019	-0.0020	0.0238	0.020	0.080
T-NH	0.0100	-0.0067	-0.0003	0.0397	0.033	0.169
Bent NH\cdotsC	0.0117	-0.0104	-0.0066	0.0531	0.036	0.196

^aValues of electron density and Laplacian at BCP 1 and 2 indicated.

Table 6.9. Values of the interaction energy (ΔE) and its different components (in kcal/mol units), for the various $B_3N_3H_6-C_6H_6$ complexes using Energy Decomposition Analysis at MP2/aug-cc-pVDZ level of theory.

Complex	E_{elec}	E_{ex-rep}	E_{pol}	E_{dis}	E_{total}
PD	-5.15	12.74	-2.98	-13.06	-8.45
T_{NH}	-3.83	7.34	-2.34	-8.72	-7.55
NH...C	-3.68	6.93	-2.25	-8.45	-7.45

Table 6.10. Values of the interaction energy (ΔE) and its different components (in kcal/mol units), for the various $B_3N_3H_6-PhAc$ complexes using Energy Decomposition Analysis at MP2/aug-cc-pVDZ level of theory.

Complex	E_{elec}	E_{ex-rep}	E_{pol}	E_{dis}	E_{total}
Stacked	-6.02	11.50	-2.54	-13.15	-10.21
T-NH	-2.92	5.99	-2.14	-8.56	-7.63
Bent NH...C	-3.71	8.43	-2.43	-9.60	-7.31

Table 6.11. NBO analysis for the B₃N₃H₆-C₆H₆ dimers, performed at MP2/aug-cc-pVDZ level of theory. The atom numbering indicated in the table is as shown in Fig. 6.1. E is the second order perturbation energy, E(j)-E(i) is the donor-acceptor energy difference and F(i,j) is the overlap between the donor and acceptor orbitals.

Complex	Orbitals involved		E(2) (kcal/mol)	E(j)-E(i) a.u.	F(i,j) a.u.
	Donor	Acceptor			
PD	LP*(1)C ₁₃	B ₈ -N ₁₁ (σ*)	3.81	0.31	0.040
T-NH	LP*(1)C ₁₃	N ₉ -H ₁₂ (σ*)	0.32	0.84	0.020
	LP*(1)C ₁₄	N ₉ -H ₁₂ (σ*)	0.27	0.84	0.020
	LP*(1)C ₁₅	N ₉ -H ₁₂ (σ*)	0.31	0.84	0.020
	LP(1)C ₁₆	N ₉ -H ₁₂ (σ*)	0.40	0.84	0.023
	LP(1)C ₁₇	N ₉ -H ₁₂ (σ*)	0.45	0.84	0.024
NH...C	LP(1)C ₁₈	N ₉ -H ₁₂ (σ*)	0.41	0.84	0.023
	LP(1) C ₁₃	N ₉ -H ₁₂ (σ*)	0.22	0.84	0.023
	LP(1) C ₁₄	N ₉ -H ₁₂ (σ*)	0.41	0.84	0.023
	LP(1) C ₁₅	N ₉ -H ₁₂ (σ*)	0.57	0.84	0.027
	LP(1) C ₁₆	N ₉ -H ₁₂ (σ*)	0.40	0.84	0.017
	LP(1) C ₁₇	N ₉ -H ₁₂ (σ*)	0.21	0.84	0.017
	LP(1) C ₁₈	N ₉ -H ₁₂ (σ*)	0.15	0.83	0.014

Table 6.12. NBO analysis for the $B_3N_3H_6$ -PhAc dimers, performed at MP2/aug-cc-pVDZ level of theory. The atom numbering indicated in the table is as shown in Fig. 6.4. E is the second order perturbation energy, $E(j)-E(i)$ is the donor-acceptor energy difference and $F(i,j)$ is the overlap between the donor and acceptor orbitals.

Complex	Orbitals involved		E (kcal/mol)	E(j)-E(i) a.u.	F(i,j) a.u.
	Donor	Acceptor			
Stacked	LP(1)C ₁₆	B ₆ -N ₁₀ (σ^*)	3.13	0.32	0.037
T-NH	LP(1)C ₁₃	H ₁ -N ₁₁ (σ^*)	0.18	0.84	0.016
	LP(1)C ₁₄	H ₁ -N ₁₁ (σ^*)	0.07	0.84	0.010
	LP(1)C ₁₅	H ₁ -N ₁₁ (σ^*)	0.13	0.85	0.013
	LP(1)C ₁₆	H ₁ -N ₁₁ (σ^*)	0.27	0.84	0.019
	LP(1)C ₁₇	H ₁ -N ₁₁ (σ^*)	0.71	0.85	0.031
	LP*(1)C ₁₈	H ₁ -N ₁₁ (σ^*)	0.53	0.84	0.027
Bent NH \cdots C	(σ)C ₂₄ -C ₂₅	N ₁₁ -H ₁ (σ^*)	1.98	1.16	0.043



Fig. 6.9. Optimized geometries of PhAc- C_6H_6 complexes at MP2/aug-cc-pVDZ

REFERENCES

- (1) Mishra, P.; Verma, K.; Bawari, D.; Viswanathan, K.S. Does borazine-water behave like benzene-water? A matrix isolation infrared and *ab initio* study. *J. Chem. Phys.* 2016, **144**, 234307-234316.
- (2) Verma, K.; Viswanathan, K.S.; Sathyamurthy, N.; Majumder, M. How different is the Borazine–Acetylene Dimer from the Benzene-Acetylene Dimer? A Matrix Isolation Infrared and *Ab Initio* Quantum Chemical Study. *Mol.Phys.* **2017**, DOI: 10.1080/00268976.2017.1284357.
- (3) Verma, K.; Viswanathan, K.S. The Borazine Dimer: Case of a Classical Hydrogen Bond Competing With a Dihydrogen Bond. *Phys. Chem. Chem. Phys.* 2017, **19**, 19067-19074.
- (4) Bettinger, H.F.; Kar, T.; Sanchez-Garcia, E. Borazine and benzene homo- and heterodimers. *J. Phys. Chem. A.* **2009**, *113*, 3353-3359.
- (5) M.J. Frisch, G.W. Trucks, H.B. Schlegel, G.E. Scuseria, M.A. Robb, J.R. Cheeseman, G. Scalmani, V. Barone, B. Mennucci, and Petersson et. al. Gaussian, Inc., Wallingford CT, 2010.
- (6) Boys, S.B.; Bernardi, F. The calculation of small molecular interactions by the differences of separate total energies. Some procedures with reduced errors. *Mol.Phys.* **1970**, *19*, 553-566.
- (7) The spectra were simulated using SYNSPEC made available by K. Irikura, National Institute of Standards and Technology, Gaithersburg, MD 20899, USA, **1995**.
- (8) R.F.W. Bader *Atoms in Molecules. A Quantum Theory* (Clarendon Press, Oxford, 1994).
- (9) R.G.A. Bone and R.F.W. Bader Identifying and analyzing intermolecular bonding interactions in van der Waals molecules *J. Phys. Chem.* **1996**, *100*, 10892-10911.
- (10) F. Bieger-König, D. Bayles, and J. Schönbohn, AIM2000 (Version 1.0); Chemical Adviser: R. F. W. Bader.
- (11) Su, P. F.; Li, H. Energy Decomposition Analysis of Covalent Bonds and Intermolecular Interactions. *J. Chem. Phys.* **2009**, *131*, 014102-014115.
- (12) Glendening, E.D.; Reed, A. E.; Carpenter, J.E.; Weinhold, F. NBO Version 3.1.
- (13) Stearns, J.A.; Zwier, T.S. Infrared and UV Spectroscopy of Jet Cooled ortho-, meta- and para- Diethynylbenzene. *J. Phys. Chem. A.* **2003**, *107*, 10717-10724.
- (14) Koch, U.; Popelier, P.L.A. Characterization of CH \cdots O hydrogen bonds on the basis of charge density. *J. Phys. Chem.* **1995**, *99*, 9747-9754.

CHAPTER 7: SUMMARY AND CONCLUSIONS

This thesis provides an insight into the hydrogen bonding interactions present in multifunctional π systems. The studies were conducted employing the technique of matrix isolation infrared spectroscopy which were corroborated by *ab initio* computations. The π systems explored in this thesis are PhAc, C_2H_2 , $B_3N_3H_6$ and C_6H_6 . Atoms in molecules (AIM) analysis, Natural Bond Orbital (NBO) analysis and Localized Molecular Orbital Energy Decomposition Analysis (LMO-EDA) have been also used in all the systems to further investigate the nature of interactions present. The scheme below gives the pairwise heterodimers, studied between the four molecules listed above. In addition, each of the molecules also has homodimer interactions, some of which have also been studied.

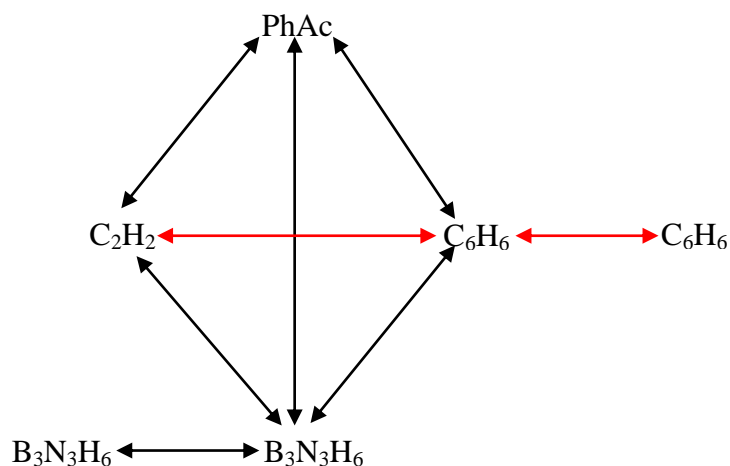


Fig.7.1 The various multifunctional π systems explored in this thesis. The red arrow indicates the interactions already reported in the literature.

The factors affecting the stabilities of the various structures and the competition between the various binding sites were the main objectives of studying hydrogen bonding interactions in these systems. Furthermore, comparing the hydrogen bonding interactions in $B_3N_3H_6$ and its organic analogue, C_6H_6 , was also expected to provide useful insights into non-covalent interactions, which led us to study the interactions of $B_3N_3H_6$ with π systems such as C_2H_2 , C_6H_6 and PhAc.

The first system that we explored was the PhAc-C₂H₂ system. Four stable minima were obtained for this system on the potential energy surface but we were able to discern only one complex in our matrix isolation experiments, where the C-H of C₂H₂ was the proton donor to the π cloud of C₂H₂ in PhAc. The formation of this complex was evidenced by shifts in the \equiv C-H asymmetric stretch of C₂H₂, \equiv C-H stretch of PhAc and \equiv C-H bend of C₂H₂. The structure where PhAc served as the proton donor to the acetylenic π -cloud was the highest energy structure at both M06-2X and MP2 levels. Experiments with PhAc deuterated at the acetylenic hydrogen (PhAc_D) were also performed, to confirm the above observation, through the isotopic effect.

As has been discussed earlier, the pK_a of C₂H₂ and PhAc are consistent with complex 3 being the global minimum, as smaller pK_a of C₂H₂ is consistent with it being the proton donor. However, gas phase acidities, which are more relevant for our matrix isolation experiments, provide a contradictory picture. The ΔH_{OAcid} for C₂H₂ and PhAc are 375.4 and 370.3 kcal/mol respectively, implying that in the gas phase, PhAc is more acidic than C₂H₂, which should therefore have favoured PhAc to be the proton donor. This seemingly contradictory observation can be explained if we recognize that a secondary interaction between the C-H group of phenyl in PhAc and the π cloud of C₂H₂ renders this complex to be more stable than the complex where the PhAc is the proton donor. This was further corroborated by NBO analysis which also indicated an orbital interaction between the C-H σ^* orbital and the π of the acetylenic system of C₂H₂ in this complex.

In hydrogen bonded interactions, one has also to examine the acidity of the proton donor and the basicity of the proton acceptor and the two properties together play a role in determining the stability of the complex. Towards this end, Gilli *et. al* had proposed that the difference in pK_a and pK_b should be considered and the smaller this difference is, the more propensity for the complex to form.

We followed our work with the study on B₃N₃H₆ complexes. B₃N₃H₆ presents an interesting case study for hydrogen bonding systems. While it is isoelectronic with C₆H₆, it is sufficiently different from its organic counterpart, in terms of the electronic distribution in the ring, to pose interesting landscapes for the study of non-covalent interactions. B₃N₃H₆ has both electron rich *p* orbitals centered on the nitrogen atoms and electron deficient *p* orbitals centered on the boron atoms. B₃N₃H₆, therefore, behaves as an amphoteric π electron system. This basic difference compared with C₆H₆ makes the comparison of B₃N₃H₆ and C₆H₆ interesting. A

number of studies on the weak interactions involving C_6H_6 are present in the literature, the most thoroughly studied being the $C_6H_6-H_2O$ system, which involves an H- π interaction. One of the first studies on $B_3N_3H_6$ by our group was to study the complexes of $B_3N_3H_6$ with H_2O and compare them with those of the $C_6H_6-H_2O$ system. The study on $B_3N_3H_6-H_2O$ by our group revealed the presence of an N-H \cdots O interaction in the matrix, where the N-H of $B_3N_3H_6$ was interacting with the O atom of water. The computations, at the MP2 and M06-2X levels on the $B_3N_3H_6-H_2O$ system yielded three minima, which is a richer landscape than the $C_6H_6-H_2O$ system. The equivalent of the H- π complex in $C_6H_6-H_2O$ was indicated to be a local minimum in the $B_3N_3H_6-H_2O$ system, which however was not observed in the experiments. In the $B_3N_3H_6-H_2O$ system, this complex showed an O-H \cdots N interaction rather than the H- π observed in $C_6H_6-H_2O$. In both systems, the H- π complex for $C_6H_6-H_2O$ and O-H \cdots N complex for $B_3N_3H_6-H_2O$, also showed near degenerate and possibly interconvertible complexes, revealing a certain floppiness in their structures. Thus, these interesting differences and similarities between the two systems led us to study the interactions of $B_3N_3H_6$ with weak complexes. We therefore studied the $B_3N_3H_6$ complexes with π systems. We chose C_2H_2 and C_6H_6 . To further investigate the competition between interactions, we incorporated PhAc, in our array of research, which contains both C_6H_6 and C_2H_2 moieties.

The $B_3N_3H_6-C_2H_2$ system was explored and was compared it with the well studied $C_6H_6-C_2H_2$ system. In the $C_6H_6-C_2H_2$ system, a T-shaped structure, where the C-H of C_2H_2 served as the proton donor to the π cloud in C_6H_6 was found to be the global minimum. In the $B_3N_3H_6-C_2H_2$ system, a bent NH \cdots C structure, where the N-H of $B_3N_3H_6$ served as a proton donor to one of the carbon atoms of C_2H_2 was found to be the global minimum. The formation of the bent NH \cdots C complex in $B_3N_3H_6-C_2H_2$ dimer was evidenced by shifts in the N-H stretch of $B_3N_3H_6$, \equiv C-H asymmetric stretch of C_2H_2 and \equiv C-H bend of C_2H_2 . Located higher in energy relative to this structure was an isomer with a bent CH \cdots N geometry in which the C-H of C_2H_2 was the proton donor to the nitrogen of $B_3N_3H_6$. This structure was also observed in our experiments, as indicated by the shift in the \equiv C-H asymmetric stretch of C_2H_2 .

We also studied the $B_3N_3H_6$ dimer system in order to compare it with the well investigated C_6H_6 dimer system. While in the case of a C_6H_6 dimer, a parallel-displaced structure was the global minimum, in the $B_3N_3H_6$ dimer, the aligned stacked structure and the parallel

displaced structures were almost isoenergetic and were found to be the global minima at all levels of theory that we explored. However, these structures could not be observed in our experiments due to the lack of any significant spectral signatures. Experimentally, two isomeric forms of the $B_3N_3H_6$ dimers were observed in our matrix. One was the T_N structure, where the N-H of one $B_3N_3H_6$ molecule pointed towards the nitrogen atom of the second $B_3N_3H_6$ molecule; a structure that was similar to the T-shaped C_6H_6 dimer. In addition to this structure, we also observed a dihydrogen bonded structure, both computationally and experimentally. In this structure, the N-H of one $B_3N_3H_6$ molecule interacted with the H attached to the boron atom of another $B_3N_3H_6$ molecule. In this structure, *two* dihydrogen bonds were in operation, probably cooperatively, which therefore placed it in terms of stability, just behind the classical hydrogen bonded T_N dimer, by about 0.5 kcal/mol. The dihydrogen bonded system has been observed in metal hydride systems, but our observation is the first of its kind in a system not involving a metal hydride.

It was appealing to investigate the nature of interactions when both $B_3N_3H_6$ and C_6H_6 were deposited together in a matrix. We therefore studied the $B_3N_3H_6$ - C_6H_6 system. This system was explored computationally by Bettinger *et al* and it was shown that the structure, where the N-H of $B_3N_3H_6$ interacted with the π cloud of C_6H_6 (T-NH-1) and the parallel displaced structure were nearly isoenergetic at the MP2/aug-cc-pVQZ level of theory. Our matrix isolation experiments revealed that the T-NH structure, along with the structure where the N-H of $B_3N_3H_6$ interacted with one of the carbon atoms in C_6H_6 were the global minimum. In both these complexes, the N-H of $B_3N_3H_6$ served as a proton donor, a conclusion consistent with our studies on the $B_3N_3H_6$ - C_2H_2 complex and $B_3N_3H_6$ dimer.

We studied the $B_3N_3H_6$ -PhAc system as PhAc has components of both C_2H_2 and C_6H_6 and is also expected to show hydrogen bonding interactions, with multiple isomers. Our previous studies on the PhAc-Ac heterodimer resulted in the C_2H_2 serving as the proton donor to the π cloud of C_2H_2 in PhAc. It was therefore interesting to see the interaction of an N-H system like $B_3N_3H_6$ with a $C-H\cdots\pi$ system such as PhAc. In this system, the N-H of $B_3N_3H_6$ served as a proton donor to the carbon atom of C_2H_2 in PhAc, a complex labeled as the bent $NH\cdots C$ complex. This complex was very similar to the bent $NH\cdots C$ complex formed in the $B_3N_3H_6$ - C_2H_2 system, where the N-H of $B_3N_3H_6$ interacted with the carbon atom of C_2H_2 . Experiments were also

carried out using PhAc_D to study the effect of isotope on this complex. These experiments also revealed, through C-D shifts, the formation of the bent NH[⋯]C complex in the matrix.

We also explored the C₆H₆-PhAc system to investigate the nature of interactions when both highly electron rich π systems interact with each other in a matrix. Experiments in both N₂ and Ar matrices did not lead to any conclusive results and hence, is not described in this thesis. However, the computations at MP2/aug-cc-pVDZ level of theory revealed the stacked structure to be the global minimum, followed by the T-shaped structure, where the C-H of PhAc served as the proton donor to the π cloud of C₆H₆, a structure similar to the T-shaped structure obtained in the C₆H₆-C₂H₂ experiments present in the literature.

In all the B₃N₃H₆ systems studied in this thesis, it was found that the N-H of B₃N₃H₆ served as the proton donor in the matrix. The stacked structures, although being the most stable structures computationally, could not be discerned in the matrix isolation experiments due to meagre shifts and thus providing no significant spectral signatures.

7.1 Scope for future work

It would be interesting to study the hydrogen bonding interactions of PhAc, substituted with electron withdrawing or donating groups on the phenyl ring. The changes in the electron withdrawing or donating substituents could lead to interesting results since the basicity of the π cloud and the acidity of the acetylenic hydrogen would now be altered.

The various B₃N₃H₆ systems studied in this thesis present a nice comparison with the well studied C₆H₆ systems. The interesting differences between the organic and inorganic analogues of C₆H₆, can open up new areas of study involving B₃N₃H₆, with other precursors such as those containing sulphur. The study of B₃N₃H₆ with alcohols could also present a very interesting scenario relative to the interactions of alcohols with C₆H₆.

The stacked structures, despite being the global minimum structures in our work on B₃N₃H₆ dimer, B₃N₃H₆-PhAc and PhAc-C₆H₆ complexes, could not be discerned in our experiments. These structures could be investigated using UV-Visible spectroscopy as a tool to study the matrix isolated species. The interaction of π electron systems in the stacked structures can be expected to present signatures in the electronic absorption spectroscopy.

Going beyond the boron systems, hydrogen bonding interactions involving phosphorus containing rings, such as phosphazenes could also be studied using matrix isolation infrared spectroscopy, as these may present surprises in the realm of hydrogen bonded contacts.

LIST OF PUBLICATIONS

List of Publications included in the thesis

1. “Hydrogen bonded complexes of Phenylacetylene-Acetylene-Who is the proton donor?” *Kanupriya Verma, Kapil Dave, K.S.Viswanathan, J. Phys. Chem. A* **2015**, 119, 12656-64.
2. “How different is the borazine acetylene dimer from the benzene acetylene dimer?-A matrix isolation infrared and *ab initio* quantum chemical study.” *K.Verma, K.S.Viswanathan, M.Majumder and N.Sathyamurthy, Mol. Phys.* **2017**, 115, 2637-48.
3. “Borazine Dimer-the case of a dihydrogen bond competing with a classical hydrogen bond” *Kanupriya Verma, K. S. Viswanathan. Phys. Chem. Chem. Phys.* **2017**, 19, 19067-19074.
4. “A Tale of Two Structures: The Stacks and Ts of Borazine and Benzene Hetero and Homo Dimers” *Kanupriya Verma, K. S. Viswanathan Chem. Select* **2018**, 3, 864-873.

Manuscript in Preparation

1. **Matrix Isolation Infrared and *ab initio* computations on the Borazine-phenylacetylene complexes.** *Kanupriya Verma, K.S. Viswanathan.*

Collaborative Publications

1. “Does borazine water behave like benzene-water?-A matrix isolation infrared and *ab initio* study.” *P.Mishra, K.Verma, D.Bawari and K.S.Viswanathan, J. Chem. Phys.* **2016**, 144, 234307-16.

Book Chapter

1. “Matrix Isolation: A window to Molecular Processes” in **Molecular and Laser Spectroscopy.** *Pankaj Dubey, Jyoti Saini, Kanupriya Verma, Ginny Karir, Anamika Mukhopadhyay, K.S.Viswanathan. Elsevier, 2017,317-340.*